CCN Consistency

Product Validation and Intercomparison Report for Consistency (CCN_D2)

Reference:	CCI-LAKES-CCN-PVIR-1.0
Issue:	1.2
Date:	Dec. 10, 21

Distribution:		
Company	Names	Contact Details
ESA	C. Albergel	clementalbergel@esa.int
BC	K. Stelzer	kerstin.stelzer@brockmann-consult.de
	D. Müller	dagmar.mueller@brockmann-consult.de
	J. Scholze	jorrit.scholze@brockmann-consult.de
CLS	B. Coulon	bcoulon@groupcls.com
	B. Calmettes	bcalmettes@groupcls.com
	A. Mangilli	amangilli@groupcls.com
	P. Thibaut	pthibaut@groupcls.com
CNR	C. Giardino	giardino.c@irea.cnr.it
	M. Pinardi	pinardi.m@irea.cnr.it
Eola	E. Zakharova	zavocado@gmail.com
GeoEcoMar	A. Scrieciu	albert.scrieciu@geoecomar.ro
H2OG	C. Duguay	claude.duguay@h2ogeomatics.com
	Y. WU	mark.wu@h2ogeomatics.com
LEGOS	J.F. Crétaux	jean-francois.cretaux@legos.obs-mip.fr
	A. Kouraev	alexei.kouraev@legos.obs-mip.fr
NORCE	E. Malnes	eirik.malnes@norceresearch.no
PML	S. G. H. Simis	stsi@pml.ac.uk
	X. Liu	liux@pml.ac.uk
SERTIT	H. Yésou	herve.yesou@unsitra.fr
TRE-ALTAMIRA	P. Blanco	Pablo.blanco@tre-altamira.com
UoR	C. Merchant	c.j.merchant@reading.ac.uk
	L. Carrea	l.carrea@reading.ac.uk
UoS	A. Tyler	a.n.tyler@stir.ac.uk
	E. Spyrakos	evangelos.spyrakos@stir.ac.uk

List of Contents

1 Introduction

1.1 Objectives of the Consistency analysis

Inconsistency between datasets of Essential Climate Variables (ECVs) or of single-variable cases can lead to misinterpretation and reduced acceptance by the user community. The Lakes_cci project baseline activities provide products for five thematic ECVs, predominantly applying existing, published algorithms to arrive at each thematic ECV, which are for the first time combined into a single Lakes_cci product. The consistency between the thematic variables needs to be assessed in detail because inconsistencies are not only probable but even expected.

The objective of the Consistency study is to investigate and improve the CCI Lakes consistency of thematic ECVs, through development of statistical tests, cross-ECV time series analysis spanning the global dataset, identification of sources of inconsistency from underlying observation data and finally proposing improvements and quality flags for the thematic and merged ECVs. The ultimate objective is to provide users of the data set with improved guidance on the correct usage of the first-ever multidisciplinary global Lakes ECV data set. The procedures developed in this work can apply also to future data sets and therefore this work represents an important legacy to cross-disciplinary lake remote sensing.

1.2 Purpose of this document

The purpose of this document is to provide an overview on the analyses performed for identifying inconsistencies within and between the thematic variables. From existing work to characterize product uncertainties we know that the Lake Water-Leaving Reflectance (LWLR) is likely to be most sensitive to algorithmic and observation inconsistencies. Therefore, advanced analyses for the reasons of inconsistencies, including between sensors, are presented for LWLR. New Optical Water Type (OWT) classes are derived based on the results from the consistency analyses and solutions for improved flagging are presented. Climatologies are derived for LSWT and optical data for the purpose of identification of unexpected results, particularly those found in the LWLR. The techniques developed here with the 250 lakes in the Climate Research Data Package (CRDP) v1 are transferable to CRDP v2.

2 Data sets and data extraction

The CRDP of the Lakes_cci consists of global, projected and merged products of five thematic data sets at daily aggregation intervals referred to as Super-collated Level 3 (L3S). They comprise data from several satellite missions, designed with different objectives, and processed by different teams in the Lakes_cci scientific community. The following abbreviations are used to refer to these distinctive parts of the L3S dataset:

- LWL: Lake Water Level; a single value per lake and day (several altimeter instruments).
- LWE: Lake water extent; a single value per lake and day (several SAR and optical instruments)
- LSWT: Lake surface water temperature; daily 1-km gridded (ATSR, AASTR, AVHRR).
- LIC: Lake ice cover; daily 1-km gridded (MODIS Terra, Aqua).
- LWLR: Lake Water-Leaving Reflectance, turbidity and chlorophyll-a concentration; daily 1-km gridded (MERIS, OLCI-A/B)

This report covers CRDP version 1.0 and (and partly also version 1.1), which contain information on 250 lakes with a global distribution.

Data of individual lakes had to be extracted from the daily gridded global L3S products for analysis. Several extraction methods were implemented. For example, to compare pixel identification (ice/water), a 3x3 macropixel at the location corresponding to maximum distance from land was extracted. For time-series analysis and cross-correlation work, daily lake-median values were used to compare to meteorological data. The following sections give an overview of the extraction

methodology and resulting datasets and metrics. Examples of their purpose in the analysis follow in the chapters that follow.

2.1 Pixel at maximum distance from land

The location corresponding to maximum distance from land is calculated from the lake shape and will often be close to the geographic centre of the lake or one of its connected sub-basins. This location is not necessarily representative of the entire lake but minimises product variability caused by shoreline effects, which could include bottom visibility, signal mixing due to adjacency effects, or strong horizontal optical gradients. Generally speaking, variability in lake physics and biogeochemistry can be expected to be higher near the shore compared to open waters. LWL and LWE data are single observation values per lake, so their time series do not allow further spatial selection.

The extraction comprises 3 by 3 pixels and includes all available variables in the L3S product. In addition, eleven variables were extracted from ERA 5. Additionally, OWT membership variables were extracted from intermediate L2 LWLR products.

Table 1: L3S Product variables extracted at maximum distance position of each lake.

L3S THEMATIC VARIABLES	VARIABLE NAMES (SHORTENED)
LWL	water_surface_height_above_reference_datum water_surface_height_uncertainty
LWE	lake_surface_water_extent and -uncertainty
LSWT	lake_surface_water_temperature, lswt_uncertainty, lswt_quality_level (categories)
LIC	lake_ice_cover (categories), uncertainty
LWLR	chla_mean, turbidity_mean (+uncertainty)
	Rw 400-900: Rw, uncertainty_relative, uncertainty_relative_unbiased

Table 2: Variables extracted from ERA 5 at the maximum distance position of each lake, at 12:00 UTC.

ERA 5 DATA VARIABLES ABBREVIATIONS	FULL VARIABLE NAMES
licd, lict	lake_ice_depth, lake_ice_temperature
lmld, lmlt	lake_mix_layer_depth, lake_mix_layer_temperature
lshf	lake_shape_factor
skt	skin_temperature
sf	Snowfall
tp	total_precipitation
tsn	temperature_of_snow_layer
u10, v10	10m wind components

Table 3: OWT product variables extracted at maximum distance from shore.

OWT PRODUCT VARIABLES
poly_owt01 - 13
poly_owt_membership_sum, _normalized
blended_dominant_owt_majority_class

2.2 Median per Lake

The daily median value of each lake for a selection of variables has been calculated and extracted for further analysis, likewise the daily standard deviation and the number of available pixels in the daily observation.

For years without LWLR data, only LSWT was extracted from the L3S. The uncertainties of Rw were not included in the extraction.

The extraction of LWL or LWE described in section 2.1 was used as the single pixel extraction covers the one value per lake (if values are available due to reduced number of lakes for this variable).

Table 4: Variables extracted for daily median values of lakes.

L3 PRODUCT THEMATIC VARS	VARIABLE NAMES	YEARS
LSWT	lake_surface_water_temperature, lswt_uncertainty	1992-2019
LWLR	chla_mean, turbidity_mean (+ uncertainty)	2002-2012, 2016-2019
	Rw 400-900: Rw for each wavelength	

ERA 5 DATA VARIABLES ABBREVIATIONS	YEARS
licd, lict, lmld, lmlt, lshf, skt, sf, tp, tsn, u10, v10	1992-2019

2.3 Median per OWT and Lake

The daily lake-median values and the number of pixels associated with each OWT, were calculated. The OWT membership was based on the dominant OWT class per pixel. Choosing the majority class for this extraction ignores the fact that Rw spectra may have high similarity to more than one class. The temporal coverage is restricted to the years 2002-2012 and 2016-2019 corresponding to MERIS and OLCI-A/B records.

The extracted data were organised in tables with columns of lake identifier (LakeID), date of daily L3S data (time), dominant OWT class (OWT between 1-13), number of pixels in that class (N_owt) and three columns for each variable giving the median, standard deviation and number of pixels in that class. The number of pixels in the specified OWT for a given date and lake (N_owt) can differ from the number of observations for water surface temperature (lswt_n), because they are derived from different instruments. The number of observations should be the same for all lake-colour based variables, e.g. Rw400_n and chla_mean_n. The Rw uncertainties were not extracted.

Table 5: Variables extracted for OWT based lake median.

L3 Product Thematic Vars	Variable names
LSWT	lake_surface_water_temperature, lswt_uncertainty
LWLR	chla_mean/uncert., turbidity_mean/uncert. Rw400 - Rw900

2.4   Median per LIC classification and per LSWT quality classification

The LSWT product comes with a pixel-wise description of estimated quality level. The five levels (and a no-data flag) are defined as 1 for bad data, 2 for worst quality, 3 for low, 4 for acceptable and 5 for best-quality data. The extraction algorithm counts the daily number of pixels for levels 1 to 5, and the total number of pixels per lake (including the no data pixels).

For each of these levels, the median and standard deviation of lake surface water temperature were calculated per day and per lake, resulting in time series of different quality levels with daily resolution for each lake.

The lake ice cover is a classification with four categories: water, ice, cloud, or bad. Again, the extraction algorithm counts the number of pixels within each category per day and lake. For the three LWLR variables Rw560, chla_mean and turbidity_mean, the median, standard deviation and number of pixels per class were calculated or counted. The combination of the LIC classification with the availability of LWLR products can address questions on flagging consistency, e.g., how well cloud and ice masking has worked in the independently derived LWLR products compared to the LIC classification (see section 3.2).

The LIC product has adopted a new classification procedure which was released as CRDP v1.1. The influence of the changes between version 1.0 and the reprocessed version 1.1 is documented in this report.

2.5   Daily Percentiles of variables per OWT

Percentile values at 5, 10, 20, 50, 80, 90 and 95% were extracted for some LSWT and LWLR product variables. The variables from LWLR are: Rw412, Rw443, Rw490, Rw510, Rw560, Rw620, Rw665, Rw681, Rw709, Rw754d, Rw779, Rw885, Rw900, chla_mean, chla_uncertainty, turbidity_mean, turbidity_uncertainty; and from LSWT: lake_surface_water_temperature and lswt_uncertainty.

The percentiles were extracted from the daily data per lake and OWT (described in section 2.3) which are further aggregated to medians of daily percentiles over all years or per sensors which led to multi-annual median of percentiles.

3   Consistency Analysis

Within this chapter we show the analyses that have been performed to test the consistency and identify inconsistencies between sensors (MERIS and OLCI) (3.1), between thematic variables (3.2) and how these findings were used to find underlying issues related to land adjacency effects (3.3) and atmospheric correction for LWLR (3.4).

3.1 Consistency of MERIS and OLCI products and dominant OWTs

Although similar in their design, it is known that MERIS and OLCI measurements are systematically different. These differences become enhanced when water leaving reflectance spectra are obtained from atmospheric correction. In the following we demonstrate how subtle spectral differences affect the OWT classification and the ranges of LWLR-derived chlorophyll-*a* concentration and turbidity. A deeper investigation of spectral characteristics of the two sensors and their representation in the OWT classes is presented in section 4.1, while investigations into the consistencies between atmospheric corrections of MERIS and OLCI are shown in section 3.4.

3.1.1 Occurrence of OWTs and distribution of daily median turbidity and chl-a

The daily per-OWT medians are evaluated for MERIS and OLCI independently (**Fehler! Verweisquelle konnte nicht gefunden werden.**, MERIS: blue, OLCI: red). Each histogram shows daily median values of turbidity or chlorophyll-*a* concentration from observations predominantly associated with a given OWT class (1 to 13). The histograms are based on yearly datasets, so that changing distributions over the years of one sensor can be seen in the intensity of the colour. The frequency distribution refers to the number of days on which any number of observations was predominantly associated with the given OWT, ultimately providing a median value for each LWLR product. The total number of observation days is different for MERIS and OLCI, which are covering the year 2002 to 2012 (MERIS) and 2016 to 2019 (OLCI), respectively.

Differences between the sensors might arise from changes in the water body itself as well as systematic spectral divergence of the sensor data including their atmospheric correction. The distribution of daily turbidity values within the dominant OWTs reveals that OWT classes 1, 5 and 10 (and to some extent also 2, 12 and 13) show systematic differences between OLCI and MERIS turbidity: in all cases, the turbidity shifted to lower values for OLCI. The yearly distributions within one sensor are more similar to each other than the distributions between sensors. The example shown in **Fehler! Verweisquelle konnte nicht gefunden werden.** (a,b) is for Lake Superior.
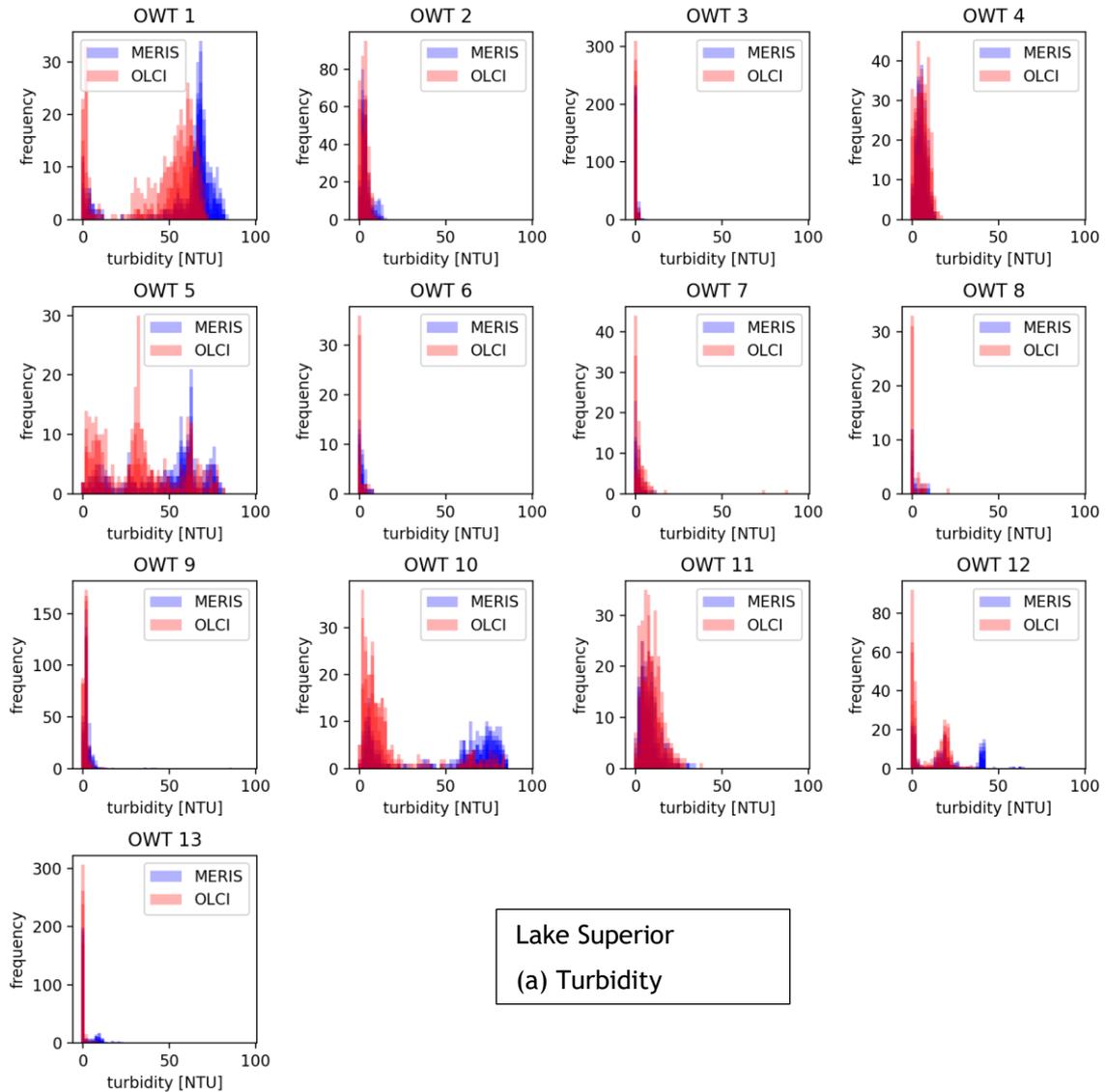
Figure 1a. Yearly distributions of daily median turbidity and chlorophyll concentration (daily, per lake, per OWT), separated for MERIS and OLCI observations. The intensity of colour highlights where distributions based on yearly observations are similar over the observation period.
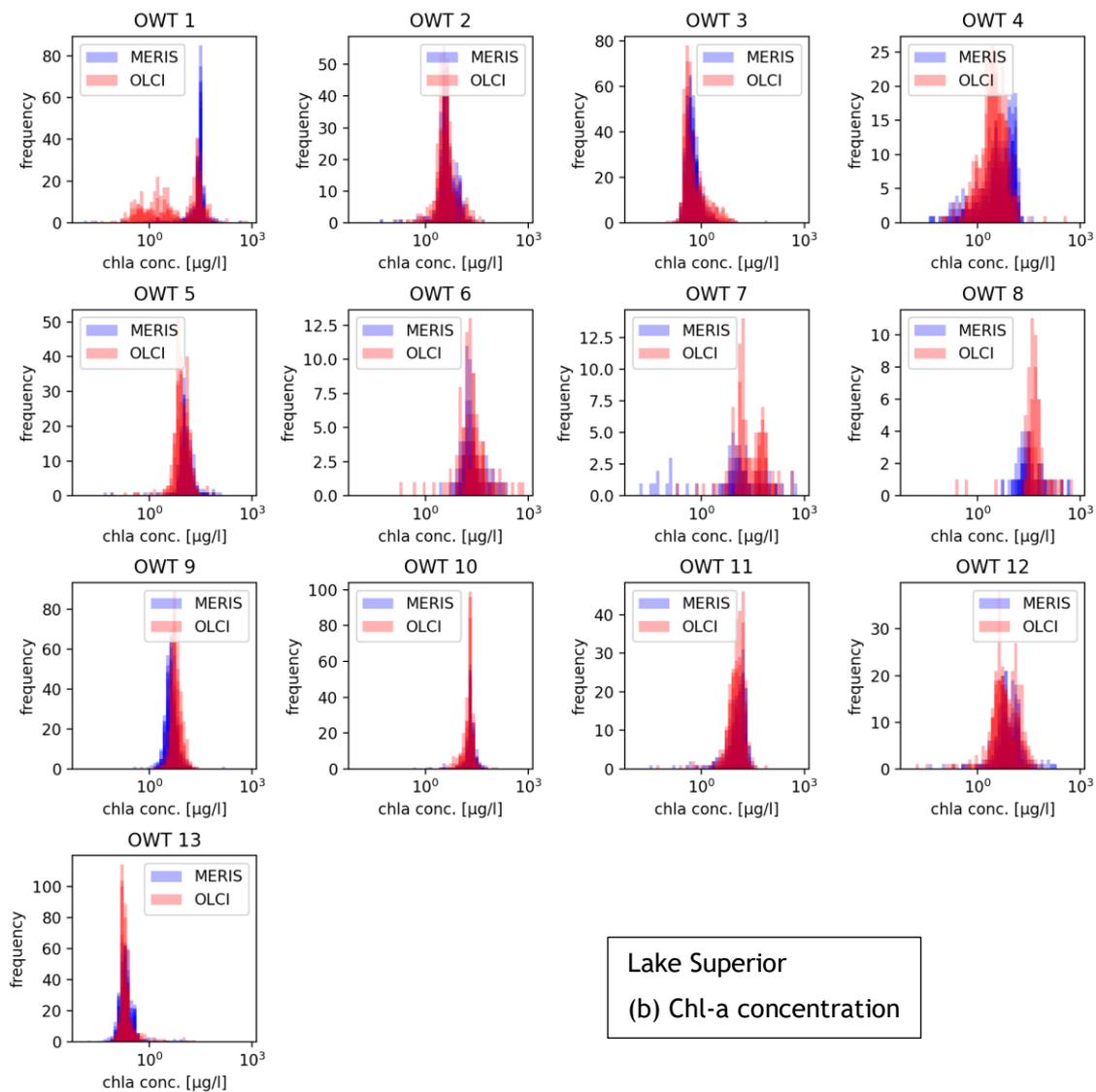
Figure 1b. Yearly distributions of daily median turbidity and chlorophyll concentration (daily, per lake, per OWT), separated for MERIS and OLCI observations. The intensity of colour highlights where distributions based on yearly observations are similar over the observation period.

3.1.2 OWT membership score and Chl-a at maximum distance from shore

Per definition of the OWTs, a relationship between OWT membership score and chlorophyll-*a* concentration is expected. The reference spectra of the OWTs were chosen from a set of spectra which are assumed to cover the natural occurring ranges of Chl-a concentration and turbidity. Ideally, if the observed MERIS and OLCI spectra are similar in shape and intensity and the optical and biological properties of the lake stayed the same in the observation period, the relationships between Chl-a concentration and OWT membership score would be similar for both sensors. If the patterns of Chl-a and membership score change systematically, e.g. some combinations only occur for one of the satellite sensors, this implies that the associated spectral shapes are observed only with one sensor (while reference spectra for the optical water types remain the same for all observations). The

reason, why different spectral shapes are observed, can originate from observation or algorithmic uncertainty, or differences in quality flagging between sensors.

The input data set for the analysis of OWT membership scores and Chl-a concentration are the macropixel extracts of the L3S, i.e. a 3 x 3 pixel extraction at maximum distance from the shoreline position. The data do not represent the entire lake, particularly if the lake contains multiple sub-basins.

Figure 2 and Figure 3 show the relationship between Chl-a and OWT membership score for each OWT class for 2 selected lakes. The MERIS data (blue crosses) shows more variability in Chl-a values, including larger numbers of high concentrations, which are only very sparsely observed with OLCI (green). It is not possible to state a single cause for this behaviour; in addition to sources of systematic uncertainty listed above, sensor-specific pixel classifications may work better for one of the sensors, and undetected ice may lead to biases in the distributions of OWT membership score and Chl-a, as demonstrated here for Lake Amadjuak (Figure 2).

Particularly, for MERIS data in Lake Chad (Figure 3), there are many spectra with lower membership values than the ones observed with OLCI (around 0.8) in all classes and a wide Chl-a concentration range. For example, OWT 10 becomes the dominant water type for many MERIS spectra at quite low membership scores, whereas for spectra from OLCI, the same dominant water class is selected at much higher membership scores.

Amadjuak, Canada
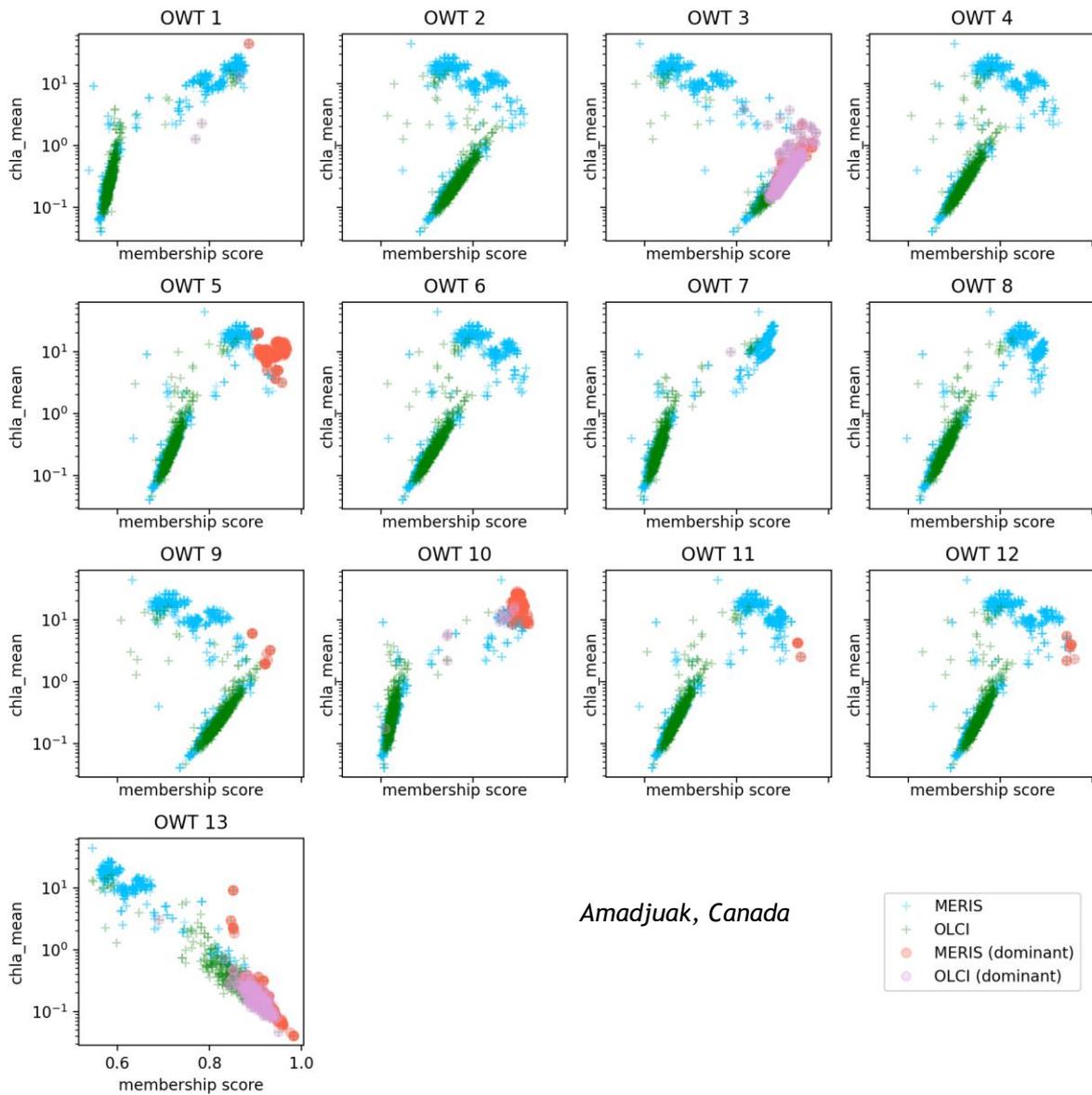
Figure 2 OWT membership score vs. chlorophyll-a mean value per OWT (data extracts from all years at centre point of the lake). The dominant water type, the class with the maximum membership score, is highlighted by filled circles (MERIS: red, OLCI: violet). Other membership scores are marked with crosses (MERIS: blue, OLCI: green)
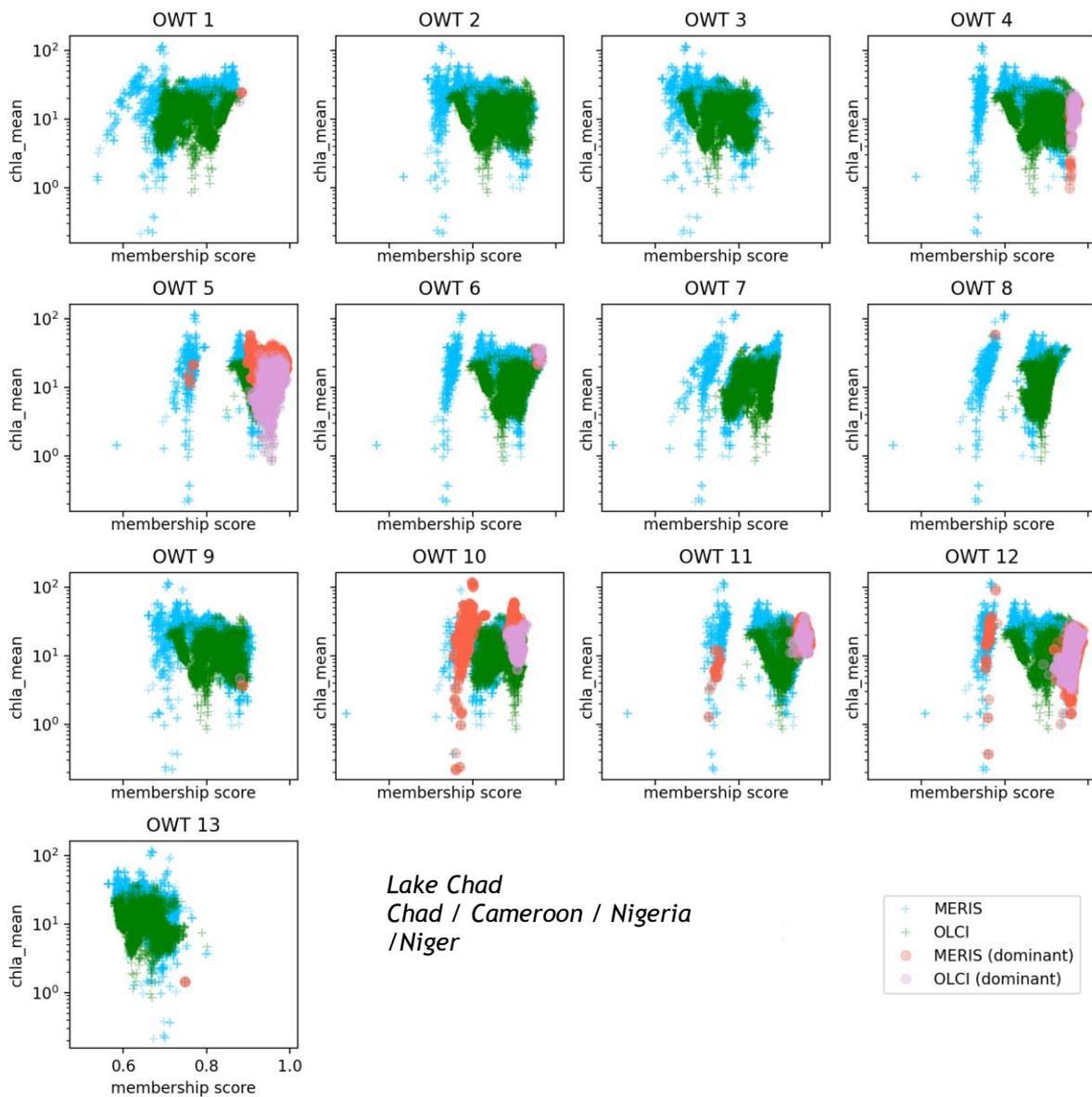
Figure 3 OWT membership score vs. chlorophyll-a mean value per OWT (data extracts from all years at centre point of the lake). The dominant water type, the class with the maximum membership score, is highlighted by filled circles (MERIS: red, OLCI: violet). Other membership scores are marked with crosses (MERIS: blue, OLCI: green)

3.1.3 Discussion

This analysis served to inform us on the severity of inter-sensor inconsistencies, and to attribute this behaviour to specific water types. However, it was quickly found that the most extreme differences were likely associate with misclassification between OWT classes rather than the algorithms for Chl-a associated with each of the classes. The misclassification could be due to observation effects (including sensor-related), but we suspect that land-adjacency, ice or possibly cloud effects are the most likely causes, even when inspecting data from the lake centre.

Ways to improve quality-filtering in post-processing were discussed and informed further analysis (below). One approach is to have a generic or lake-specific thresholding function, using the percentiles of LWLR products to determine realistic vs suspect value ranges. Thus far we have been cautious to apply strict thresholds because there is no reference framework to inform a decision on

when high values become suspect or extremely suspect. The data extraction strategy, working on lake centre observations, does not necessarily inform this process as well as we might like, either. Further analyses presented below focus on using other Lakes ECV variables to inform the process. Furthermore, section 4.1 aim to relate retrieval accuracy to the presence of adjacent land.

3.2 Consistency of LIC, LSWT and LWLR products

3.2.1 Analysis performed with LIC version 1.0

To compare the consistency of the LIC classification from MODIS data with the snow/ice flagging of LWLR data from MERIS and OLCI and the LSWT product, we used data extracted at the position of the maximum distance from the shore. This data extract comprises all variables of the L3S Lakes_cci product within a 3 x 3 macro-pixel. Each pixel within the macro-pixel is uses as an independent observation. Treating all observations within the macro-pixel independently was considered a reasonable compromise to address data gaps that resulted from sparse data availability between the individual products, caused by using different underlying sensors with varying observation times, and is considered to provide some additional sensitivity to spatial inhomogeneity.

Comparisons are shown between lake ice cover classification, LWLR at 490nm and LSWT (Figure 4). Only data points for which observations are obtained on the same day are shown, while there can be several hours between the overpass of individual sensors. If the pixel is classified by the LIC product as ice, it is marked with a red dot. If the LSWT quality is above three (the recommended quality classes) and the pixel is not classified as ice, the data points are marked in dark blue; points of poor LSWT quality (LSWT quality = 3) and not classified as ice are marked in light blue.

The expectation towards perfect consistency between the three thematic products would be:

- Ice only occurs when temperatures are close to or below freezing point, ignoring variations caused by lake salinity.
- Where ice is observed, LSWT and LWLR cannot be observed.

All observations of LSWT and LWLR, which are at the same time identified as ice by the LIC product, are at least suspect because LIC should be considered the most diagnostic product. If the temperature is close to freezing point and LIC is identified, both may be correct due to different observation times or thresholding for sub-pixel occurrence. If the temperature is well above zero degrees and observed with high certainty, the LIC v1.0 classification is suspicious.

In an extreme example from Aral Sea, Kazahkstan (Figure 4), many pixels were classified as ice in the LIC product while they are neither very bright (LWLR) or near freezing temperature. The histogram representation of the data tells the same story: at the top the distribution of LSWT shows that LSWT is well above the freezing point. We know this lake to experience siltation (which would further lower the freezing point), and strong decreases of lake water extent. In this case, the classification algorithm of the LIC v1.0 product was inconsistent because ice occurrence was highly improbable.
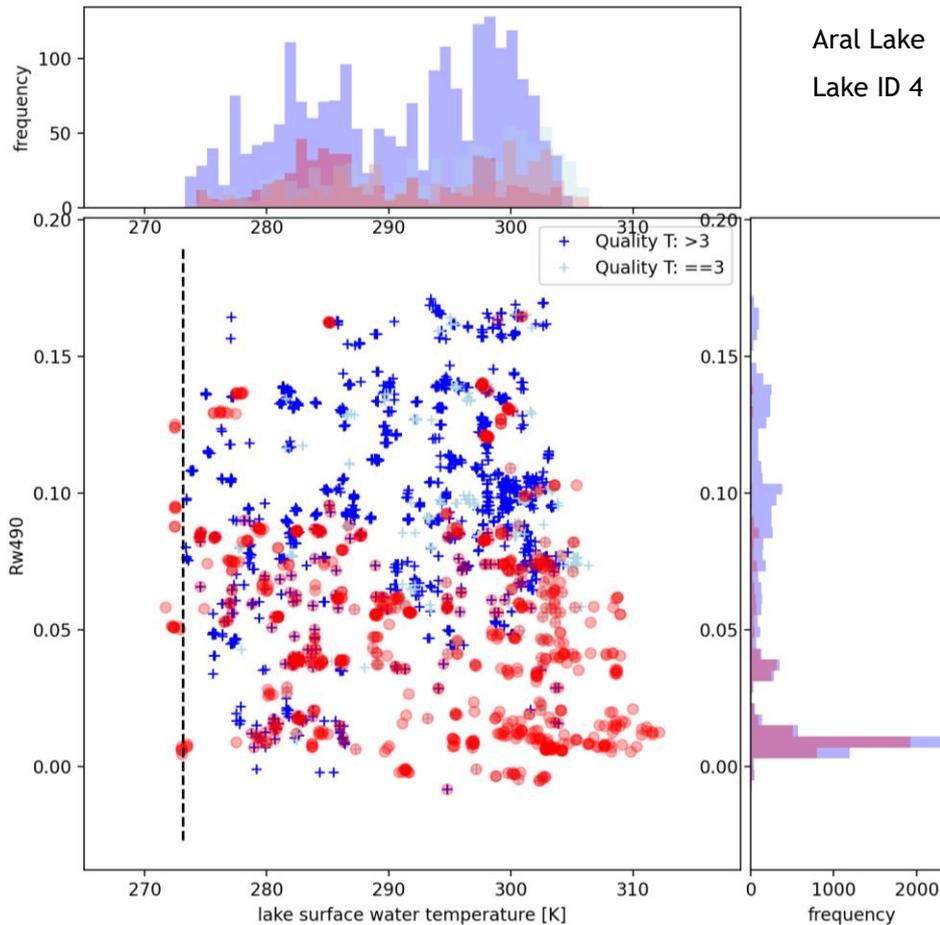
Figure 4 LSWT, LWLR (Rw490) and LIC classification of Aral Sea (LakeID 4). Pixels from 3x3 macropixel at lake centre are analysed, if all three products are available at the same time (scatterplot) or of two products are available (histograms). Colours code the classification of ice (red dots). If the pixel is not classified as ice, the data points is marked as a blue cross. Two qualities of the LSWT product are distinguished: recommended quality (dark blue or red), and poor quality (light blue or red). (data source: L3S v1.0)

For Lake Amudjuak the ice classification of the LIC v1.0 product worked well (Figure 5). The few remaining ice observations are all close to the freezing point. Both histograms which are based on the coinciding observations of two variables confirm this interpretation. The distribution of LSWT data which are classified as ice by the LIC product (red histogram) is tilted towards the freezing point. The data points classified as ice also correspond to relatively high LWLR (histogram on the right, coinciding measurements of LWLR and LIC). These are most certainly ice observations, which have not been correctly identified by the pixel identification for MERIS and OLCI data. So, in combining all three product branches, the snow/ice flagging for the LWLR products can be corrected in post-processing and these observations can be flagged as suspicious.
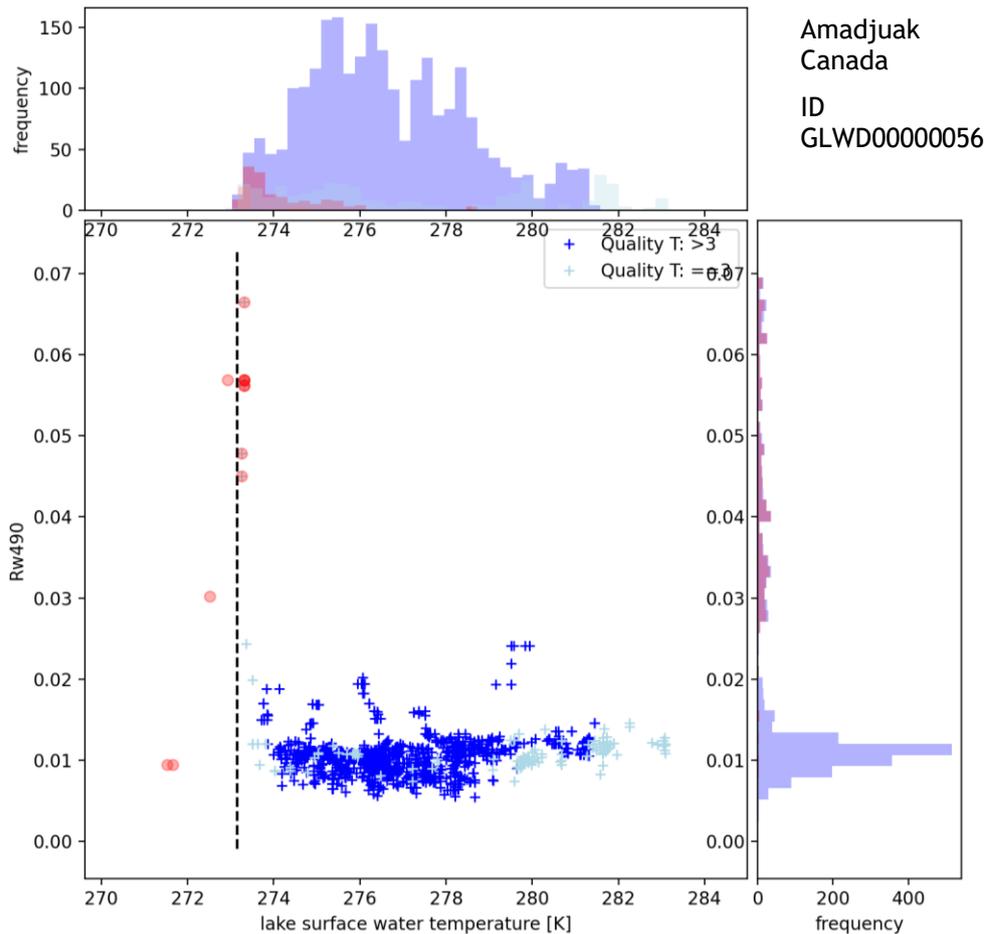
Figure 5 LSWT, LWLR (Rw490) and LIC classification of Lake Amadjuak (LakeID 56) observed on the same day (centre). The histograms are based on only two coinciding observations, either LIC + LWLR (right), or LIC + LSWT (top). The LIC classification and the LSWT can help to identify short-comings in the ice/snow flagging of LWLR product. Further explanations, see text. (L3 v1.0)

3.2.2 Improvements of LIC classification from version 1.0 to 1.1

The issue described above with the LIC classification in version 1.0 has been addressed and is partially solved in version 1.1 (Figure 6). The Aral Sea underwent dramatic changes in lake water extent which are reflected in the falling maximum number of water pixels. At the same time, ice observations increased diametrically in version 1.0, which points to the misclassification of land pixels as ice (upper panel, version 1.0). In the timeseries of version 1.1 the maxima of ice observations are restricted to January. There are still quite a lot of ice observations during summer months, which are improbable, but the diametrical trend in number of water and number of ice observations is resolved.

In general, the number of ice observations are reduced between LIC results versions 1.0 and 1.1. Although the maximum extent of Lake Amadjuak is quite stable during the time, the occurrence of days with full maximum number of pixels (equalling the maximum number of pixels covering the lake) is lower in version 1.1 (Figure 7).
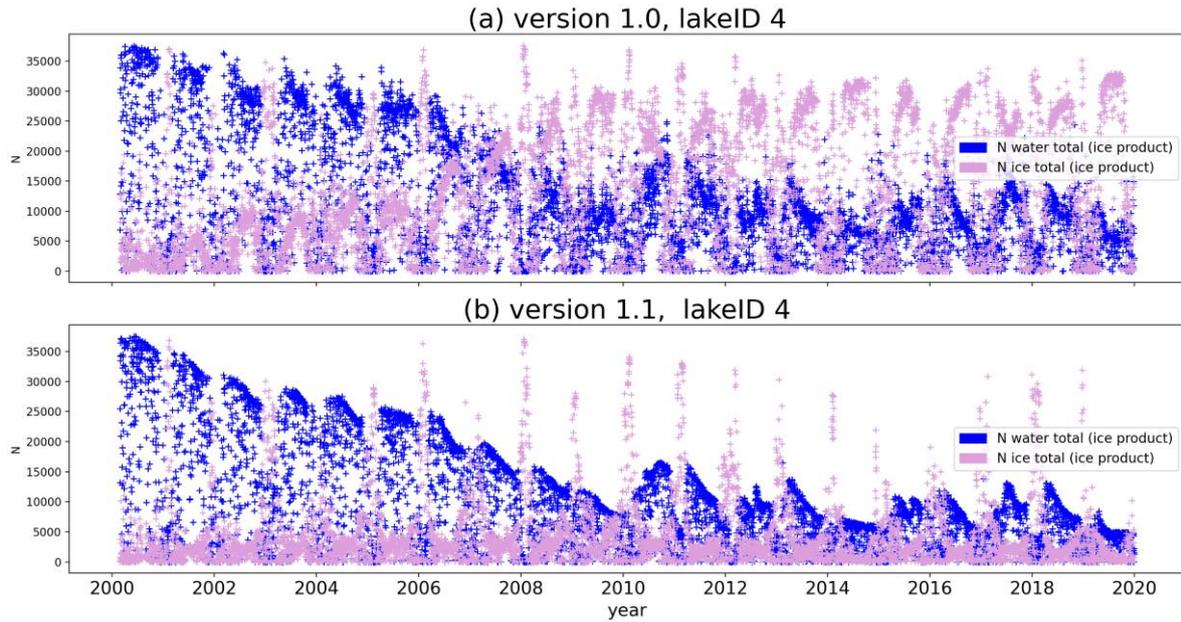
Figure 6 Daily counts of pixels classified as water (blue) and ice (redish) from the LIC classification, MODIS data, for version 1.0 (a, upper panel) and version 1.1 (b, lower panel) of the L3 CCI-Lakes product. Aral Sea, Lake ID GWLD00000004.
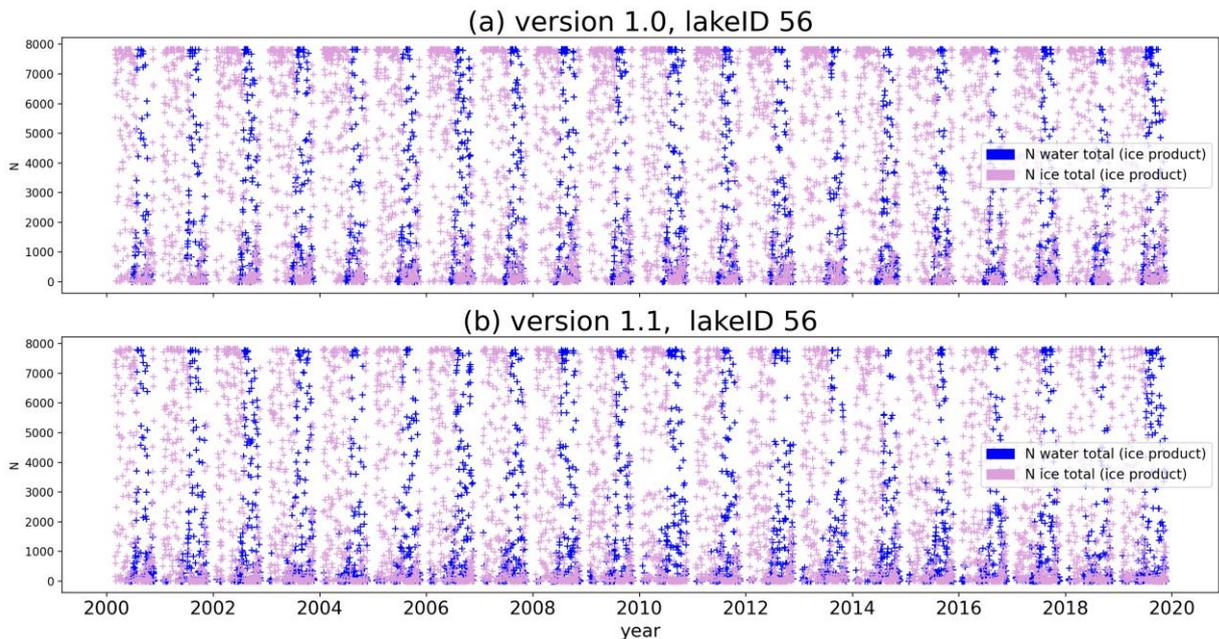
Figure 7 Daily counts of pixels classified as water (blue) and ice (redish) from the LIC classification, MODIS data, for version 1.0 (a, upper panel) and version 1.1 (b, lower panel) of the L3S Lakes_cci product. Lake Amadjuak, Lake ID GLWD00000056.

The changes in the population of the classes are shown in Figure 8 for two highlighted lakes. The histograms show the differences in counts per LIC class (N v1.0/N v1.1). When the ratio is lower than 1, the class occurs more often in v1.1 and vice versa. The red line indicates the ratio of 1. The changes from v1.0 to v1.1 are systematic over all lakes: there are fewer water observations in v1.1, and more cloud identifications. The ice observations are reduced significantly which is seen as improved consistency. This analysis was based on the extraction of lake median LIC class, which includes the daily counts per class. It is therefore not possible to tell precisely how classes converted between the two product versions on a pixel-basis.
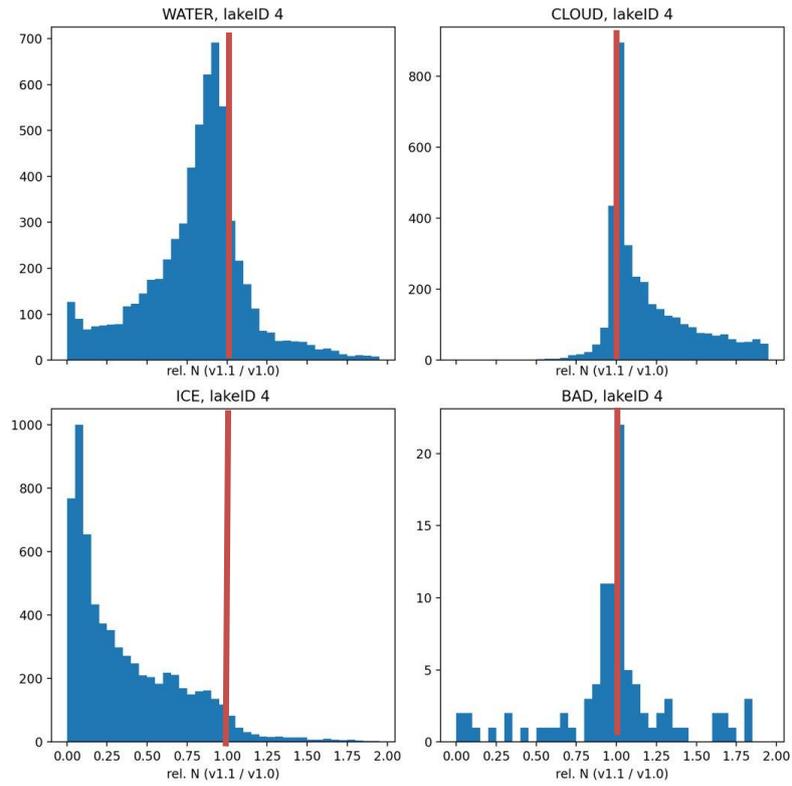
(a) Aral Sea
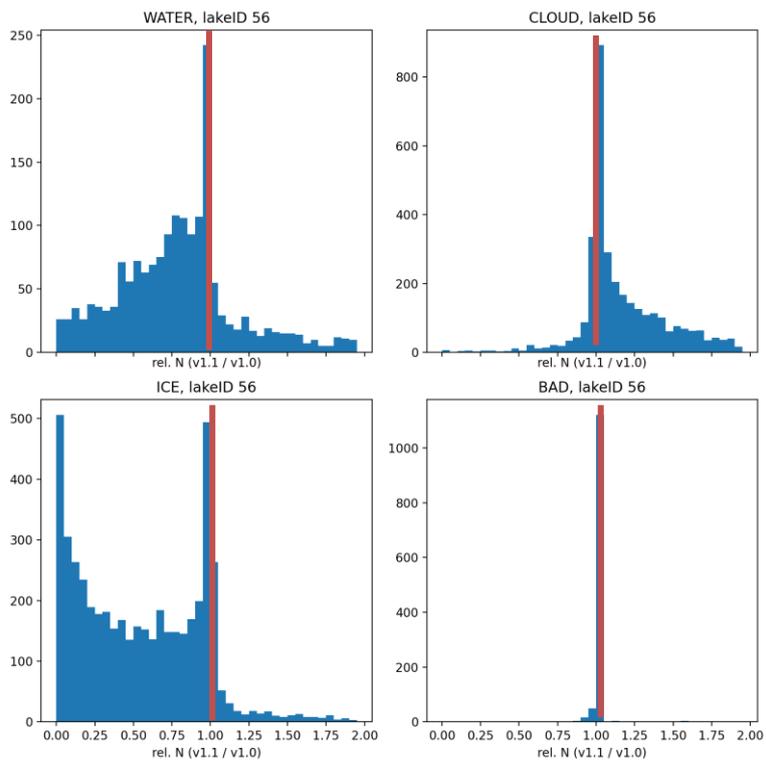
(b) Lake Amadjuak

Figure 8 Distribution of changes in the daily counts per LIC class (water, cloud, ice, bad) for Aral Sea (lake ID GLWD00000004, upper panel) and Lake Amadjuak (lake ID GLWD00000056, lower panel).

3.2.3 Conclusions

The combined availability of LIC, LSWT and LWLR variables in the L3S product creates important new opportunities to address shortcomings in individual pixel identification of these product branches, by vastly increasing the amount of information collected from multiple sensors. This is demonstrated to work well at the daily aggregation level. Suspicious ice observations at high temperatures in the LIC product could be flagged as well as high LWRL values which coincide with an ice classification in the LIC product.

The translation of these findings from lake-averaged data into pixel-based flags is not entirely straightforward, because spatial data gaps between sensors (due to sensor swath or changing cloud cover between overpasses) are more common at the individual pixel level. To address this, probabilistic or generalized quality flagging procedures are needed, as further discussed in section 4.2.

3.3   Consistency of LWLR between lake centre and lake shore

Monitoring of nearshore and inland waters from optical remote sensors is often hindered by adjacency effects due to the significantly sharp contrast between water and land targets, i.e. low radiance from water adjacent to high radiance from land. Small inland water bodies are most susceptible to adjacency effects compared to large water bodies, coastal waters and open oceans and the strong signal from nearby land may affect observations across these lakes, depending on the strength of land and water signal mixing in the atmosphere. To analyse these effects on the MERIS and OLCI observations, water-leaving reflectance spectra were extracted from the lake centre to the lake shore from Lake Rusken and Lake Bolmen in Sweden. The two lakes were selected because of their small size (34 km^2 for Lake Rusken, 170 km^2 for Lake Bolmen), irregularities in shape and the presence of islands within the lake. These characteristics are expected to significantly amplify adjacency effects in the reflectance spectra. These two lakes were also included in the Brownification use case.

Three points from the centre to the shore at Lake Rusken were selected in four directions (Figure 9), i.e., from centre to eastern shore (C0-E2), from centre to northern shore (C0-N2), from centre to western shore (C0-W2), and from centre to southern shore (C0-S2). Similarly, four points were selected from the centre to shore of Lake Bolmen in four directions (Figure 10). The spectra were extracted from both MERIS and OLCI time series, at 1km and 300m equivalent pixel size, respectively. MERIS processing for LWLR is based on the Reduced Resolution satellite data archive because this has better global availability compared to the Full Resolution product. However, the reduced resolution may enhance adjacency effects.
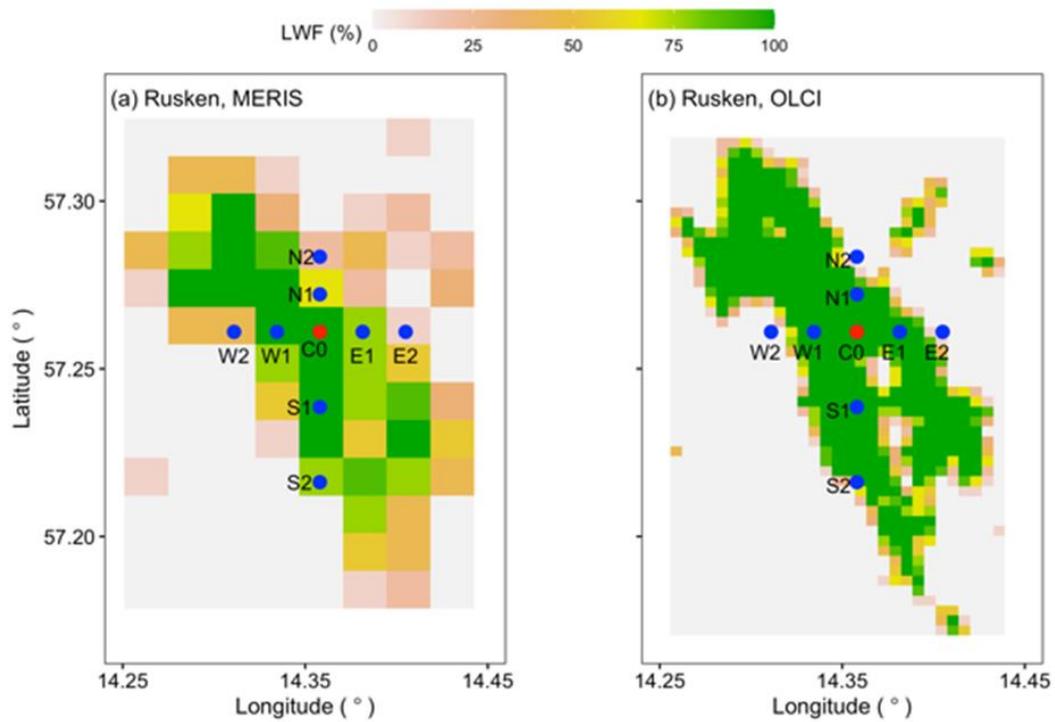
Figure 9 Locations for spectral analysis in Lake Rusken in the (a) MERIS and (b) OLCI imagery. Color indicates the land-water fraction (LWF) determined from a high-resolution land-water mask (which is not used in the standard processing).
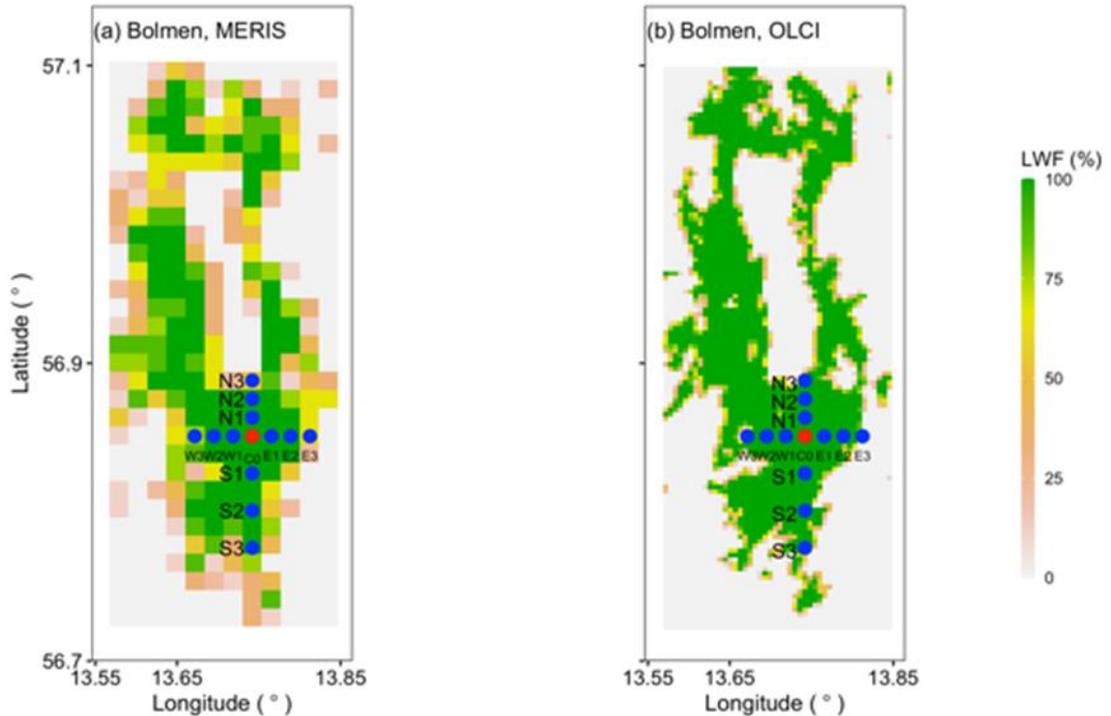
Figure 10 Locations for spectra analysis in Lake Bolmen for (a) MERIS and (b) OLCI imagery. Color indicates the land-water fraction (LWF) derived from a high-resolution land/water mask.

Figure 11 and Figure 12 show the water-leaving reflectance spectra extracted from lake centre to lake shore for Lake Rusken (from column 1 to 3). For Lake Rusken, it is shown that both spectral magnitude and spectral shape changes from lake centre to lake shore. In terms of spectral magnitude, the LWLR increases gradually from lake centre to lake shore, e.g. , from C0 to E2 in the east of Lake Rusken (Figure 11a-c). In terms of spectral shape, the reflectance decreases from visible bands to NIR bands in lake centre, and the reflectance in NIR bands is near zero (e.g. Figure 11a). Moving to the lake shore, the reflectance in NIR bands clearly increased (e.g., Figure 11c) as is expected from increased land reflectance represented in the mixed signal. These features were found in both MERIS and OLCI images.

The reflectance at the lake centre is lower in OLCI images (Figure 12) than that from MERIS images e.g. comparing Figure 11a with Figure 12a. The spectral shape at the lake shore in OLCI images is different when compared to the ones from MERIS images. OLCI data showed higher reflectance in NIR bands, e.g. comparing Figure 11c with Figure 12c.
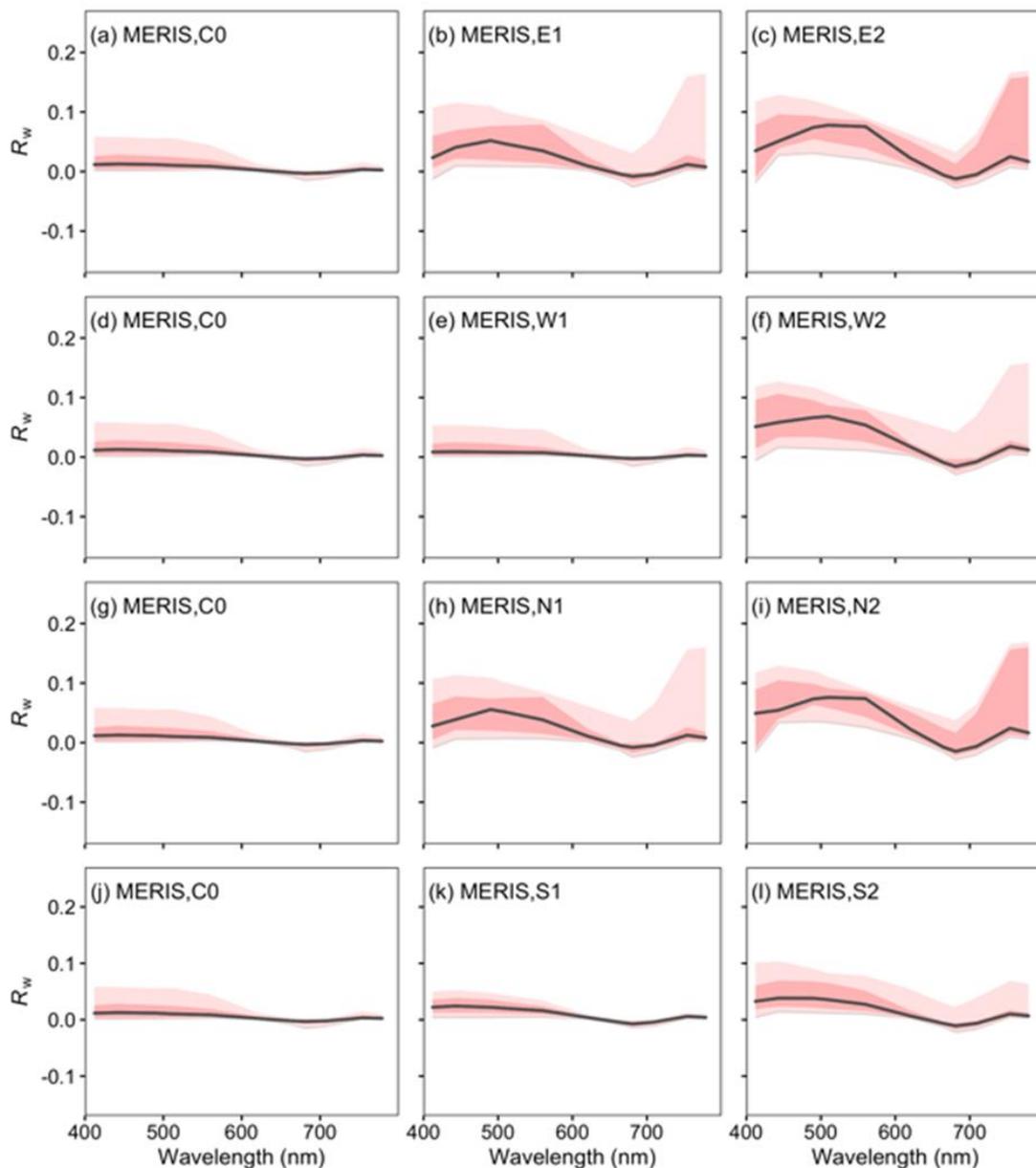
Figure 11 Statistics of MERIS spectra at the selected points in Lake Rusken. (a)-(c): eastern lake (C0-E2). (d)-(f): western lake (C0-W2). (g)-(i): northern lake (C0-N2). (j)-(l): southern lake (C0-S2). Black solid line represents median value, red area represents 25%-75% quantiles, and light red area represents 10%-90% quantiles.
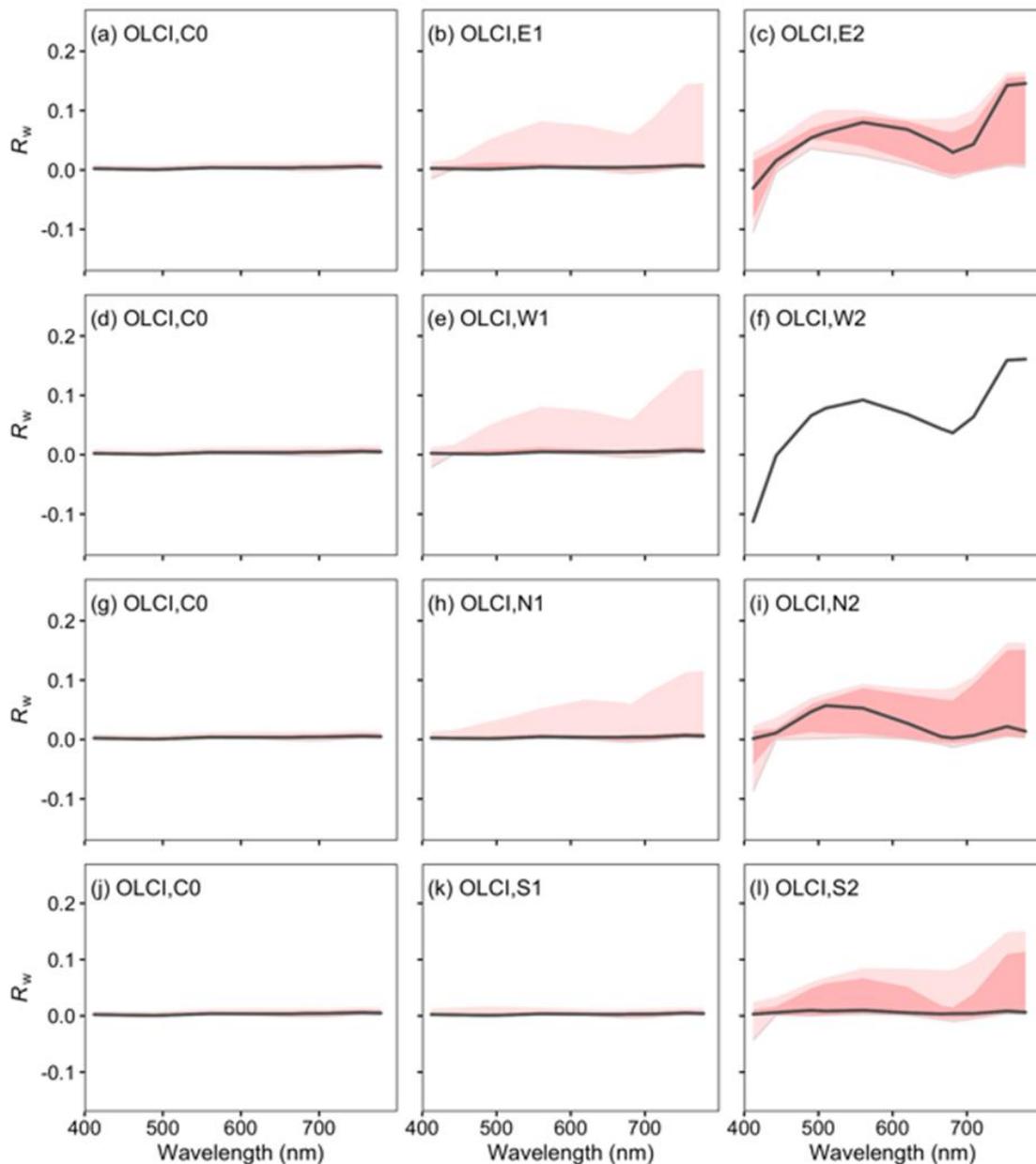
Figure 12 Statistics of OLCI spectra at the selected points in Lake Rusken. (a)-(c): eastern lake (C0-E2). (d)-(f): western lake (C0-W2). (g)-(i): northern lake (C0-N2). (j)-(l): southern lake (C0-S2). Black solid line represents median value, red area represents 25%-75% quantiles, and light red area represents 10%-90% quantiles.

Similar results were obtained from Lake Bolmen. For both MERIS and OLCI images, it is shown that spectral magnitude and spectral shape changes from lake centre to lake shore. Spectral magnitude increases from the lake centre to the lake shore, e.g, from C0 to E3 in the east of Lake Bolmen (Figure 13a-d). The spectral magnitude of the second point in each direction was typically still low in Lake Bolmen (i.e., E1, W1, N1 and S1 in Figure 13 and Figure 14). In terms of spectral shape, the reflectance value in NIR bands increased clearly from lake centre to shore, e.g. comparing Figure 13a with Figure 13d.

In contrast to results from Lake Rusken, the extracted spectra from MERIS and OLCI at the lake centre were all close to zero in Lake Bolmen (the adjacency effect was lower at the lake centre). However, when moving from lake centre to lake shore, spectra extracted from MERIS showed a stronger

adjacency effect than seen with OLCI. For example, spectra at point E2 showed high reflectance values with MERIS but low reflectance values from OLCI. In addition, the spectral shape at the lake shore in OLCI images was different to that in MERIS images, where OLCI showed higher reflectance in NIR bands, e.g. comparing Figure 13d with Figure 14d.

Comparing the spectra extracted at the lake shore, the spectral shape is similar between MERIS images in Lake Rusken and MERIS images in Lake Bolmen (Figure 11c, f, i, l, and Figure 13d, h, l, p), and the spectral shape is similar between OLCI images in Lake Rusken and OLCI images in Lake Bolmen as well (Figure 12c, f, i, l, and Figure 14d, h, l, p). This consistency in shape between lakes gives us the chance to identify those pixels influenced by adjacency effects using the spectral shape, described in the next section.
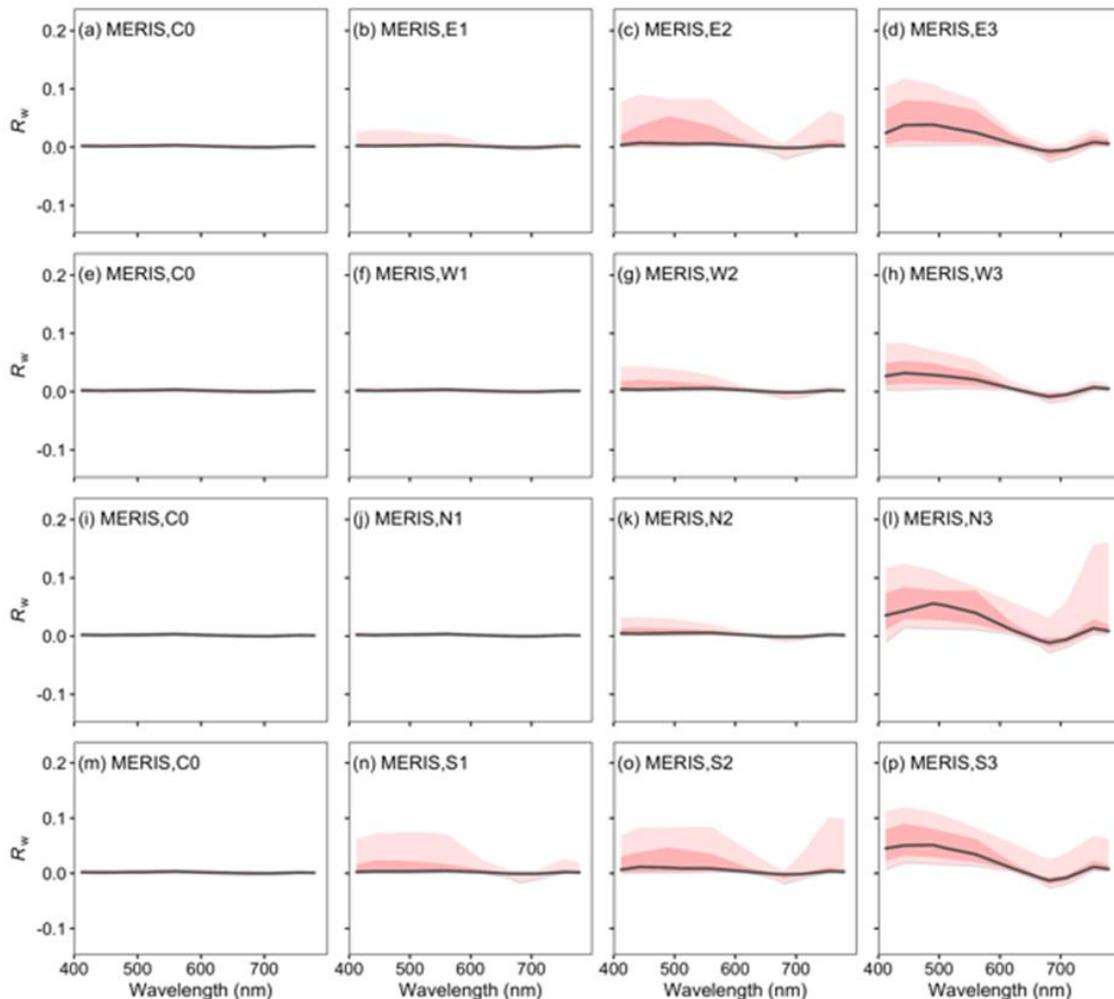

Figure 13 Statistics of MERIS spectra at the selected points in Lake Bolmen. (a)-(d): eastern lake (C0-E3). (e)-(h): western lake (C0-W3). (i)-(l): northern lake (C0-N3). (m)-(p): southern lake (C0-S3). Black solid line represents median value, red area represents 25%-75% quantiles, and light red area represents 10%-90% quantiles.
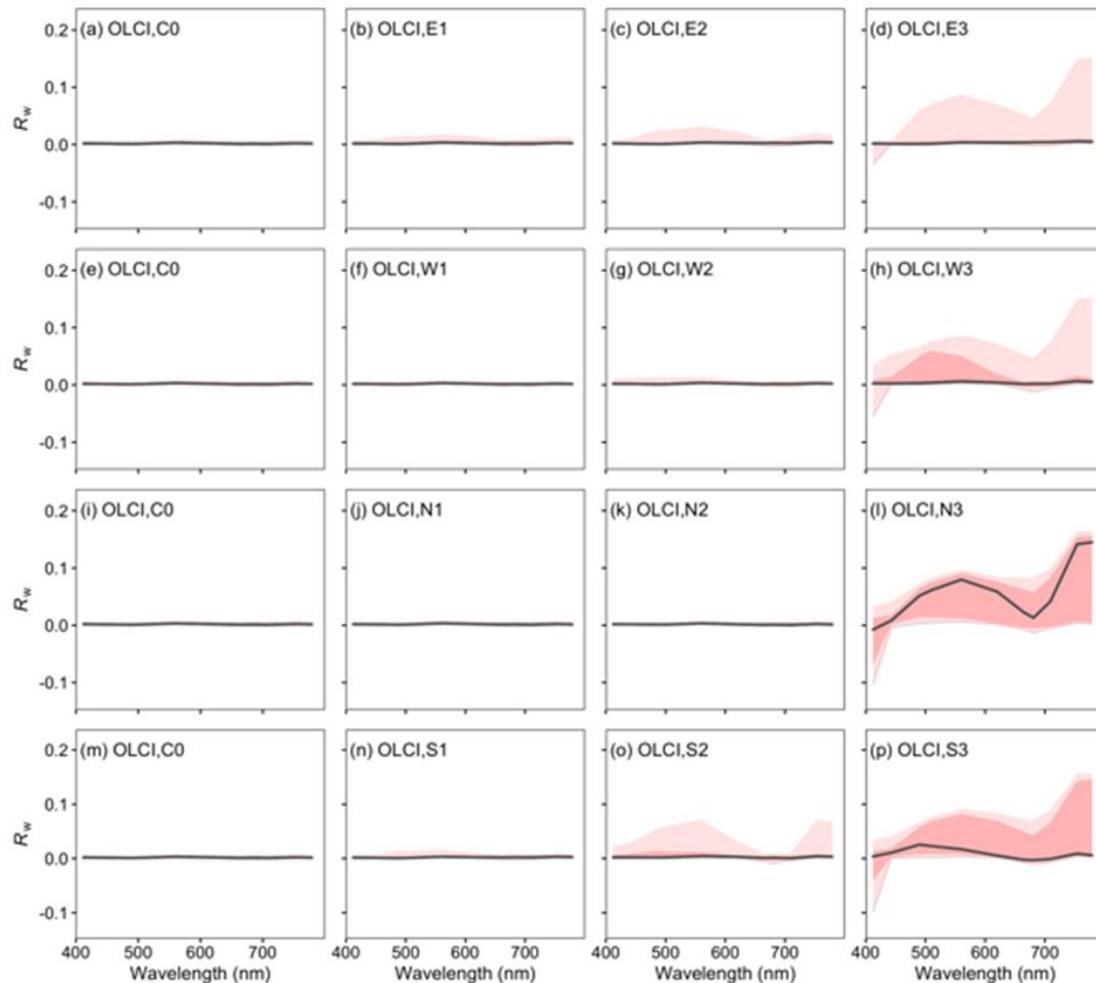
Figure 14 Statistics of OLCI spectra at the selected points in Lake Bolmen. (a)-(d): eastern lake (C0-E3). (e)-(h): western lake (C0-W3). (i)-(l): northern lake (C0-N3). (m)-(p): southern lake (C0-S3). Black solid line represents median value, red area represents 25%-75% quantiles, and light red area represents 10%-90% quantiles.

3.4 Parameterisation of POLYMER for OLCI processing

The Lakes_cci consistency team and the team of the use case for brownification have found that in some high-latitude lakes (typically those that are small and highly absorbing), Polymer-corrected MERIS Rw spectrum give consistent, fairly realistic results, whereas OLCI does not. Therefore, some further analyses, beyond the variable influence of adjacent land between sensor products, were performed to find a possible explanation for this inconsistency in Rw between MERIS and OLCI. The analysis focusses on the spectral bands used in the atmospheric correction using POLYMER for OLCI, the influence of the band selection is investigated with respect to spatial distribution of differences.

The current Polymer band settings for MERIS include bands: 412, 443, 490, 510, 560, 620, 665, 754, 779 and 865 nm. OLCI has the same default band selection as MERIS in Polymer v4.10 (and versions before that), which was adopted for the processing of LWLR products in Lakes_cci v1.0. For Polymer v4.11 and after, band 412 nm is removed for the OLCI in the default band configuration.

The tested parameterisations of Polymer for OLCI include the following:

Bands 412, 443, 490, 510, 560, 620, 665, 754, 779 and 865, hereafter labelled 'with 412 nm'

Bands 443, 490, 510, 560, 620, 665, 754, 779 and 865, hereafter labelled 'no 412 nm'

Bands 443, 490, 510, 560, 620, 665, 681, 754, 779 and 865, hereafter labelled 'add 681 nm'

This experiment was conducted in several lakes in Sweden including lakes Vättern (1888 km^2), Rusken (34 km^2), Glan (77 km^2) and Bolmen (184 km^2), among which Vättern is a large oligotrophic clear (deep) lake while the other three are particularly dark (strongly absorbing) lakes.

3.4.1 Spectral comparison of Polymer-corrected Rw for MERIS and OLCI

Figure 15 shows a spectral comparison of Polymer-corrected Rw with different band configurations for MERIS and OLCI in Lake Rusken. The spectra were extracted from the location indicated by the black triangle in Figure 15a for MERIS and OLCI during the time periods of 2009-2011 and 2017-2019, respectively. The spectral shapes of MERIS and OLCI Rw show different characteristics (Figure 15b): MERIS Rw was elevated in short wavebands, with a second peak between 700 and 800 nm and negative Rw in the red, suggesting over-correction for atmospheric effects. OLCI Rw spectra corrected using all the tested band configurations were generally low in short wavebands and gradually elevated in longer wavebands, which is not realistic for relatively clear (non-turbid) open water. There were no significant differences between the median Rw spectral for OLCI from different band settings (Figure 15). Similar results were found in another extracted location in Lake Rusken, which was further from the lake shore (Figure 16).
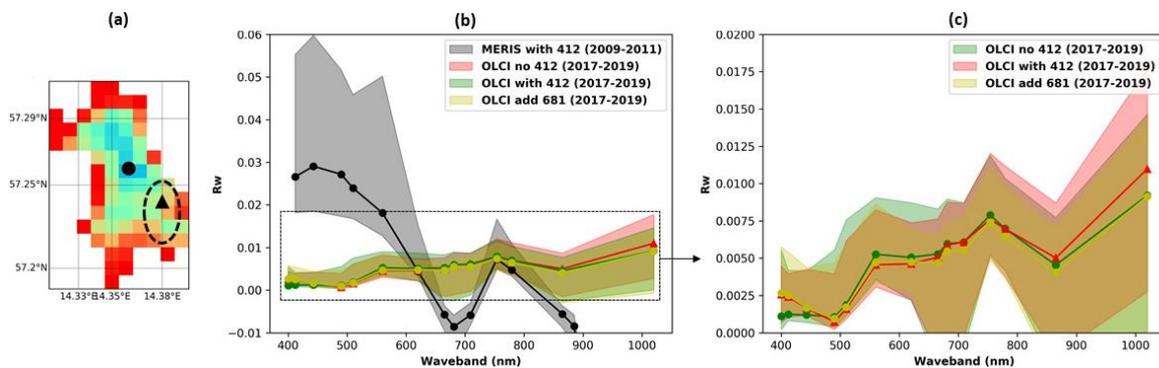
Figure 15 Spectral comparison of Polymer-corrected water-leaving reflectance (Rw) with different band configurations for MERIS (2009-2011) and OLCI (2017-2019) in Lake Rusken. (a) location of the extracted pixel, (b) spectral distribution for MERIS and OLCI and (c) highlight of the differences between different Polymer band configurations for OLCI. The central line shows the median value of each dataset. Upper and lower boundaries of the shaded areas are 20th and 80th percentiles, respectively.
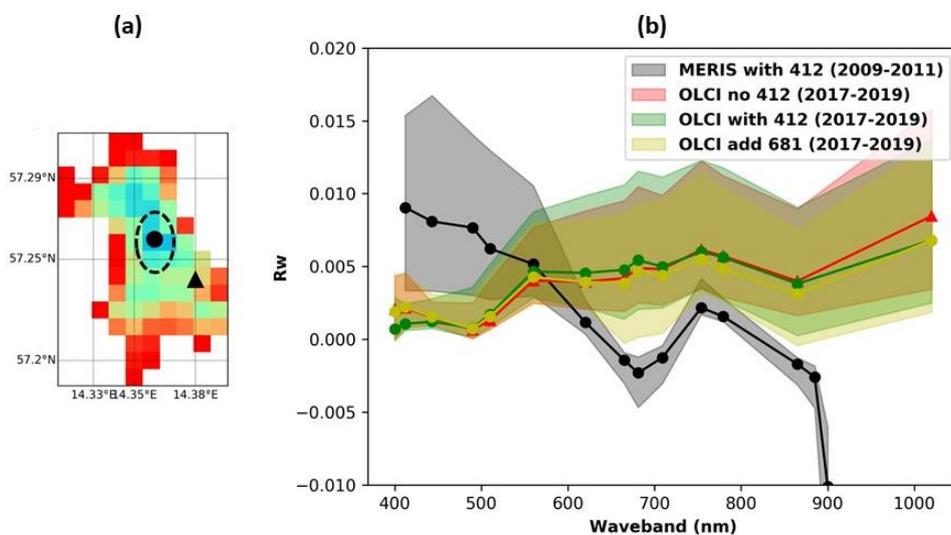
**Figure 16 Spectral comparison of Polymer-corrected water-leaving reflectance (Rw) with different band configurations for MERIS (2009-2011) and OLCI (2017-2019) in Lake Rusken. (a) location of the extracted pixel, (b) spectral distribution for MERIS and OLCI. Central line shows the median value. Upper and lower boundary are 20th and 80th percentiles, respectively.**

3.4.2 Spatial comparison of Polymer-corrected Rw for MERIS and OLCI

The spatial distribution of Rw 443, 665 and 865 nm for MERIS and OLCI is shown in Figure 17. The maps were calculated as yearly average of 2011 and 2017 for MERIS and OLCI, respectively. Rw at 443 nm for MERIS showed generally high values in the whole lake compared to other bands, with extremely high values observed close to lakeshores (Figure 17a). MERIS Rw at 665 nm was low across the whole lake and there was no clear spatial pattern (Figure 17b). While for band 865 nm, MERIS Rw show increasing trend from lake centre to shore, with extremely high values observed occasionally close to lakeshore (Figure 17c). Bands 443, 665 and 865 nm for OLCI corrected using 'no 412 nm' Polymer band setting show similar spatial pattern across the lake, with increasing values from lake centre to shore (Figure 17d, e and f). For OLCI Rw corrected using 'with 412 nm' Polymer band setting, band 443 nm elevated in regions close to lakeshore (Figure 17g) while bands 665 and 865 nm didn't show distinct spatial pattern (Figure 17h and i).
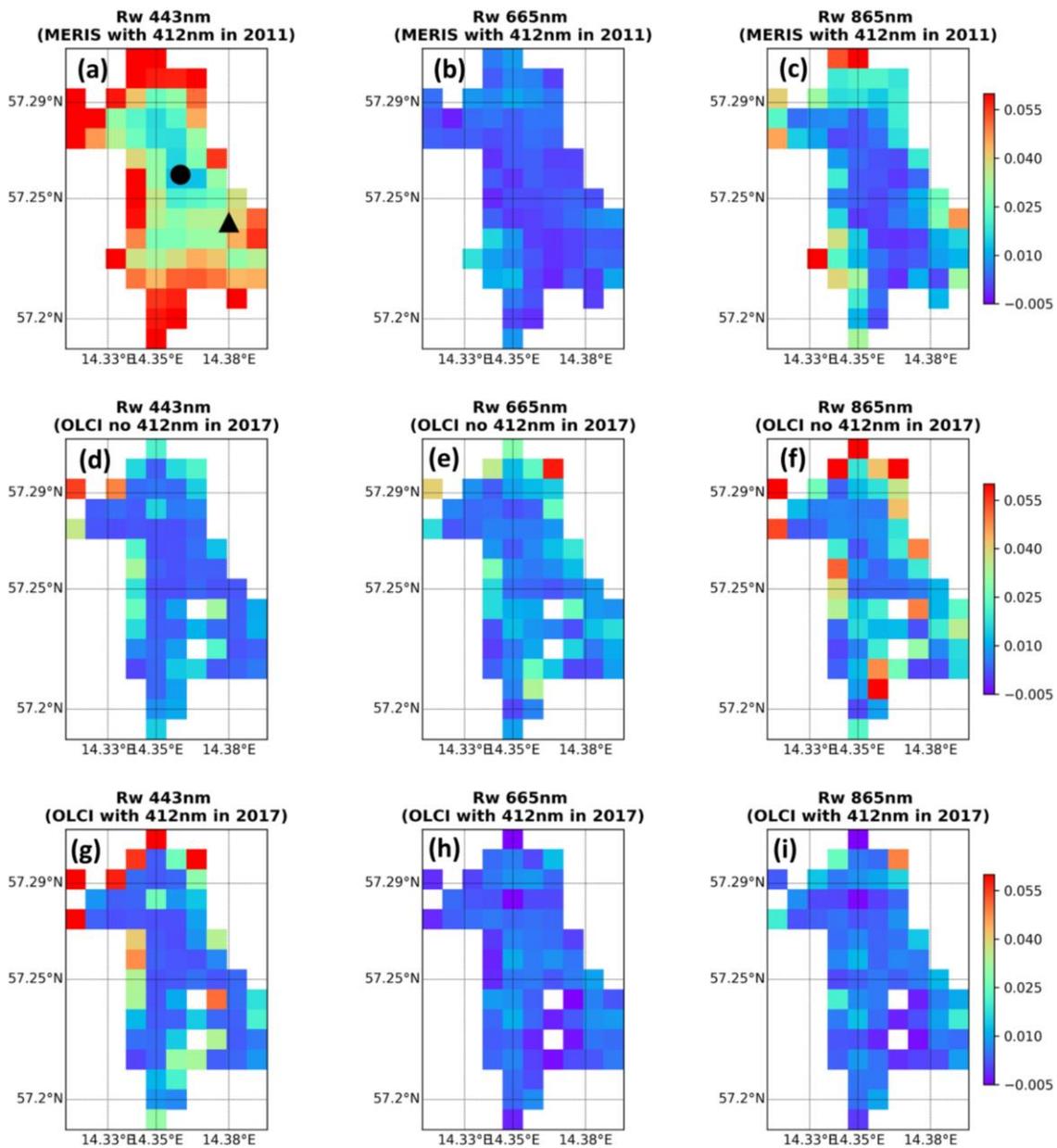
Figure 17 Spatial comparison of Polymer-corrected water-leaving reflectance (Rw) from MERIS and OLCI data in Lake Rusken for bands 443, 665 and 865 nm. The maps were averaged in year 2011 and 2017 for MERIS and OLCI, respectively.

3.4.3 Spectral comparison of Polymer-corrected Rw between MERIS and OLCI in other high-latitude lakes

MERIS and OLCI Rw spectra corrected using the same Polymer band settings were compared in lake centres of Vättern, Glan and Bolmen. The spectra include all the satellite observations extracted from the labelled location during the periods of 2009-2011 and 2017-2019 for MERIS and OLCI, respectively (Figure 29Figure 18a, b and c). The spectral shape of Rw for lakes Vättern generally matches between MERIS and OLCI, both showing typical clear water reflectance features with high reflectance at shorter wavelengths and low reflectance values in the red region of the spectra, similar to clear oceanic waters (Figure 18a'). In lake Glan, MERIS and OLCI Rw are also showing good agreement in terms of spectral shape (Figure 18b'). While in lake Bolmen, the MERIS and OLCI Rw spectra are showing different pattern, likely due to the fact that the extracted location in this lake is close to lakeshore, therefore introducing strong adjacency effect by land (Figure 18c').
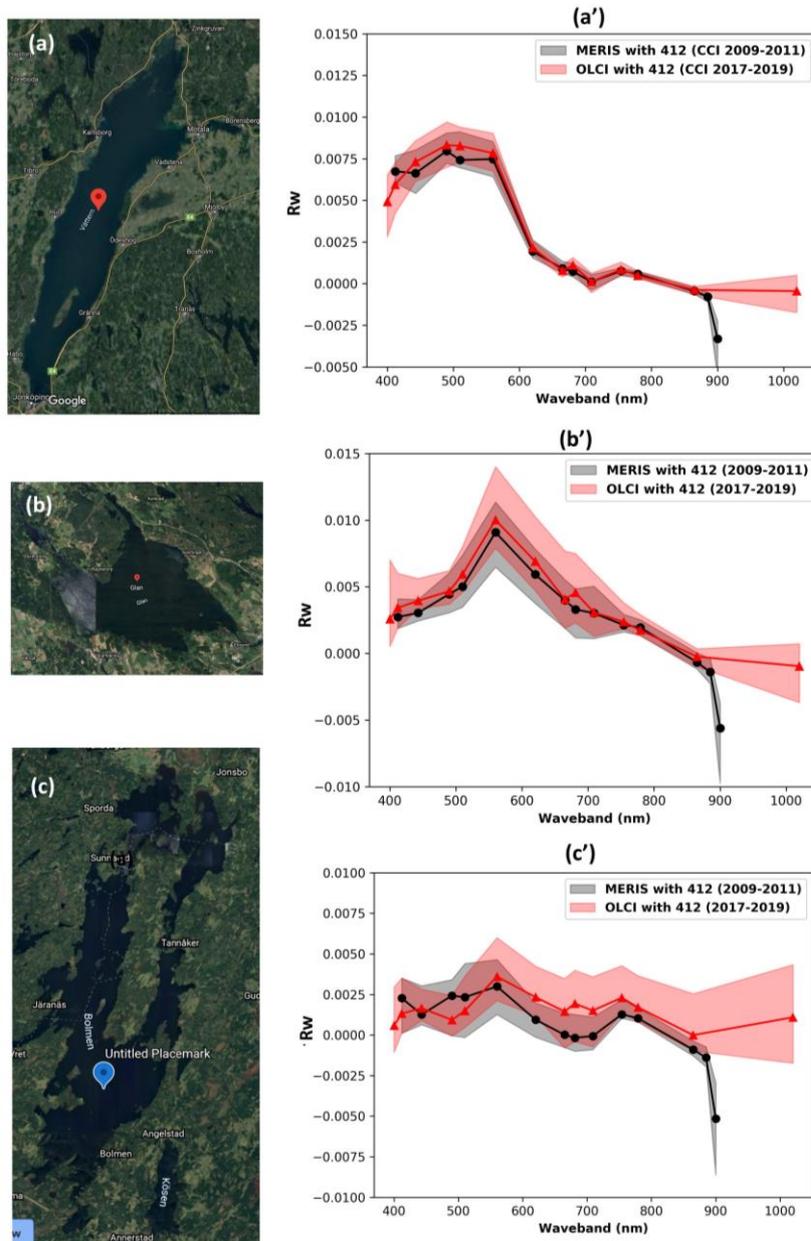
Figure 18 Extracted locations and spectral comparison of Polymer-corrected Rw in lakes (a and a') Vättern, (b and b') Glan and (c and c') Bolmen, for MERIS (2009-2011) and OLCI (2017-2019). Central line shows the median value. Upper and lower boundary are 20th and 80th percentiles, respectively.

3.4.4 Conclusions

Based on this brief analysis, we find that small highly absorbing lakes (Lake Rusken) with high absorption by CDOM are more likely to result in unrealistic LWLR spectra, whereas the different selection of bands to optimize the atmospheric correction procedure is not a key factors for the inconsistency between MERIS and OLCI products. At lake centres that are distant from the lake shore, which are less impacted by land adjacency (e.g., Lake Glan and Lake Vättern), the spectral shape of Rw matched between MERIS and OLCI. Therefore, the inconsistency in Rw between MERIS and OLCI in small high-absorbing lakes (e.g., Lake Rusken and Lake Bolmen) are expected to be mainly introduced by the differences in responses of the two sensors to land adjacency effect (both from lakeshore and small islands). In case of MERIS, this initially resulted in presumedly realistic spectral shapes (and therefore, lake Colour observed in the brownification use case), but on closer inspection these turned out to have negative reflectance, suggesting over-correction of atmospheric effects, likely caused by adjacent land. It remains curious that these results cannot be replicated using OLCI even when the same band selection is applied.

4   Solutions

Based on the analyses described in chapter 3, these results were translated into improved flagging of suspect observations, by introduction of new OWTs (sections 4.1) and by multi-variate filtering (section 4.2).

4.1   Enhancement of Optical water type classification

Spatial inconsistencies in lake colour derived from subsequent optical sensors was observed and reported within the Brownification use case in the Lakes_cci project. Further analyses into potential causes were performed within the consistency analysis presented here (see section 3.3). As a result, two additional OWT classes are proposed which identify the variable influence of adjacent land on the atmospherically corrected LWLR. For this analysis, a limited set of lakes was considered using the full spatiotemporal detail available in the L2 intermediary LWLR data set.

4.1.1   Identification of new OWTs

Based on the analysis of spectra from the lake centre to the shore in section 3.3, it is evident that the elevated in NIR bands may be exploited to capture the adjacency effect in affected observations. The high reflectance in NIR bands is most likely caused by reflectance from vegetated land pixels

To identify the general shape of pixels which influenced by adjacency effects, the spectra of those pixels which land-water fraction between 0-100% were extracted from all available MERIS and OLCI products for both Lake Rusken and Lake Bolmen. The extracted spectra from all available MERIS images and all available OLCI images were firstly standardized using the method in Spyrakos et al. (2018), and then statistical analysis was carried out for each band. The median value of the standardized spectra from MERIS and OLCI images were labelled OWT-14 and OWT-15 respectively, as an extension of the 13 OWTs identified in Spyrakos et al. (2018). Because OWT-14 and OWT-15 were identified from adjacency effects influenced pixels, they will be used to quantify adjacency effects in MERIS and OLCI images.

Figure 19 shows the identified OWT-14 and OWT-15 from MERIS and OLCI images respectively (solid black lines), both OWT-14 and OWT-15 shows high reflectance in NIR bands.
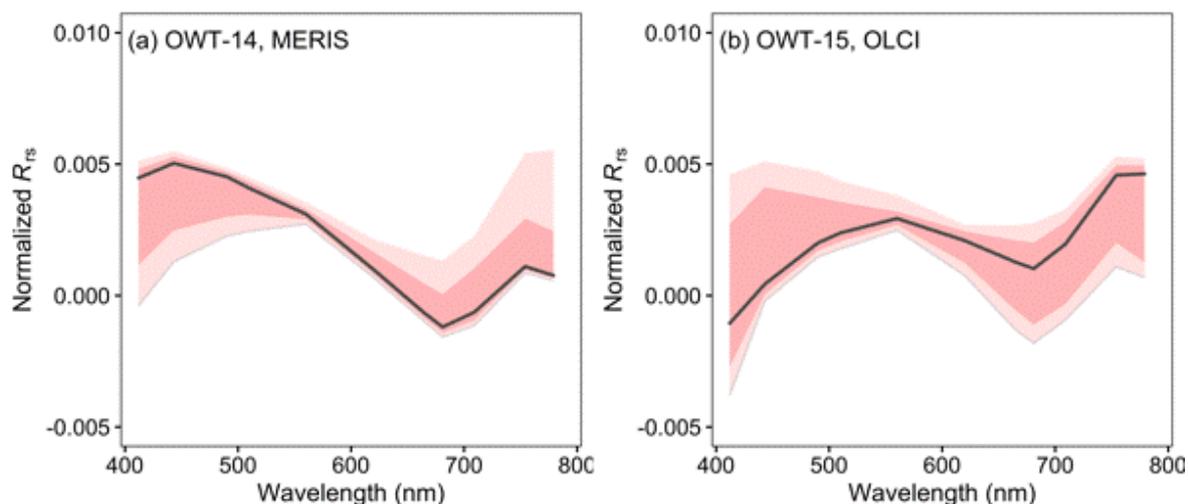
Figure 19 Identified new OWTs for flagging adjacency effects. Left: OWT-14 identified from MERIS images (solid black line). Right: OWT-15 identified from OLCI images (solid black line).

4.1.2 Application of the new OWTs

The identified OWT-14 and OWT-15 were applied to MERIS and OLCI imagery of Lake Rusken and Bolmen to check their performance in adjacency effects flagging. The framework of the adjacency effects flagging is: (1) for a given pixel, the spectrum of this pixel is standardized using the method in Spyrakos et al. (2018); (2) the spectral angle (α) between the 15 OWTs and the standardized pixel spectrum is calculated, and the OWT membership score is defined as $S_{OWT} = 1-\alpha/\pi$; (3) the OWT which has maximum S_{OWT} is identified as the dominant OWT of the observation. When OWT-14 or OWT-15 is identified as dominant the observation is considered significantly affected by adjacent land. In all other cases, the pixel is treated as water. More quality-control classes could be added in this way in future.

This method was first applied to all available MERIS and OLCI images of Lake Rusken and Bolmen, to explore their usefulness in adjacency effects flagging in the area where it was first observed to be a problem in the CRDP v1.0. Figure 20 shows the identified OWTs from OLCI image on May 3rd, 2016 in Lake Rusken and Bolmen. Pixels identified as water (OWT1-13 dominant) are shown in blue and pixels identified as OWT-14 or OWT-15 are shown in red. Pixels along the lake shore are consistently identified as OWT-14 or OWT-15. Pixels in the lake centre were generally identified as OWT1-13 and less likely influenced by adjacency effects.
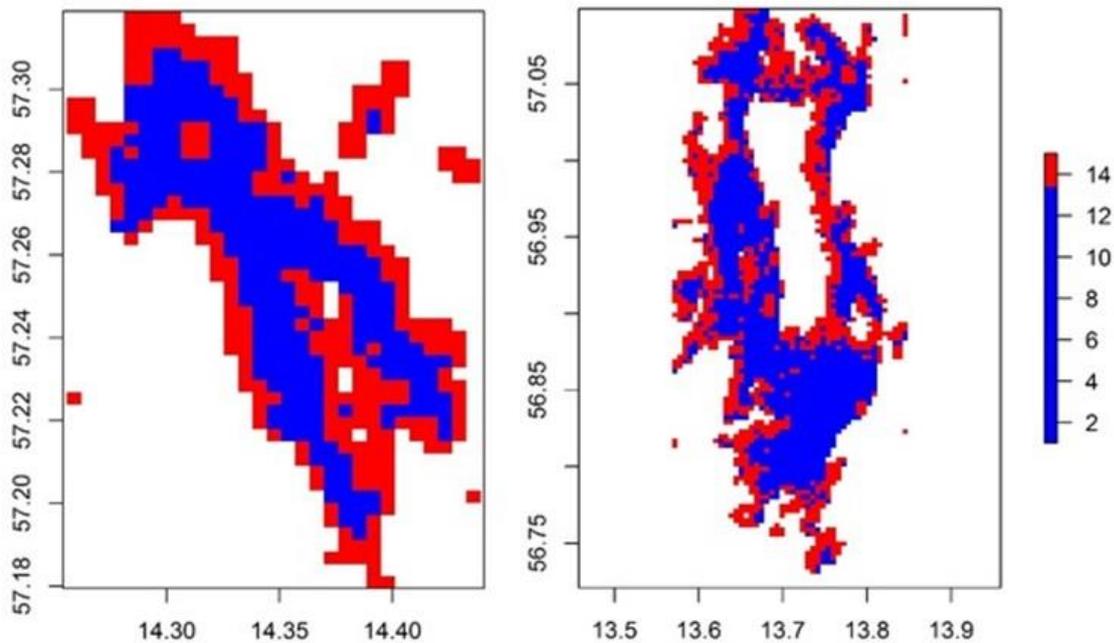
Figure 20 Example of identified OWTs in Lake Rusken and Bolmen and adjacent water bodies in the L2 intermediary LWLR product. Red pixels are identified as OWT-14 or OWT-15, blue pixels are identified as one of the non-affected water types (OWT1-13). Left: OWTs in Lake Rusken, OLCI image on May 3rd, 2016. Right: OWTs in Lake Bolmen, OLCI image on May 3rd, 2016.

To clearly show the spatial distribution of adjacency effects in the lake, an adjacency effect intensity (AEI) index was calculated for MERIS and OLCI images in Lake Rusken and Bolmen. For a given pixel, AEI is defined as the ratio between the number of images identified as OWT-14 or OWT-15 and the number of all valid images. Therefore, a high AEI value means this pixel is highly influenced by adjacency effects, and a low AEI value means this pixel has small impacts from adjacency effects. In theory, for a lake, the pixels along shoreline would have high AEI values, and the pixels in the centre of a lake would have low AEI values.

Figure 21 and Figure 22 show the AEI values calculated from all available MERIS and OLCI images respectively in Lake Rusken and Lake Bolmen, respectively. In terms of spatial distribution, it is clear that the AEI value in the lake centre is consistently lowest, the AEI values increased gradually from lake centre to lake shore, and the highest AEI values are those pixels along the shore of the lake or the islands. The larger Lake Bolmen shows lower AEI in the lake centre. Comparing the AEI values from MERIS with those from OLCI, it can be seen that the AEI values from MERIS are higher than from OLCI, especially in the lake centre. A potential reason is the lower spatial resolution of MERIS RR, such that one pixel will cover a wider area compared with OLCI and has a higher possibility to include reflectance from nearby land pixels. However, other observation effects, or differences between sensors in the ability of the atmospheric correction procedure to work out the water reflectance, cannot be ruled out.
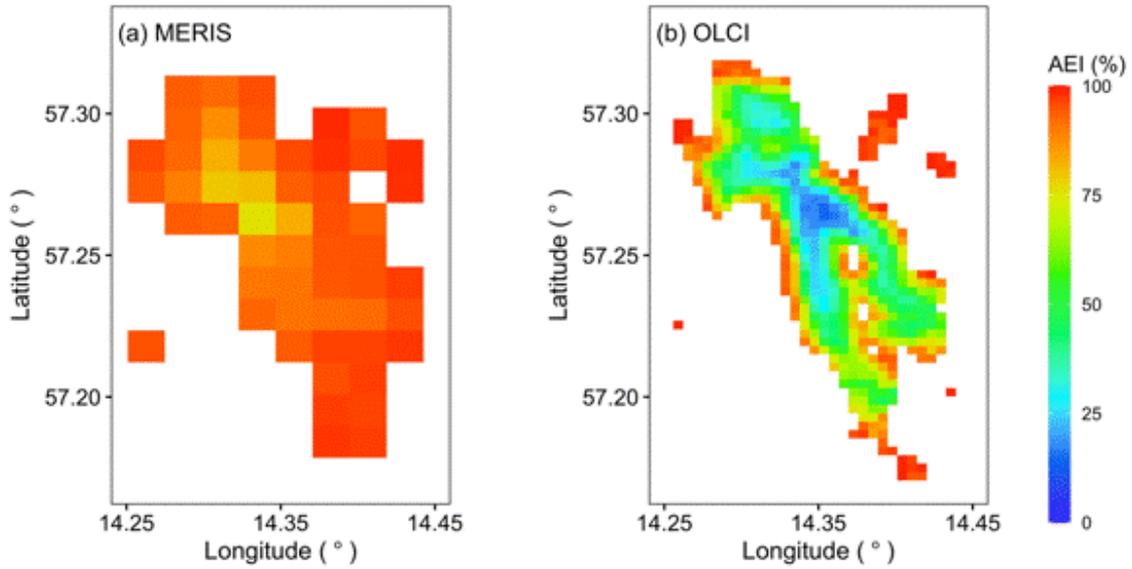
Figure 21 Adjacency effect intensity maps for Lake Rusken. (a) from MERIS. (b) from OLCI.
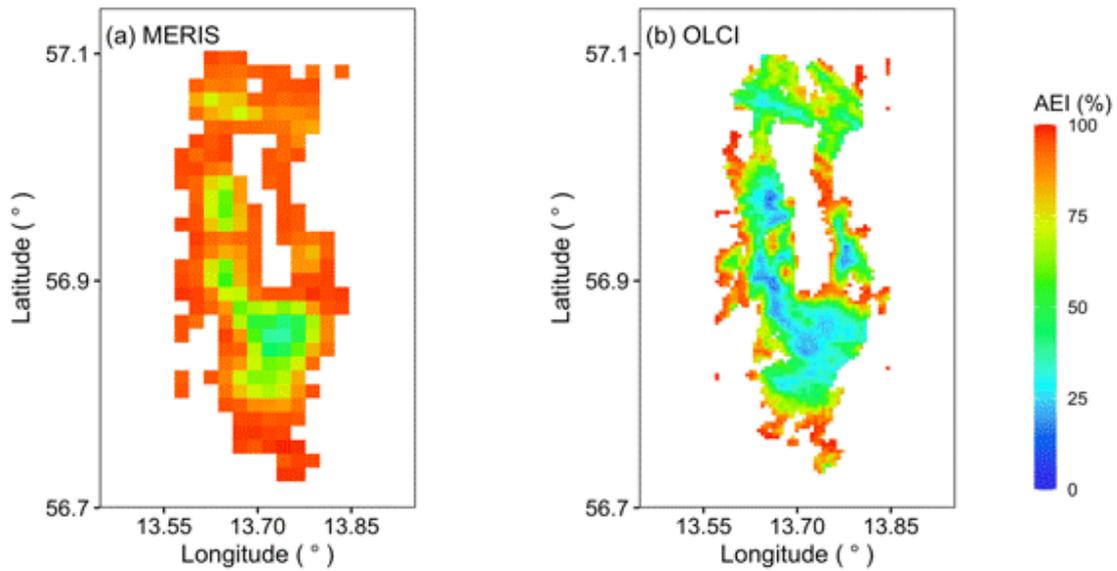
Figure 22 Adjacency effect intensity maps for Lake Bolmen. (a) from MERIS. (b) from OLCI.

To study the applicability of the new OWTs in adjacency effects flagging, the new OWTs based adjacency flagging method was applied to another two lakes in Sweden, Lake östra Ringsjön and Lake Ivösjön, these are independent cases not used in the development of the added OWTs.

Lake östra Ringsjön and Lake Ivösjön are small lakes, with a similar water area as Lake Rusken. The Adjacency effects flagging results in those two lakes are shown in Figure 23 and Figure 24, it is clearly shown that the AEI values increase from lake centre to lake shore in both lakes, and the AEI values from MERIS image are higher than that from OLCI image. Those results are consistent with the adjacency effects flagging results in Lake Rusken and Bolmen, which indicate the identified new OWTs can likely be extended to other lakes.
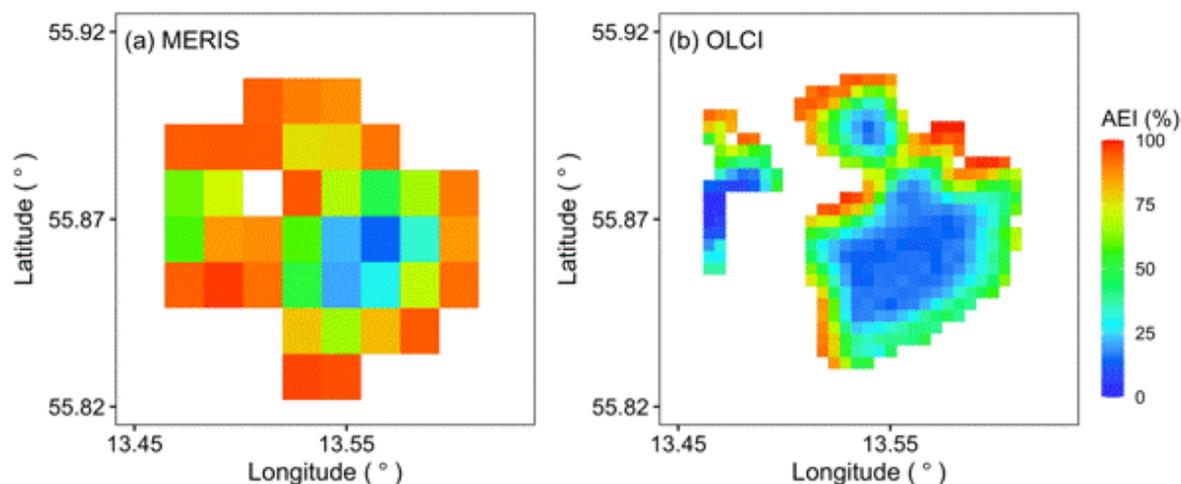
Figure 23 Adjacency effect intensity maps for Lake Oestra Ringsjoen. (a) from MERIS. (b) from OLCI.
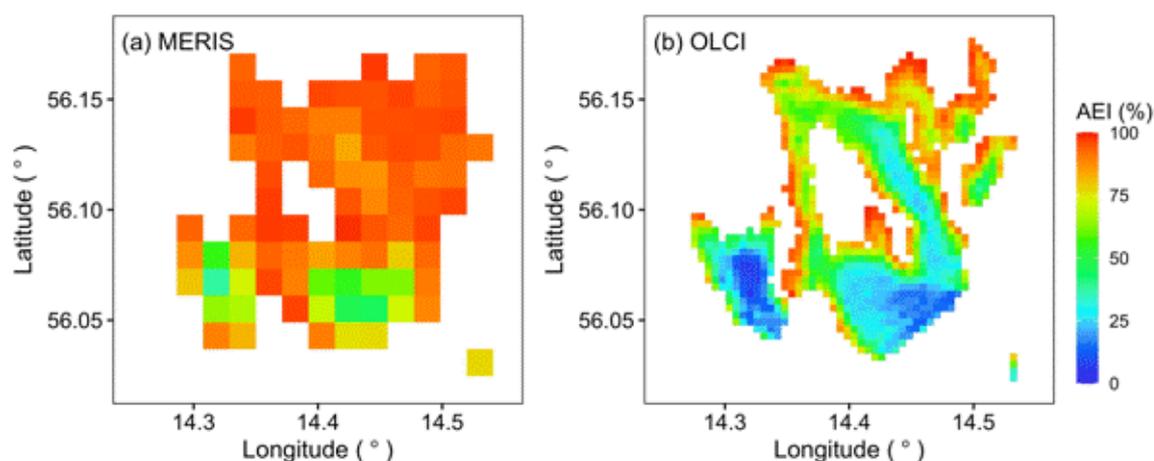
Figure 24: Adjacency effect intensity maps for Lake Ivoesjoen. (a) from MERIS. (b) from OLCI.

Further application of the new OWT classes and the effects of flagging are described in section 4.1.

4.1.3 Summary

Two new OWTs (OWT-14 and OWT-15) were identified from MERIS and OLCI images based on data from small lakes in high latitudes. The analysis and results in this section indicate that the new OWTs could be integrated in the data processing chain to identify pixels which are influenced by adjacency effects.

4.2 Multivariate filtering based on climatologies

As shown in section 3.2, ice flagging in several thematic variables and especially in LWLR products needs improvement. Undetected ice observations by the LWLR quality flagging can strongly affect algorithms that derive biogeochemical products (e.g. lead to high turbidity values), which distort daily average observations in the time series of all LWLR products and thus the interpretation of climate trends. As shown, the information from the LSWT products can help identify undetected ice pixels in the LWLR products. We propose here an approach using LSWT climatologies for filtering and

thus a method to take advantage of the synoptic datasets, without relying on coincident observations. The procedure is described in this section and illustrated in Figure 25.

From the Lake CCI CRPD v1.0 (daily, global L3S at 1km spatial resolution), data of initially 250 lakes were extracted. The LWLR and LSWT variables were extracted as daily median and standard deviation per lake. For LSWT the data were filtered based on the provided quality flag. Daily median and standard deviation were calculated per lake and quality class.

For 239 of 250 lakes, an LSWT temperature climatology could be derived. For the Caspian Sea and ten smaller lakes no LSWT product has been computed. Caspian Sea was removed from CRDP due to computing consumption and the smaller lakes lacked sufficient quality due to their size/shape.
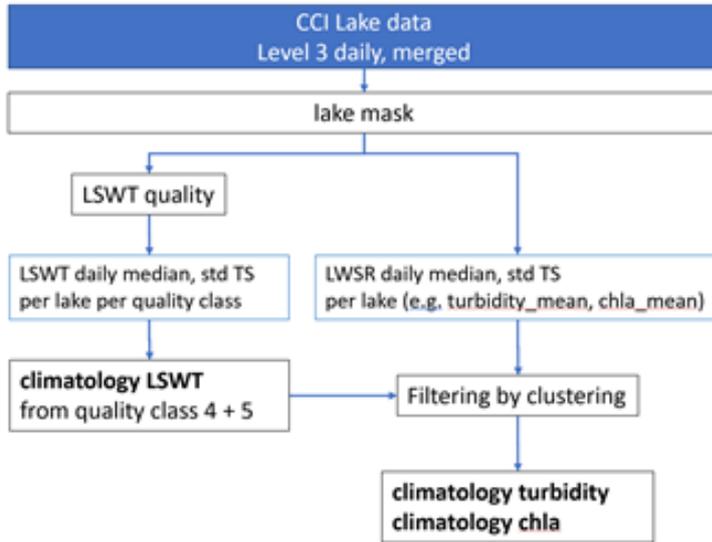
Figure 25 Overview of data extraction and dependencies for calculation of climatologies.

4.2.1 Climatology of lake surface water temperature

Temperature data were collected for the complete time period (1992-2019) and with good consistency within the v1.0 L3S product.

The LSWT data are provided with a categorical quality flag, ranging in value from 0 to 5, which translates into no data, bad data, worst quality, low, acceptable and best quality. Only temperature measurements with quality 4 and 5 were considered to derive lake climatologies. For data of each quality level the daily median and the standard deviation per lake was determined independently (see classification-based extractions of daily averages, section 2.4). These time series of quality 4 and 5 were used to derive the weighted localized mean per DOY, which is our temperature climatology.

The standard deviation of temperature values in a lake on a specific day was transformed into weights for the localized averaging. Days with a smaller standard deviation represent the entire lake temperature LSWT in a better way than days with more spatial variability and higher standard deviation. Therefore, the weights w for a daily average of quality $q \in \{4, 5\}$ are defined as:

$$w_{min} = \min\left(sd(LSWT(q,t))\right)$$

$$w_{max} = \max\left(sd(LSWT(q,t))\right)$$

$$w(q,t) = 1 - \frac{sd(LSWT(q,t)) - w_{min}}{w_{max} - w_{min}}$$

where the minimum and maximum of the standard deviation (w_{min}, w_{max}) were determined from all time steps t and both quality categories included.

To model the annual cycle of temperature values properly, locally weighted means over a 40-day span (-20 / +20 days) were used and sequences at the start and end of the year were duplicated to extend the series by -20 and +20 days.

For each day-of-year (*doy*), data within the span of the time window were selected and their weighted mean calculated. The underlying LSWT observations consist of the daily median observations of quality 4 and 5 combined. Using the weights as defined above, the climatological temperature of the *doy* and a weighted standard deviation to this climatological value were then calculated as:

$$T_{clim}(doy) = \frac{\sum w(|t-20| \le doy) * T(|t-20| \le doy)}{\sum w(|t-20| \le doy)}$$

$$wsd(T_{clim}(doy)) = \sqrt{\frac{\sum w(|t-20| \le doy) * \left(T(|t-20| \le doy) - T_{clim}(doy)\right)^2}{\sum w(|t-20| \le doy)}}$$

In most cases, the LSWT climatology derived with this approach is a smooth function of time (see Figure 26). For the Aral Sea (Lake ID GLWD00000004) LSWT data can be gathered throughout the year, so that the climatological annual cycle extends over the full period. For other lakes with long periods of ice cover, temperature observations are not contiguous, and the climatological annual cycle will have gaps (Lake Amadjuak, ID GLWD00000056).
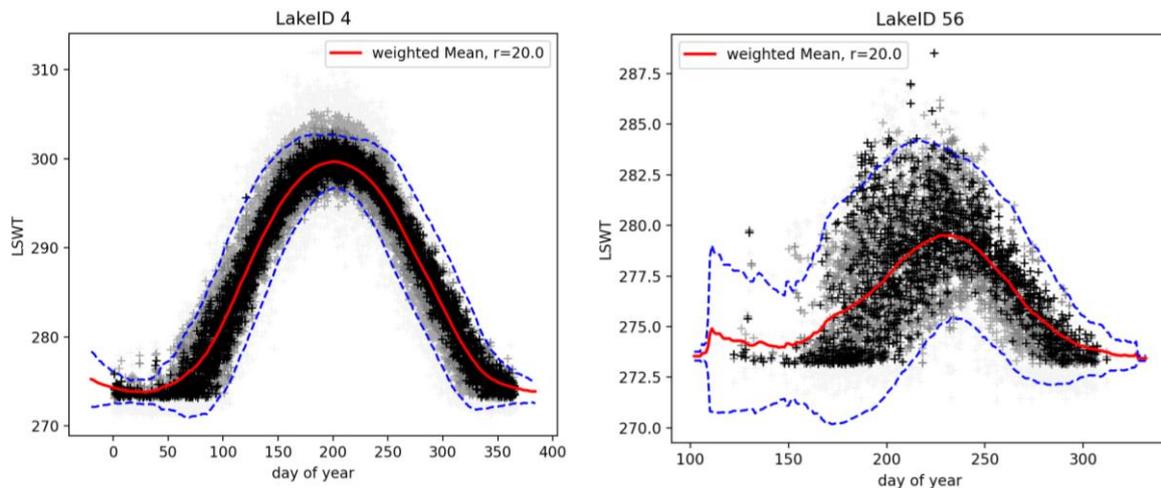
Figure 26 LSWT daily median per lake and quality class, and LSWT climatology as weighted localized mean. The quality class is represented by colour, light greys are omitted from the climatology calculation (poor quality), darker greys and black are the basis of the climatology (best quality). Examples are from Aral Sea (left, lake ID GLWD00000004) and lake Amadjuak (right, lake ID GLWD00000056) The climatological annual cycle is shown as a red line with two times the localized standard deviation indicated by blue dashed lines.

For filtering undetected ice from the optical data with the help of LSWT, the climatologies require gap filling. If there are fewer than 20 observations within the span of 40 days, the climatology value is not used. If the median LSWT in the climatology is below 276K during such a gap, it is filled with a value of 273.15K. Only days of the year with a low number of observations are considered in the gap filling, although it may be reasonable to extend it to all days within the respective winter. E.g., for Lake Amadjuak it would be a sound choice, as the LIC classification and the LSWT data (and its general position on higher latitudes on the Northern Hemisphere) suggest an extended winter period with persistent ice cover.

4.2.2 Threshold-filtering informed by climatologies - Turbidity

The LWLR processing contains a dedicated pixel identification procedure to retain only observations of water, but inconsistencies remain and are now understood to benefit from incorporating the additional thermal observations and/or additional optical sensors. In particular, the classification of ice in the LWLR is insufficient: shallow areas with bottom reflection can be marked as ice and melting ice is often misclassified leading to distorted of turbidity and chlorophyll-a concentration trends.

Pixels classified as non-water in the LWLR are not atmospherically corrected and therefore excluded from any further analysis. This means that false negatives cannot be identified here. In the time series of turbidity vs day-of-year, unrealistically high turbidity values are sometimes observed during winter. While some regions are already flagged as ice-covered and thus removed, others (possibly submerged ice, sub-pixel ice cover, or melting ice) are not excluded in the same manner, leading to these erroneous results. Using the temperature climatology, these omissions can be better identified and filtered out before calculating a climatology, or even excluded from the L3S product in future. Overall, a representative climatological annual cycle and its variance are a good starting point to flag suspicious data points in a time series. In particular, the daily median values per lake of the respective variable can be filtered with the climatological information, but it may take more effort to provide a good set of thresholds as an annual cycle for unaggregated spatial data.

The general idea is, that if water temperatures are close to freezing point, the probability that a large turbidity value arises from undetected ice is high. By clustering the turbidity (or chl-a concentration) and the climatological LSWT using the BIRCH (Balanced Iterative Reducing and Clustering using Hierarchies) clustering method (Zhang et al. 1996, 1997), outliers and potential ice cluster can be separated from valid data.

Filtering by clustering the turbidity values with LSWT climatologies follows these steps:

- BIRCH clustering (median turbidity, LSWT climatology) with n clusters (here: n=4).
- Determine cluster centre (median LSWT and median turbidity), then sort cluster centres by turbidity.
- Start with cluster of highest turbidity value, work through clusters with decreasing turbidity values. Adjust threshold to minimum turbidity of dedicated cluster (start value = 0).

From the CRDP v1 these empirical thresholds and conditions have been derived for 250 lakes. The procedure is illustrated in Figure 27 and contains the following criteria:

- If a cluster has a population which is smaller than the ratio of the total number of observations (N) and the number of clusters, it is checked for further conditions. A large cluster size means that the data points can represent a common feature of the data set. If the cluster with the highest turbidity value is already large, high values do not count as outliers and the filtering procedure is stopped. We note that this first step in the decision tree is omitted in the chlorophyll-*a* filtering, as larger clusters of high values are more common.
- If a cluster centre temperature is lower than 285K and turbidity is lower than 20, the filtering proceeds. Otherwise, it is stopped.
- If the number of points in a cluster is smaller than 20, the cluster is likely to consist entirely of outliers, which are marked as such. The acceptable maximum turbidity threshold is set to the minimum turbidity value in this cluster. The threshold cluster size of 20 is currently selected arbitrarily.
- If the cluster is larger than 20 points, it is checked, whether the cluster centre temperature is below 277K and turbidity is above 10. If this is the case, the cluster likely represents undetected ice, and each point is marked as such. Again, the acceptable maximum turbidity threshold is adjusted to the turbidity minimum of this cluster. If the condition is not true, the search is stopped at this point.
- If the search has not been stopped before and reaches a point, where invalid flag and acceptable maximum turbidity threshold is set, the procedure returns to the first step in the decision tree starting with the next cluster in line.

If the acceptable maximum turbidity threshold is greater than zero (start value), it has been adjusted during the described decision flow chart. This threshold value can now be used to filter turbidity observations within periods not covered by the LSWT climatology and therefore not

included in this approach. Gaps in LSWT climatology occur primarily due to ice coverage or due to cloudiness in tropical summer or rainfall period.
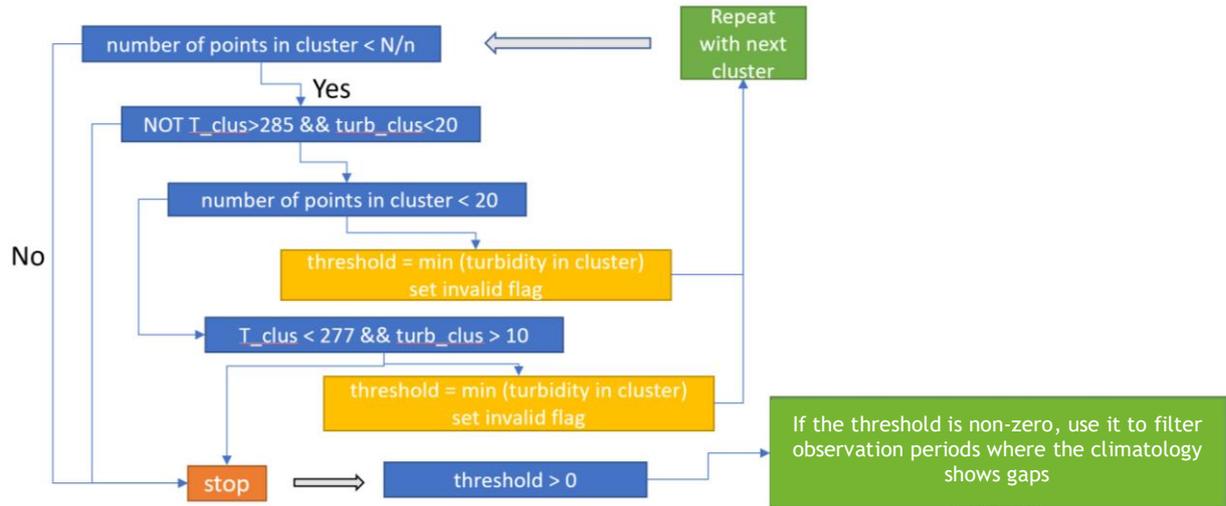

Figure 27 Turbidity filtering by clustering. Decision tree is starting with the cluster with highest turbidity centre.

4.2.2.1 Example 1 – Aral Sea, GLWD00000004

The LIC v1.0 product for the Aral Sea previously showed that strong silt accumulation and changes in lake level and extent, likely including frequent large mixed land/water observations, can lead to misclassifications. The revision of the LIC product in version 1.1 improved the issue of too many ice observations. The combined observations of LIC, LSWT and LWLR (Figure 4) already raised the expectation, that the flagging of the LWLR product is also affected.

The turbidity time series (particularly for MERIS data, Figure 28) shows data points with very high turbidity during winter. The OLCI period has high values of turbidity as well, but they are not clustered in winter months but scattered throughout the year. The clustering of LSWT climatology values and turbidity suggests, that one cluster with high turbidity and low temperature most likely represents undetected ice and should therefore be removed (green points). The silting of the Aral Sea creates a difficult example: the second highest turbidity cluster likely originates from mixed land/water pixels rather than ice cover (higher temperatures exclude this option). These high turbidity values are filtered out using the multi-variate clustering approach. They correspond to low numbers of observations in the daily average (Figure 29), indicating that the pixel identification in the LWLR product generally works and the improvement applied here should be preferred over a systematic re-training of the pixel classifier.
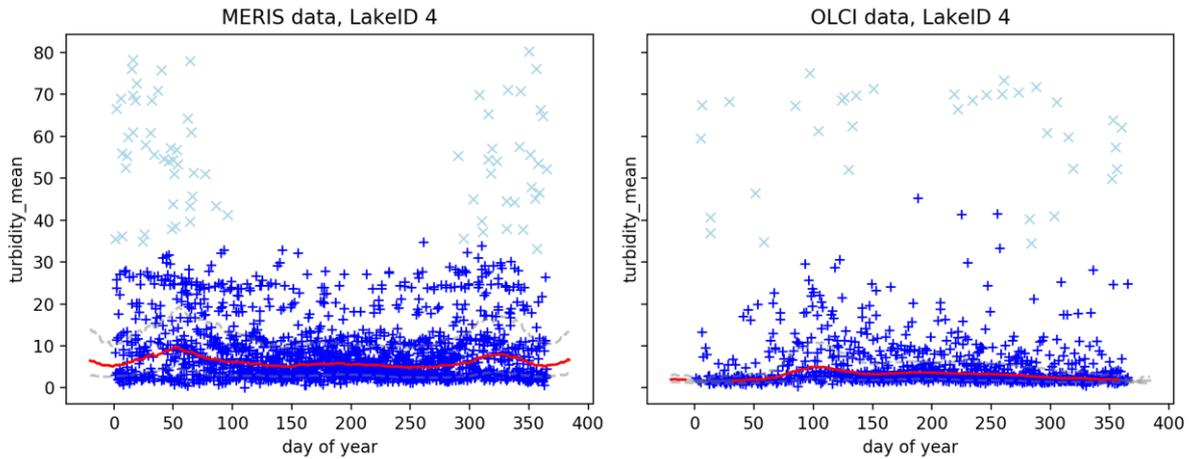
Figure 28 Climatological annual cycle of turbidity for MERIS and OLCI observations of Aral Sea (red line). The multivariate filtering with the LSWT climatology rejects some data points (light blue). See also times series and cluster analysis in Figure 30.
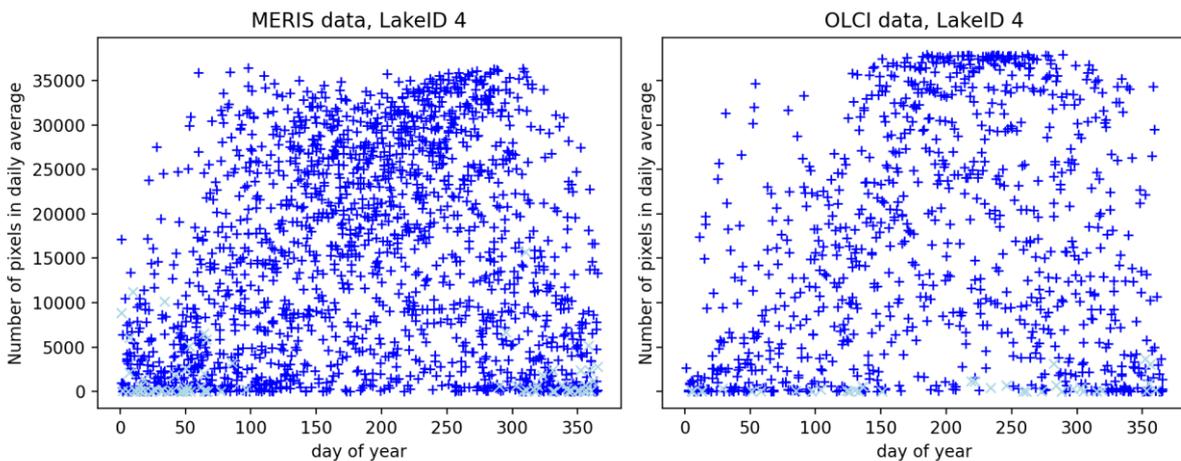
Figure 29 Number of pixels of the daily averages, which are basis of the turbidity climatology for Aral Sea. Colours represent again the status after filtering with the LSWT climatology. The high turbidity values which are cast out (light blue) correspond to very small numbers of daily observations.
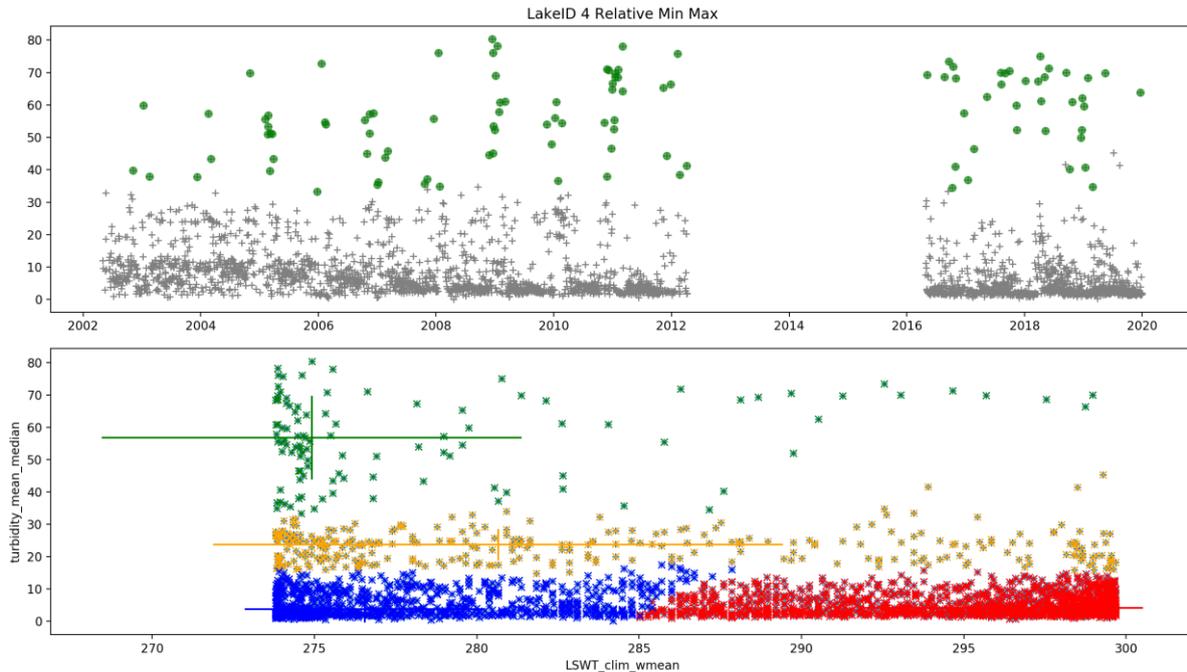
Figure 30 Turbidity time series and cluster analysis of daily lake-median turbidity and LSWT climatology. The green cluster, with its centre at low temperature and high turbidity values, is excluded because these data points are suspected to be undetected ice.

4.2.2.2 Example 2 – Lake Amadjuak, Canada, GLWD00000056

Lake Amadjuak is located on Buffin Island, in the NE of Canada. From the LIC classification and the LSWT climatology it becomes clear, that for a period lasting nearly half of the year Lake Amadjuak can be covered by ice. The quality flagging of the LWLR product concerning ice clearly works better on the OLCI than on the MERIS data, possibly owing to the extended band set of OLCI. It is reasonable to expect a data gap in winter and spring months, like the OLCI data shows (Figure 31). The high turbidity values in the daily lake-averages in the MERIS dataset represent a large number of underlying observations, so in this example the misclassification is highly common. During the winter months, nearly one fourth of the total number of pixels (N) is regularly observed and classified as water, although it is most likely ice (Figure 32).

With the clustering approach most of the suspect MERIS and OLCI datapoints can be successfully identified and omitted from the climatology calculation (Figure 33). The LSWT climatology does not extend over the entire year and the threshold criterion for data which cannot be clustered does not catch all the suspect data points, particularly in January (MERIS). Filling the winter gap in the LSWT climatological annual cycle could prevent this.
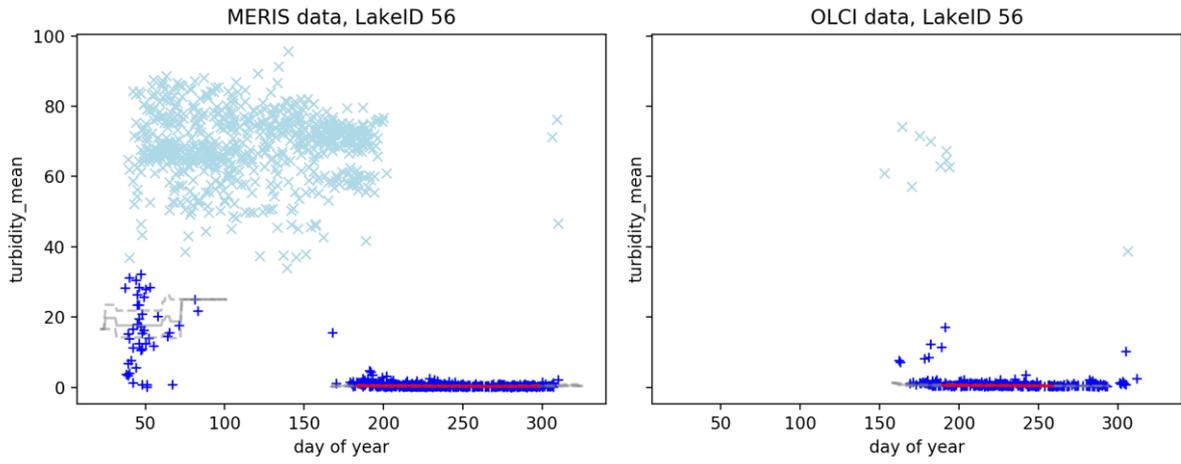
Figure 31 Turbidity climatology of Lake Amadjuak with long period of ice cover (see LIC time series, Figure 7). High turbidity values coincide with low temperatures (see Figure 33 bottom) and the suspect data points of undetected ice are filtered out. Climatological annual cycle of turbidity (red line). Clearly, the filtering of ice in the LWLR product is working better for OLCI than for MERIS.
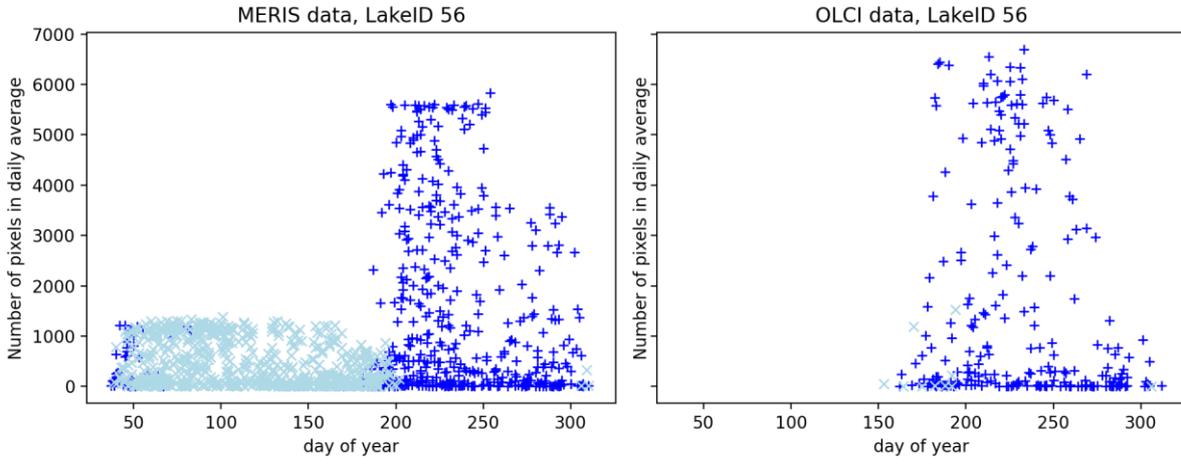
Figure 32 Number of pixels of the daily averages, which are basis of the turbidity climatology for Lake Amadjuak. Colours represent again the status after filtering with the LSWT climatology (light blue – excluded, dark blue – part of the climatology).
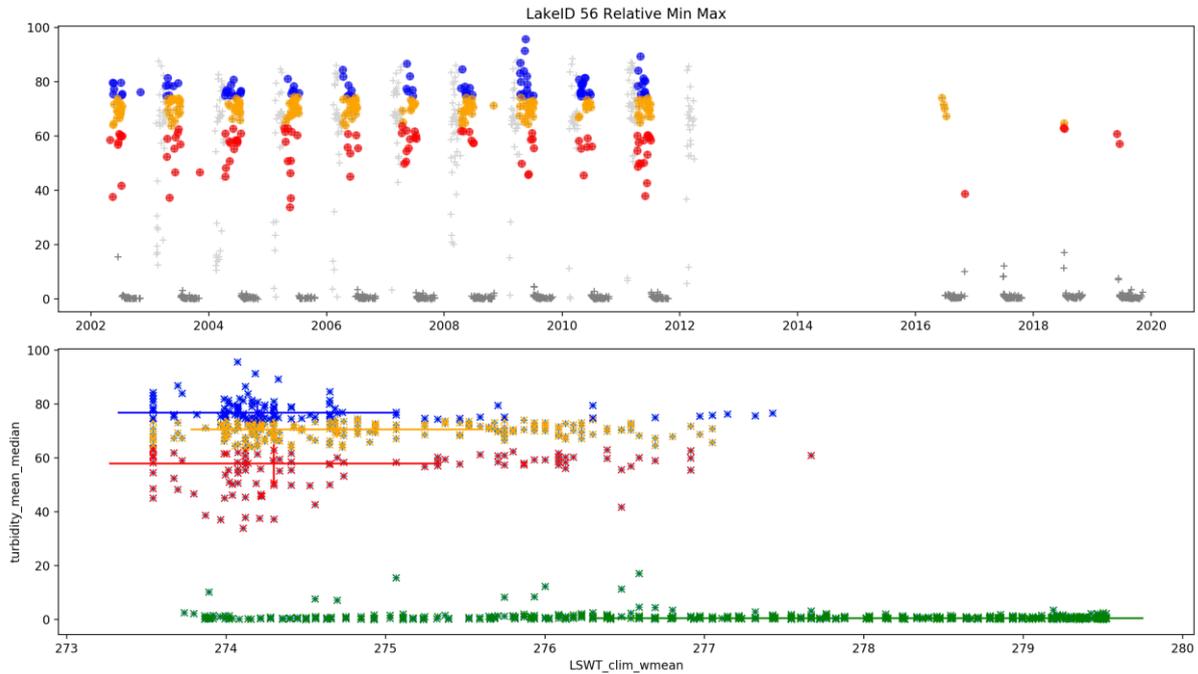
Figure 33 Turbidity time series (daily median per lake, top) and clustering of turbidity and LSWT climatology (bottom). The LSWT climatology has not been derived for all days of the year (light grey points in turbidity time series), so some data points cannot be directly filtered by clustering. Cluster centres are very distinct with high turbidity and low temperatures, identifying the undetected ice cover.

4.2.2.3 Example 3 – Lake Ngoring, China, GLWD00000300

Lake Ngoring is covered by ice in winter, so that the LSWT climatology does not cover January (Figure 34). Still, the filtering by clustering of high turbidity and low LSWT resolves the turbidity timeseries well, so that a turbidity climatology can ultimately be derived (Figure 35).

The high values of turbidity correspond in most cases with rather low numbers of observations, which suggests that the general pixel identification in the LWLR performed well within its means. The OLCI classification seems to work better than the MERIS classification. The latter shows larger number of pixels with suspiciously high turbidity averages (Figure 36).

In this case, the clustering removes a large number of data points with moderate turbidity and temperatures well above freezing point. Compared with the number of observations in the averages, which are generally low in the OLCI dataset, it becomes clear, that the filtering technique does not remove meaningful extreme values, but only outliers, with limited spatial coverage.
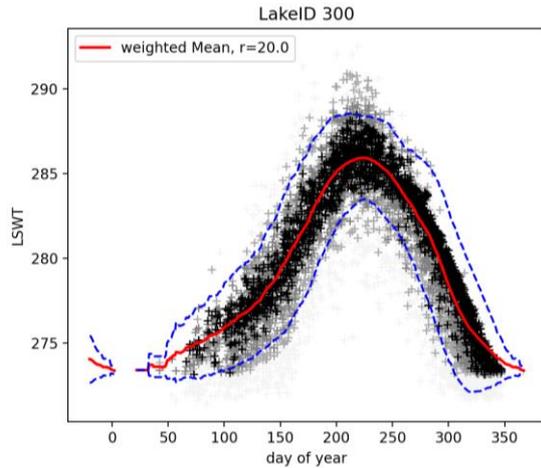
Figure 34 LSWT climatological annual cycle for Ngoring, China, GLWD00000300. Due to ice cover in winter the climatology has a gap during that period.
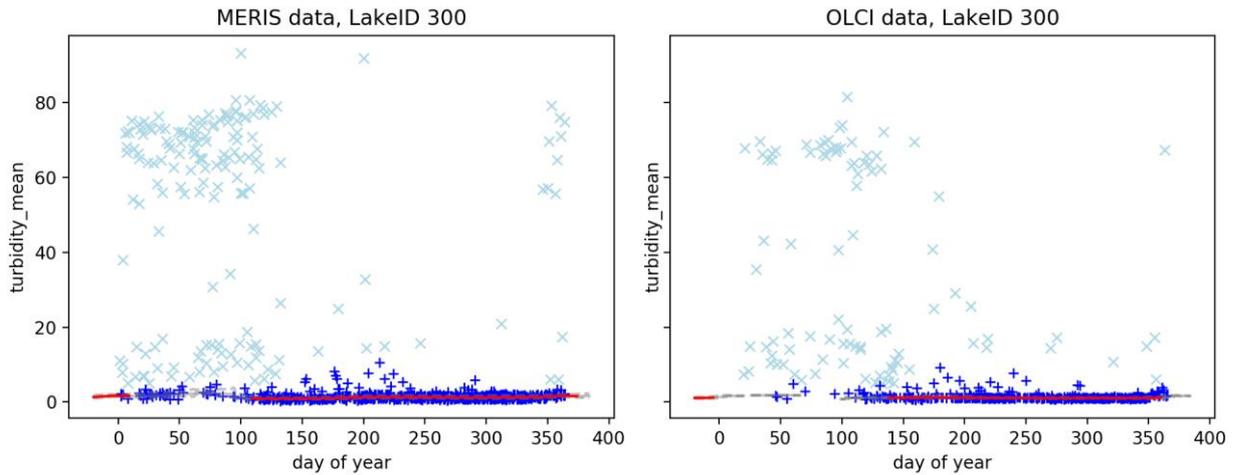
Figure 35 Climatology of turbidity of Lake Ngoring for MERIS and OLCI data based on valid data points (dark blue) after filtering with clusters based on turbidity and temperature (invalid: light blue). The recommended climatology is marked as a red line.
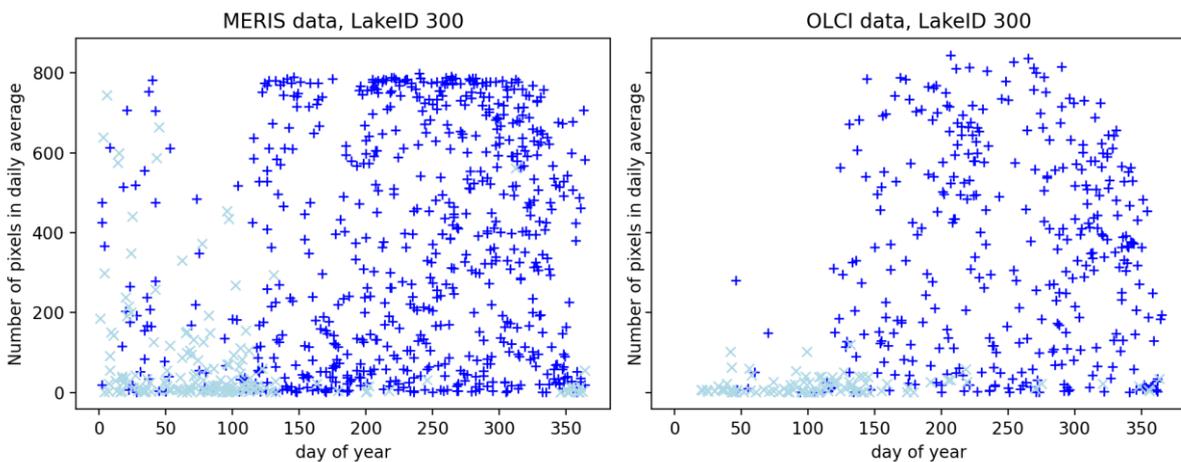
Figure 36 Number of pixels of the daily averages, which are basis of the turbidity climatology for Lake Ngoring. Colours represent again the status after filtering with the LSWT climatology. Most of the discarded high turbidity values (light blue) correspond with small numbers of observations.
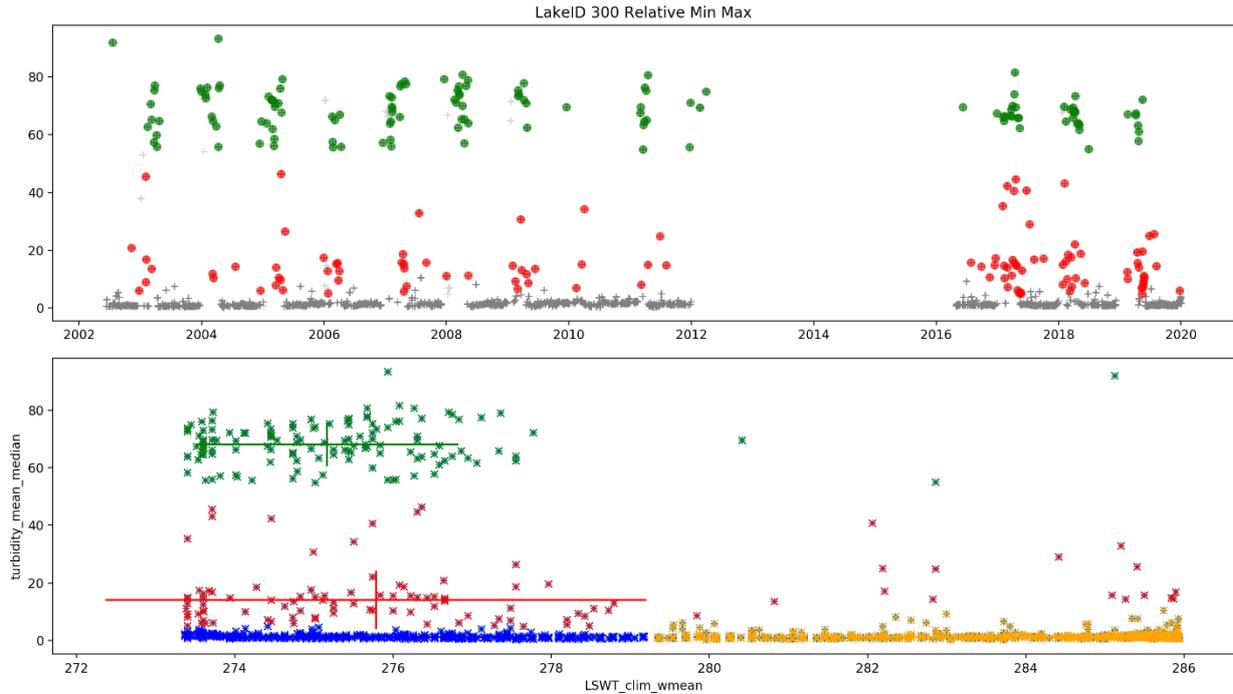
Figure 37 Turbidity times series (top) with identified suspect values from clustering result (bottom) for Lake Ngoring. Points with no corresponding temperature climatology (light grey crosses) are excluded if they are above the minimum value of the data points in the red and green clusters. The cluster with highest turbidity and lowest temperature covers most of the undetected ice influence.

4.2.3 Threshold-filtering using climatologies - Chl-a concentration

The filtering of chlorophyll-*a* concentration values follows a similar idea as for the turbidity data (overview in Figure 38). During the consistency investigation (section 3.1), the concentration values originating from MERIS and OLCI data partly show significant differences. Between the sensors, we observe different outlier behaviours, some of which are associated with specific OWTs. This investigation was done before removing adjacency effects, which may partly explain these differences. Here we look at whether additional climatology-based clustering and filtering can also help identify outliers. With the four-year gap between MERIS and OLCI, it is difficult to decide, whether the bias is natural or introduced by the sensor.

For a good clustering result it was necessary to split the data according to sensor and filter them independently. Further steps are:

- BIRCH clustering (chl-*a* (linear), LSWT) with n clusters (here: n=4).

- Determine cluster centre (median LSWT and median chl-*a*) and sort cluster centres by chl-*a*.

- Start with cluster of highest chl-*a* value, work through clusters with decreasing chl-*a* concentration along the decision tree. Adjust threshold (start value = 0)
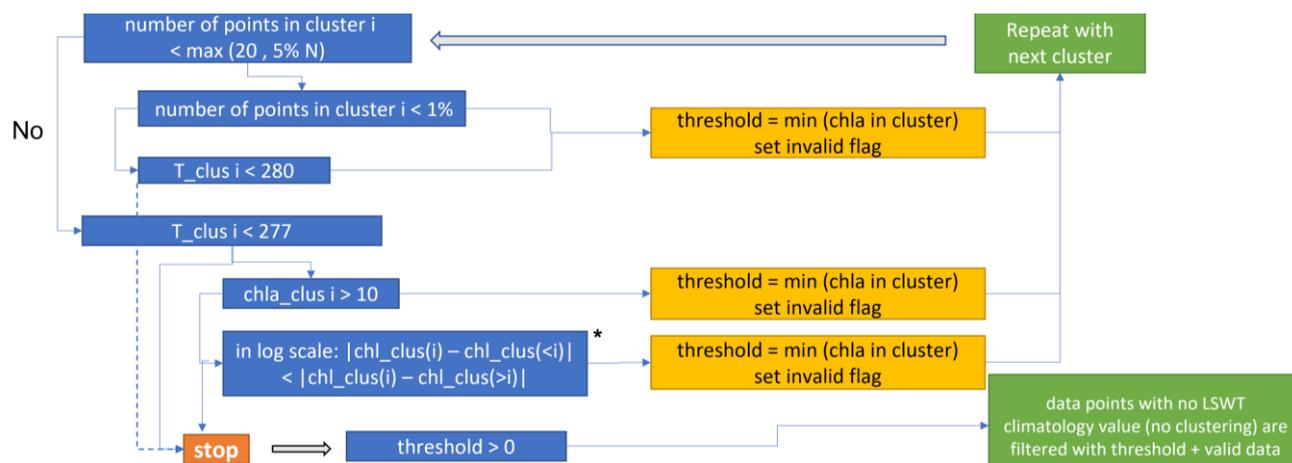
Figure 38 Chlorophyll-a concentration, filtering by clustering. Algorithm overview, decision tree. This condition marked (*) translates to: the distance of cluster centre _i_ to clusters with higher chl-a has to be smaller than distance to following clusters with lower chl-a.

The decisions for the chl-_a_ filtering start with an outlier check. If the number of points in the current cluster is smaller than the threshold value N_thresh = maximum (20, 5% of total data points), the cluster most likely represents outliers.

If the number of points in the cluster is even smaller than N_thresh/5 (i.e. which corresponds to 1% of the data), they are most certainly outliers. They are flagged as invalid, and the global chl-_a_ threshold is set to the minimum of the chl-_a_ values of this cluster.

If the cluster size is between N_tresh/5 and N_tresh, the temperature of the cluster centre becomes deciding. If T_clust is below 280K, the values can be affected by undetected ice. The invalid flag is set and the global chl-_a_ threshold is adjusted. If the temperature is higher than 280K, the filtering procedure comes to a halt.

If the cluster size is larger than N_tresh, the temperature at the cluster centre is checked. If T_clust is below 277K, further decisions have to be taken, otherwise, the filtering stops here. If the chl-_a_ value of the cluster centre is above 10µg/l, the cluster most likely represent undetected ice at this low temperature. Again, invalid flag and global chl-_a_ threshold are updated.

If chl-_a_ at the cluster centre is below 10µg/l, the distance between clusters (on a log-scale) is checked. If the distance of cluster centre i to clusters with higher chl-_a_ is smaller than the distance to following clusters with lower chl-_a_, the cluster is most likely still affected by undetected ice and should be excluded. Again, invalid flag and global chl-_a_ threshold are updated.

As soon as a cluster in order of decreasing chl-_a_ concentration is no longer considered to be potentially undetected ice, the next cluster with lower concentrations most definitely is not at risk. After updating the invalid flag and the global chl-_a_ threshold, the next cluster is checked with the same conditions starting from the top.

When the cluster filtering has ended, the global threshold is used to filter chl-_a_ data, which has not been part of the clustering due to gaps in the temperature climatology. Chl-_a_ values above this threshold are excluded.

After filtering the data in this fashion, the same calculation of a climatology is performed as it has been done for the LSWT data.

The chl-_a_ concentration climatology is based on the filtered daily median chl-_a_ concentration per day of year, converted to log-scale, the weights are derived from the daily standard deviation of chl-_a_ per lake (see LSWT algorithm). The climatological value is the weighted mean of a moving window with a radius of 20 days.

4.2.3.1 Example 1 – Aral Sea, GLWD00000004

The chlorophyll-*a* product appears less affected by undetected ice than the turbidity product (compare time series in Figure 39, Figure 40 and Figure 30. The consistency between sensors seems lower for chla concentration than for turbidity and the cut between possibly ice influenced pixels and the correctly flagged data is not as pronounced as it is in the turbidity time series. For the MERIS time series, the pixels selected for exclusion appear very close to the overall range of averaged observations (Figure 41), whereas in the OLCI observations the ice influenced cluster is much more separated from the rest of the data points (Figure 40).
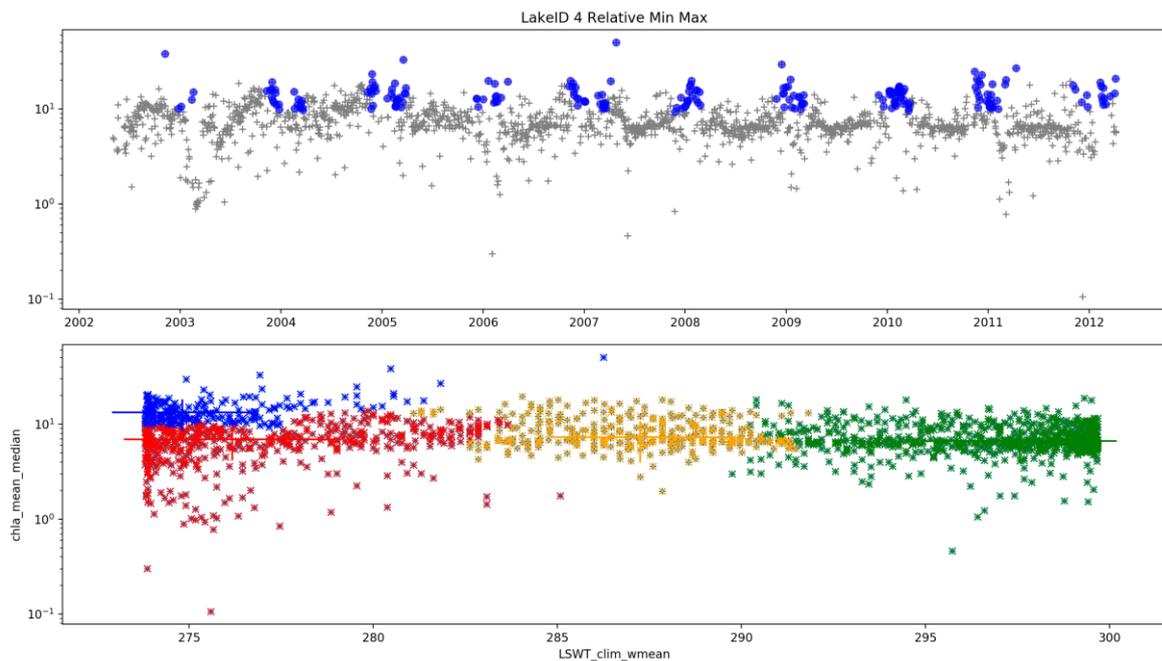

**Figure 39 Chlorophyll timeseries and clustering with LSWT climatology (Aral Sea, MERIS)**
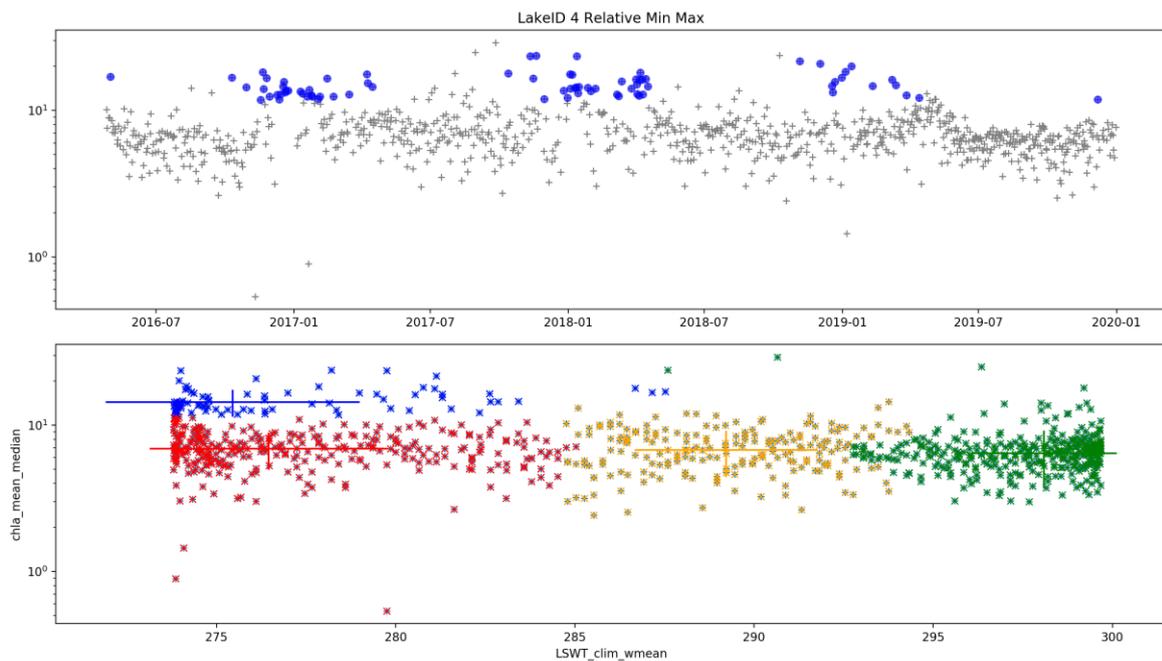
Figure 40 Chlorophyll timeseries and clustering with LSWT climatology (Aral Sea, OLCI)
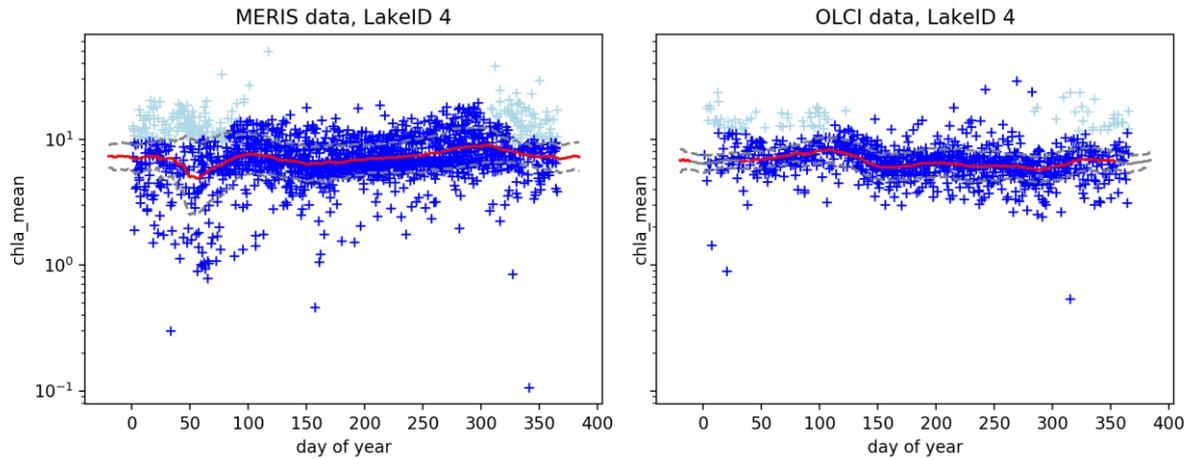
Figure 41 Chlorophyll-a multi-annual time series of daily median values, filtered with LSWT climatology. Dark blue: valid data points; light blue: pixels affected by filtering with clusters based on turbidity and temperature. Filtering and climatological annual cycle is calculated for each LWLR sensor independently.

4.2.3.2 Example 2 – Lake Amadjuak GLWD00000056

From the turbidity example of lake Amadjuak and the LSWT climatology, it is already known that the winter and spring months are governed by ice cover. Ice influence again leads to elevated chlorophyll-*a* values, particularly for MERIS (Figure 42). These high values relate to small numbers of observations per day (see Figure 32). Most pixels are already flagged in the LWLR product, but small numbers to up to a quarter of the maximum number of pixels remain unflagged, which needs further investigation in the LWLR classification.

The filtering approach with LSWT climatology data leads to reasonable identification of outliers, especially in wintertime.
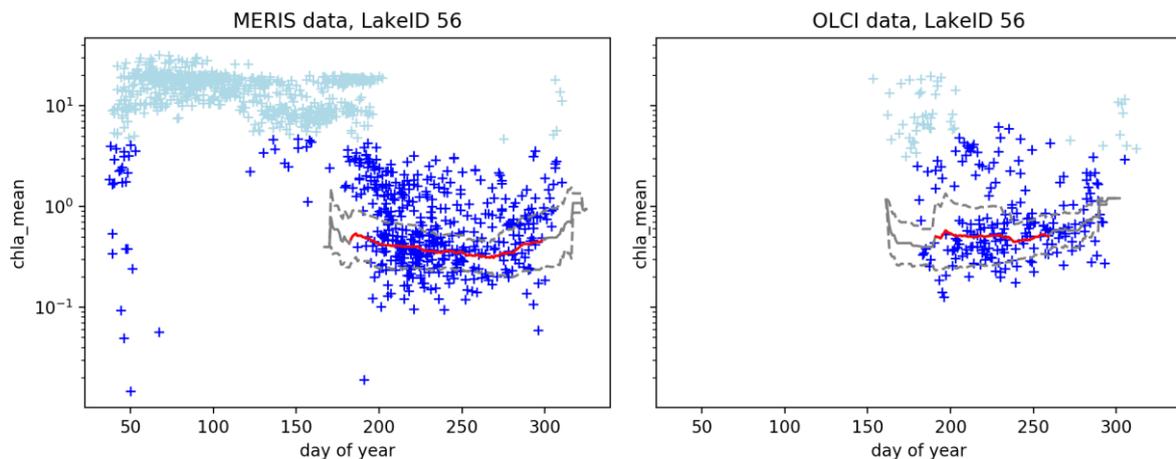
Figure 42 Daily median value of chlorophyll-a concentration for MERIS and OLCI in Lake Amadjuak. Dark blue: valid data points; light blue: pixels affected by filtering with clusters based on turbidity and temperature; red line: climatology
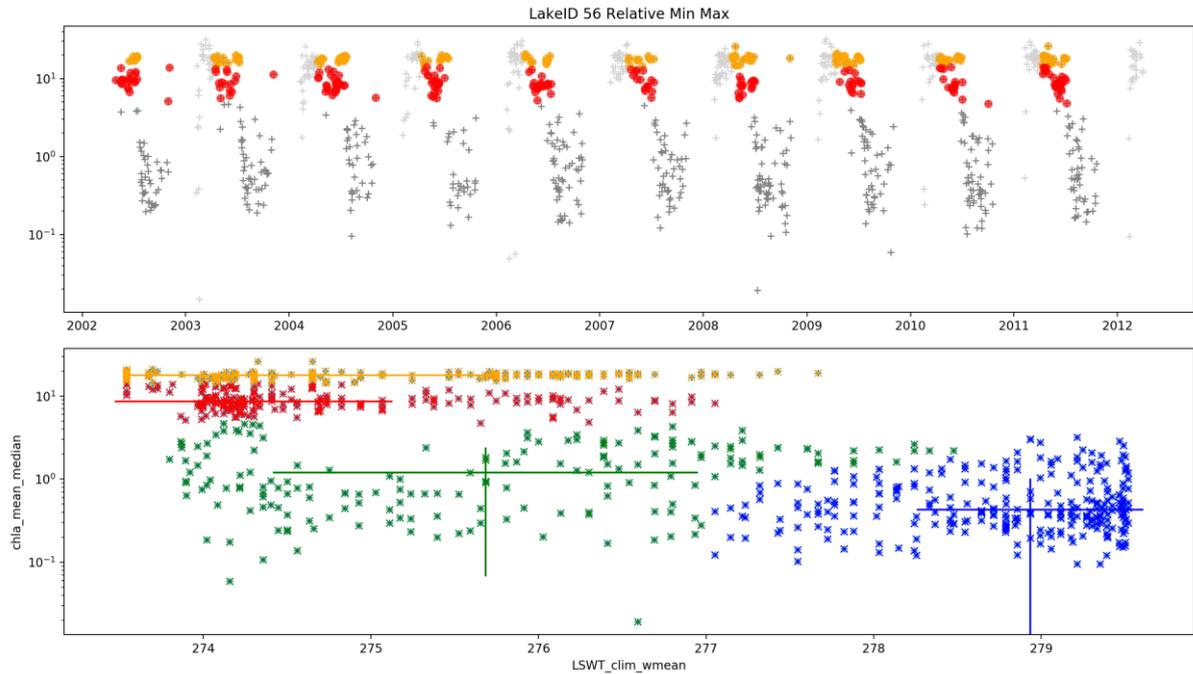
Figure 43 Time series of chlorophyll-a and clustering results with LSWT for Lake Amadjuak (MERIS period)
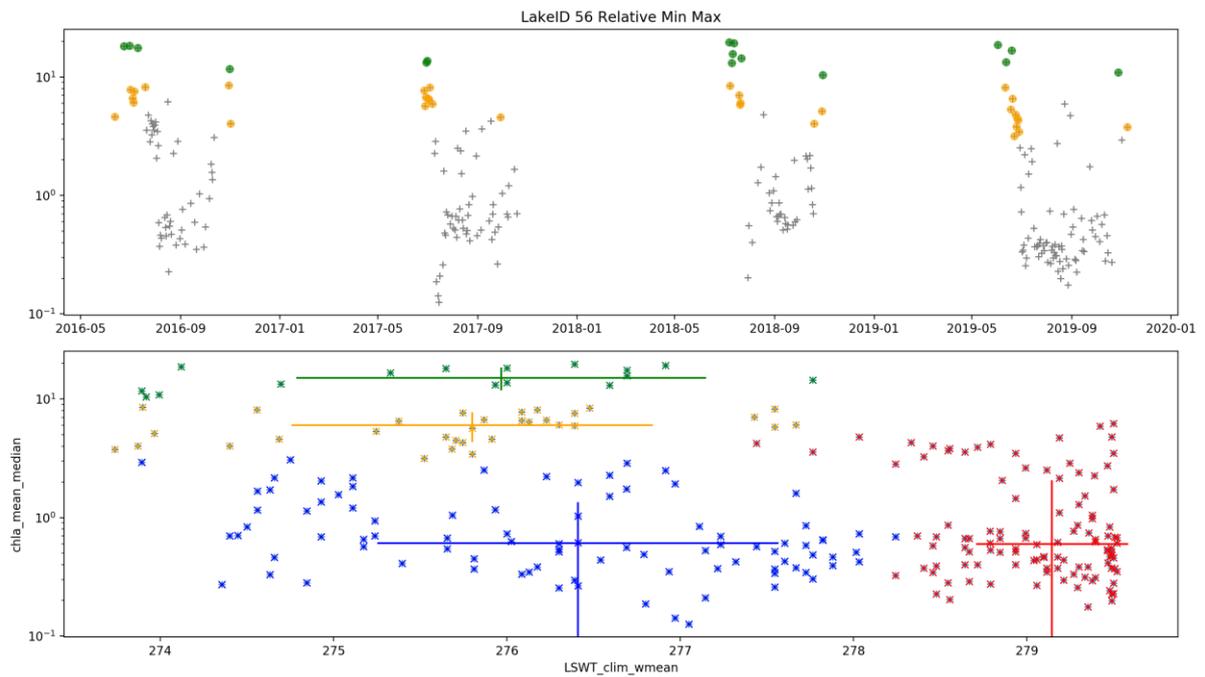
Figure 44 Time series of chlorophyll-a and clustering results with LSWT for Lake Amadjuak (OLCI period)

4.2.3.3 Example 3 - Ngoring, China, GLWD00000300

Most of the ice influence on chlorophyll-*a* algorithms is identified successfully as high outliers and filtered out with the clustering approach for both sensors (Figure 45, Figure 46). The increase in chlorophyll-*a* concentrations at the beginning of winter might still be an issue caused by undetected

ice. The high values from days 1-120 (green cluster) are excluded from the calculation of the climatology (Figure 47).
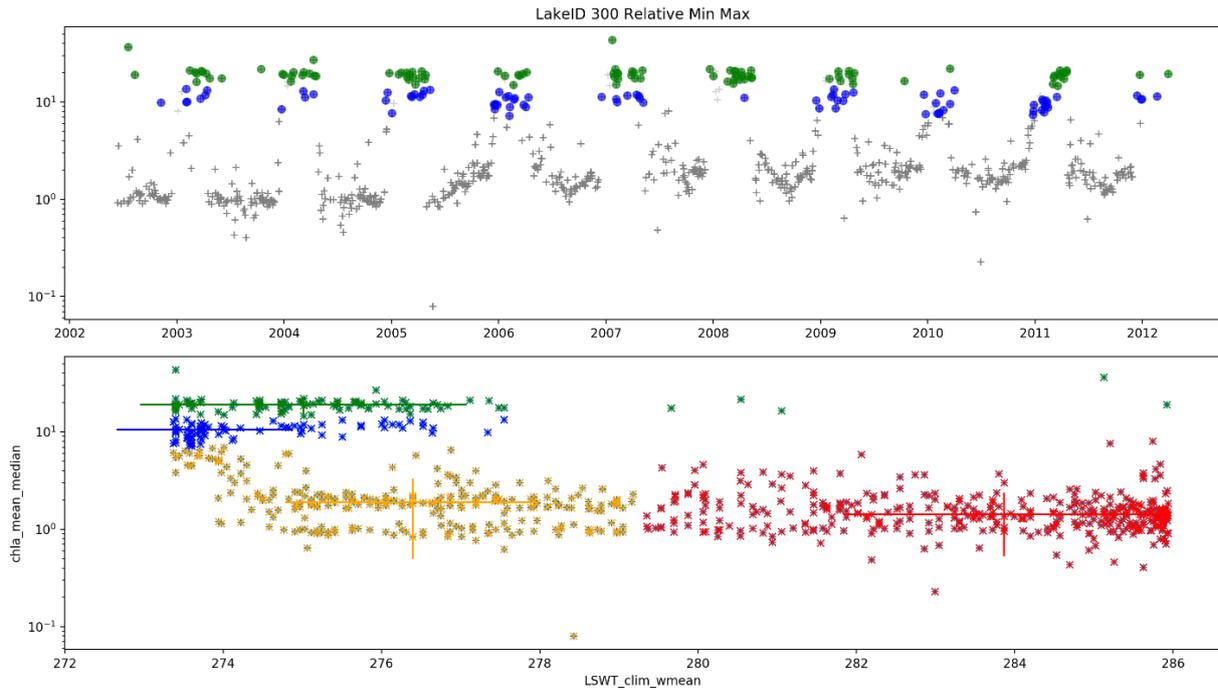
Figure 45 Chlorophyll-a time series for MERIS years in Lake Ngoring. Two clusters are identified to hold ice influenced values and their data points are excluded (blue, green). Some points of the yellow cluster are still close to the ice values.
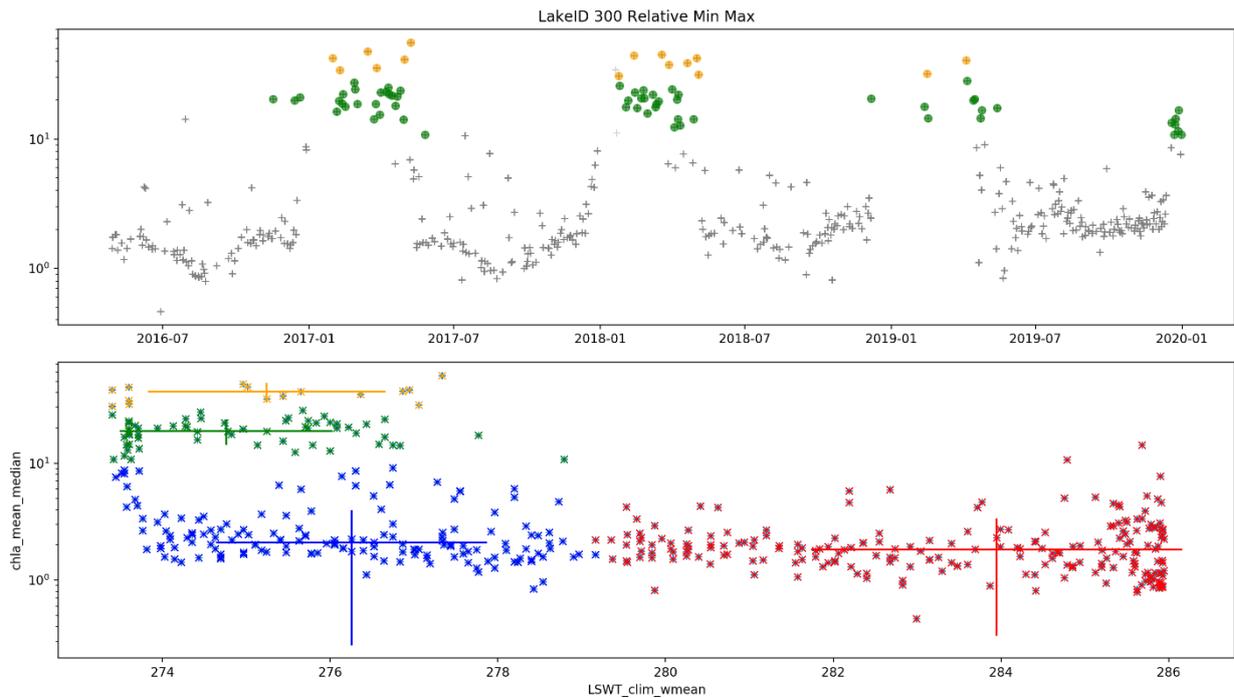
Figure 46 Chlorophyll-a time series for OLCI years in Lake Ngoring. Two clusters are identified to hold ice influenced values and their data points are excluded (yellow, green). Some points of the blue cluster are still close to the ice values.
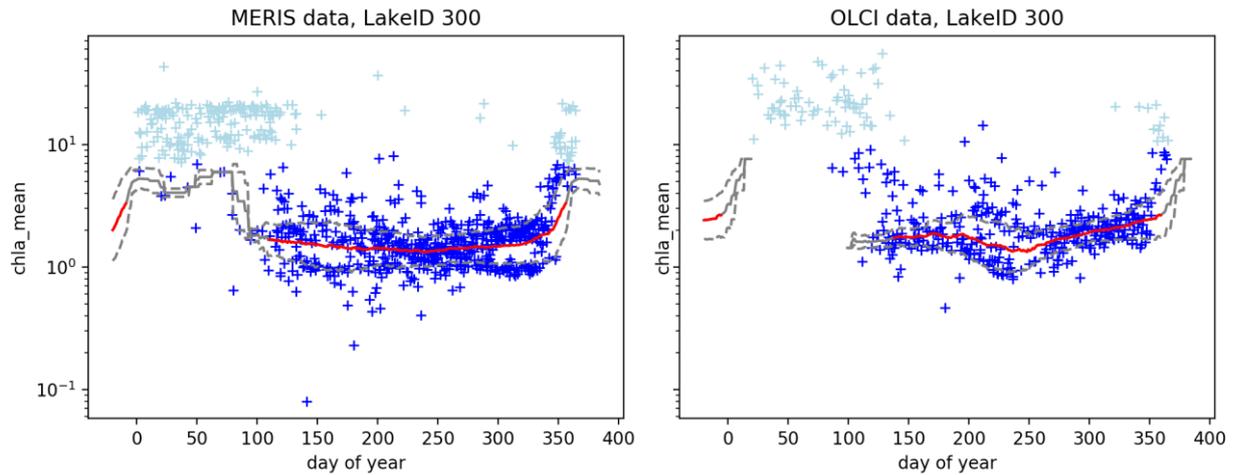
Figure 47 Climatology for chl-a concentration Dark blue: valid data points; light blue: pixels affected by filtering with clusters based on turbidity and temperature; red line: climatology

4.2.4 Classification of lakes by LSWT climatology: ice occurrence probability

The completeness of LSWT climatologies can be used to determine which sets of lakes likely have ice coverage. All lakes that are not affected by ice are more likely to be observed in a consistent manner in the LSWT and especially the LWLR products. The success of the applied pixel classification in v.1 varies between MERIS and OLCI, which in turn leads to more (MERIS) or less (OLCI) effect on the daily median values of the derived LWLR parameters by misclassified water leaving reflectance spectra.

For 237 lakes with LSWT data the climatology has been derived. There are 107 lakes with contiguous observations for each time step with at least 20 observations within each 40-day timespan. 60 of 107 lakes are never ice covered according to the temperature data, which remain above 276K. The climatologies of 47 lakes of 107 include LSWT values below 276K, for which partial ice coverage can occur. In these cases, filtering the LWLR daily median per lake data with the help of the LSWT climatology can be necessary, because ice flagging of the LWLR level 2 product might not have been sufficient.

If there are time steps with fewer than 20 observations within the 40-day timespan of the weighted mean, the climatology is less dependable at those steps. For 38 lakes, these limited numbers of observations coincide with temperatures above 276K, often associated with a gap in the maximum of the annual temperature cycle. For 91 lakes there are gaps in the observations because of ice cover, which again leads to a need of filtering the LWLR products.

Table 6 Overview of LSWT climatologies and their general characteristics of completeness in time (no gap) and occurrence of ice cover.

LSWT CLIMATOLOGY CHARACTERISTIC	NUMBER OF LAKES [INTERNAL LAKE ID]
No gap (ice possible)	**47** [100000012, 1028, 103, 113, 122, 12, 131, 135, 146, 1498, 15, 163, 165, 16, 18, 197, 201, 215, 219, 2358, 241, 267, 26, 296, 29, 2, 300000140, 300000773, 300013156, 300013182, 300165102, 310, 34, 358, 383, 439, 4, 50, 543, 565, 5, 6, 71, 87, 883, 91, 95]
No gap (T >276K)	**60** [100000002, 100000013, 10679, 10694, 117, 1196, 133, 1526, 1529, 153, 1562, 1659, 173, 188, 194, 19, 200000071, 209, 20, 216, 22, 234, 244, 25, 278, 279, 300000138, 300000177, 300000991, 300009360, 300009739, 300014185, 300015455, 327, 328, 352, 380, 390, 3, 411, 481, 484, 488, 48, 505, 51, 526, 542, 55, 576, 65, 66, 67, 729, 77, 7, 84, 8527, 948, 94]

Ice related gap	**91** [1044, 105, 1096, 110, 11, 121, 1240, 124, 13377, 13, 142, 1432, 157, 158, 159, 168, 179, 17, 181, 1891, 190, 192, 198, 202, 2199, 226, 236, 239, 23, 246, 247, 254, 264, 297, 300000182, 300000185, 300001038, 300001297, 300001744, 300002545, 300002685, 300002892, 300003969, 300013043, 300013070, 300013104, 300015002, 300, 312, 31, 3211, 3219, 32, 33, 354, 356, 37, 39, 41, 444, 44, 4503, 456, 45, 47, 49, 516, 520, 53, 56, 572, 57, 58, 592, 59, 63, 676, 6785, 679, 725, 744, 75, 812, 83, 88, 8, 92, 93, 97, 989, 9]
High temperature gap	**38** [100000011, 109, 10, 116, 1204, 129, 14, 154, 15600, 176, 18140, 182, 200000013, 200000072, 21, 245, 24, 2540, 256, 274, 30, 359, 35, 36, 42, 477, 4947, 4953, 507, 515, 52, 620, 6561, 687, 69, 7840, 78, 81]
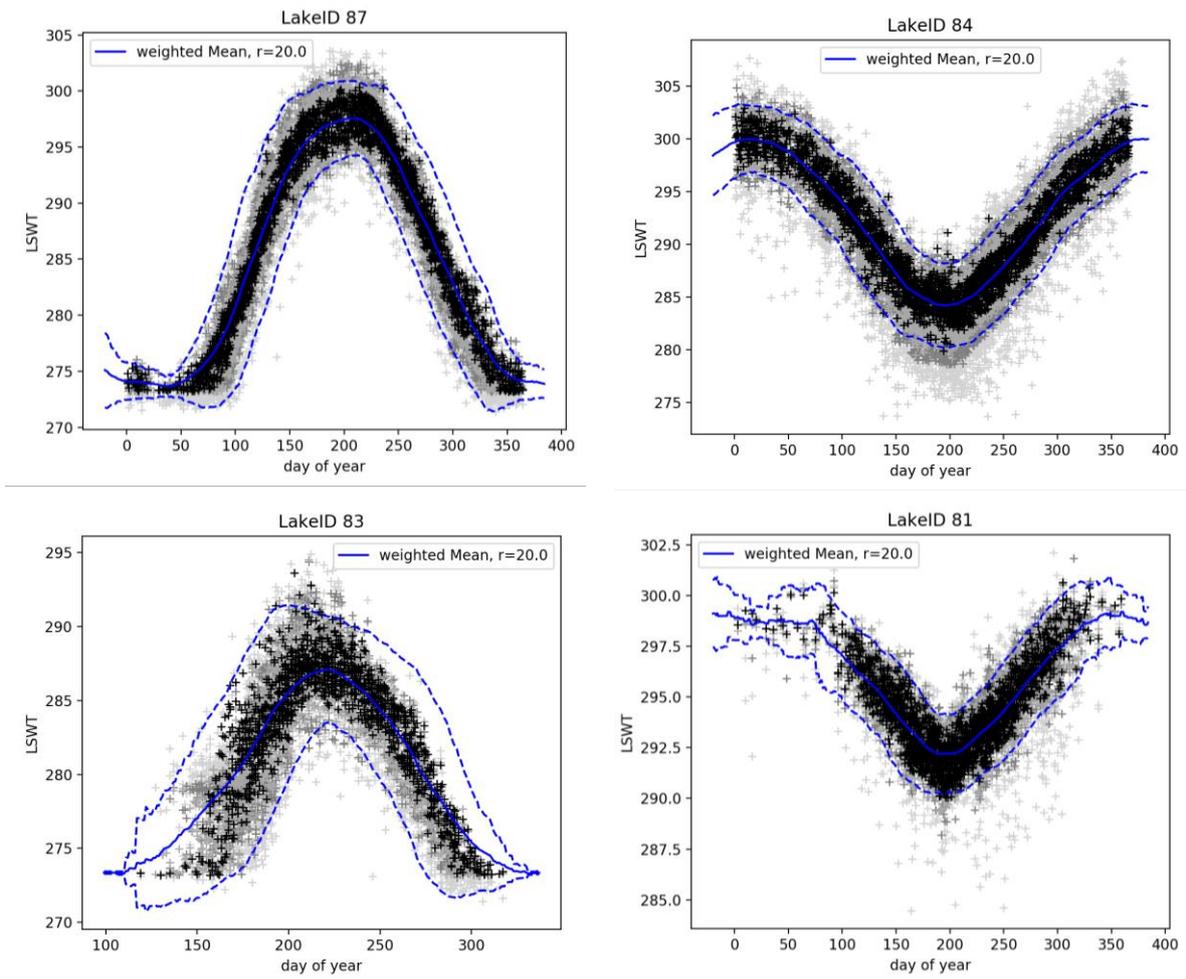
Figure 48 Examples of climatological annual cycles of LSWT (blue line, weighted mean within 20-day radius; weighted standard deviation as dashed line): timeseries of LWLR product from lakes with ice occurrence can profit from the filtering approach to account for unidentified ice observations (continuous time series for lake Kremenshugskoye, Ukraine ID 87; gap due to ice cover for lake Nueltin, Canada ID 83). Gaps in the annual cycle of LSWT can also occur during rainfall period (Bangweulu, Zambia ID 81). A very stable LSWT climatology is recorded for Mar Chiquita, Argentina ID 84.

4.2.5 Conclusions

Consistency between LWLR, LIC and LSWT is dramatically improved wherever the presence of ice is informed by thermal observations, with LWLR benefitting most from improved stability in time-series. A combination of statistical behaviours and dynamic thresholding of products derived from the LWLR is needed to achieve best results, which can be achieved with the L3S products. Upstream (L2) identification of adjacent land also proves critical in improving LWLR product quality, and adjacency masks generated in this way may be useful in other processing lines; this has not yet been explored. Such changes in L2 product generation will in turn influence the dynamic thresholding methodology – this can only be fully tested after generating the next version (2.0) of the LWLR which include adjacency effect filters, while our expectation is that reducing the variability observed in variables such as turbidity by masking adjacent land effects, will improve the sensitivity of this method to remaining outliers. For lakes without large variability or strong gradients, the dynamic thresholding based on climatologies already provides a good thresholding criterion, which removes outliers originating from unidentified mixed pixels at the shoreline or undetected ice.

Differences between MERIS and OLCI, in the ability of upstream (L2) pixel identification to classify ice, are too large to be explained just by observation (viewing angles) or sensor effects (band settings). It is recommended to investigate the MERIS ice flagging, to *a priori* remove more of the misclassifications. This will also improve dynamic threshold-based filtering on the L3 product. The climatologies derived from daily medians would become more reliable.

To harmonize the filtering approach by climatologies the turbidity climatology may be used as a proxy as it is the more sensitive one and less subject to horizontal, biological variability. The separation of suspect daily averages from the time series by clustering has the clearest results with the combination of turbidity and LSWT. We note that the dynamic thresholding methodology cannot yet be implemented in CRDPv2.0 processing, because LSWT climatologies first need to be generated for all considered lakes. Also, the adjacency mask will change in turn the lake-median values of LWLR products, so that it is advised to run the clustering algorithm again. The dynamic thresholding methodology remains a mean of L3S product flagging.

5   Validation

This chapter shows how the retrieved solutions are applied and how they influence the outcome of the data sets. While section 5.1 addresses the application and further refinement of the new OWTs, section 5.2 is showing the influence of climatology filtering on selected lakes. In section 5.3 we show how the filtered climatologies of different thematic variables and/or sensors correlate in dependency of geographic and topographic characteristic of the lakes (global distribution of patterns).

5.1   Flagging of adjacency effected pixels using newly identified OWTs

Results in section 3.2 have shown that the two newly identified OWTs (OWT-14 and OWT-15) from small brownification lakes have the protential in identifying pixels that are influenced by adjacency effects. In this section, we tested this hypothesis in various type of lakes and investigated the appropriate procedure in terms of its application.

The lakes included in this evaluation covers a wide range of bio-optical/topographical types, including Lake Vattern (large deep clear oligotrophic lake), Lake Taihu (large shallow turbid eutrophic lake), Lake Tanganyika (large deep clear alkaline lake), Lake Balaton (shallow turbid eutrophic lake) and Lake Rusken (small shallow brownification lake).

5.1.1 Spatial distribution of dominant OWT in various type of lakes (dominant-OWT-based approach)

Figure 49 shows the spatial distribution of dominant OWT in lakes Vattern, Taihu, Tanganyika, Balaton and Rusken from MERIS L2 products. It is found that the pixels influenced by adjacent land can be

identified in Lakes Taihu, Balaton and Rusken using the two OWTs (Figure 49b, d and e). While in clear lakes of Vattern and Tanganyika, some pixels in the lake centre are identified as dominant by OWTs 14 (Figure 49a and c), which are potentially misidentifications. It is also noted that in the small Lake Rusken, nearly all MERIS pixels are identified as most strongly associated with OWTs 14 or 15 (Figure 49e).
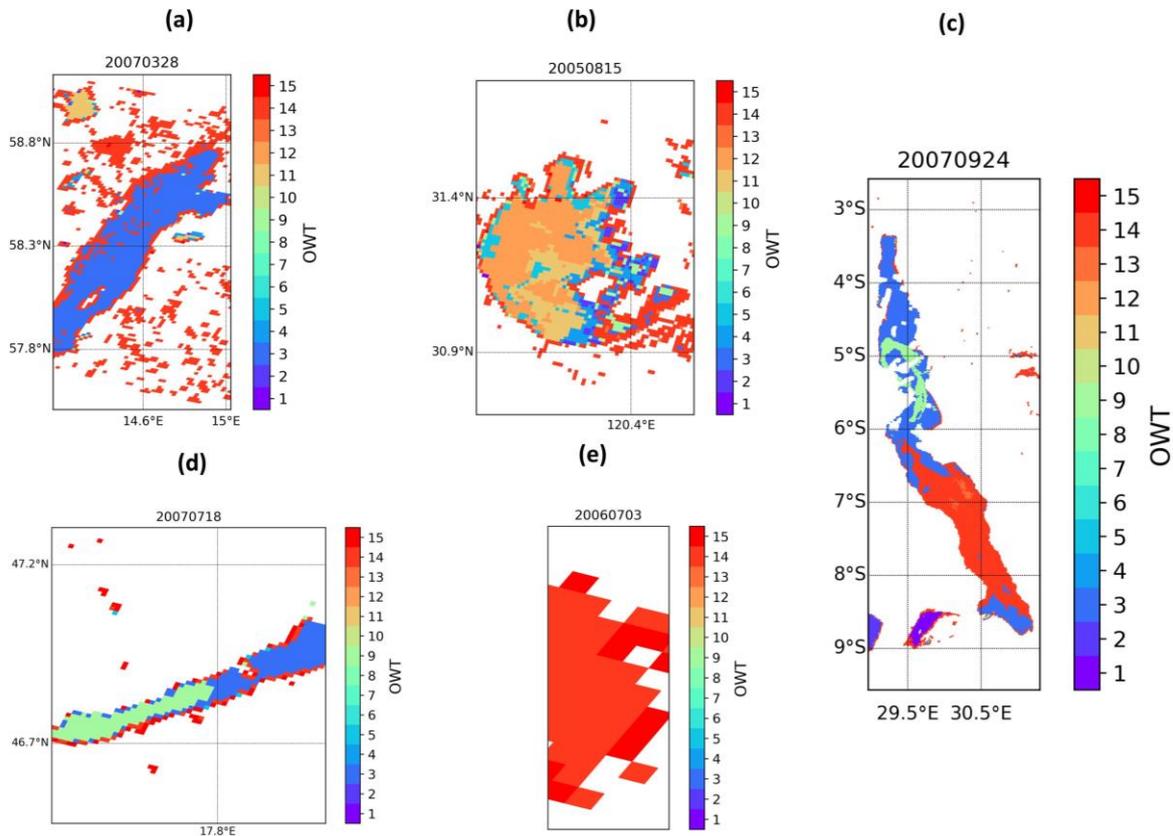
Figure 49 Spatial distribution of dominant OWT in lakes (a) Vattern, (b) Taihu, (c) Tanganyika, (d) Balaton and (e) Rusken from MERIS L2 products.

The spatial distribution of dominant OWT in OLCI L2 images is shown in Figure 50. Generally, fewer pixels are identified as OWTs 14 and 15 compared to MERIS. This confirms the results from the smaller selection of Lakes in section 4.1.2. Pixels adjacent to land are correctly identified in Lakes Taihu, Balaton and Rusken (Figure 50 b, d and e). While in clear lakes Vattern and Tanganyika, like for MERIS, some pixels in the lake centre are misclassified as having land-adjacency effects through OWT 14 (Figure 50 a and c).
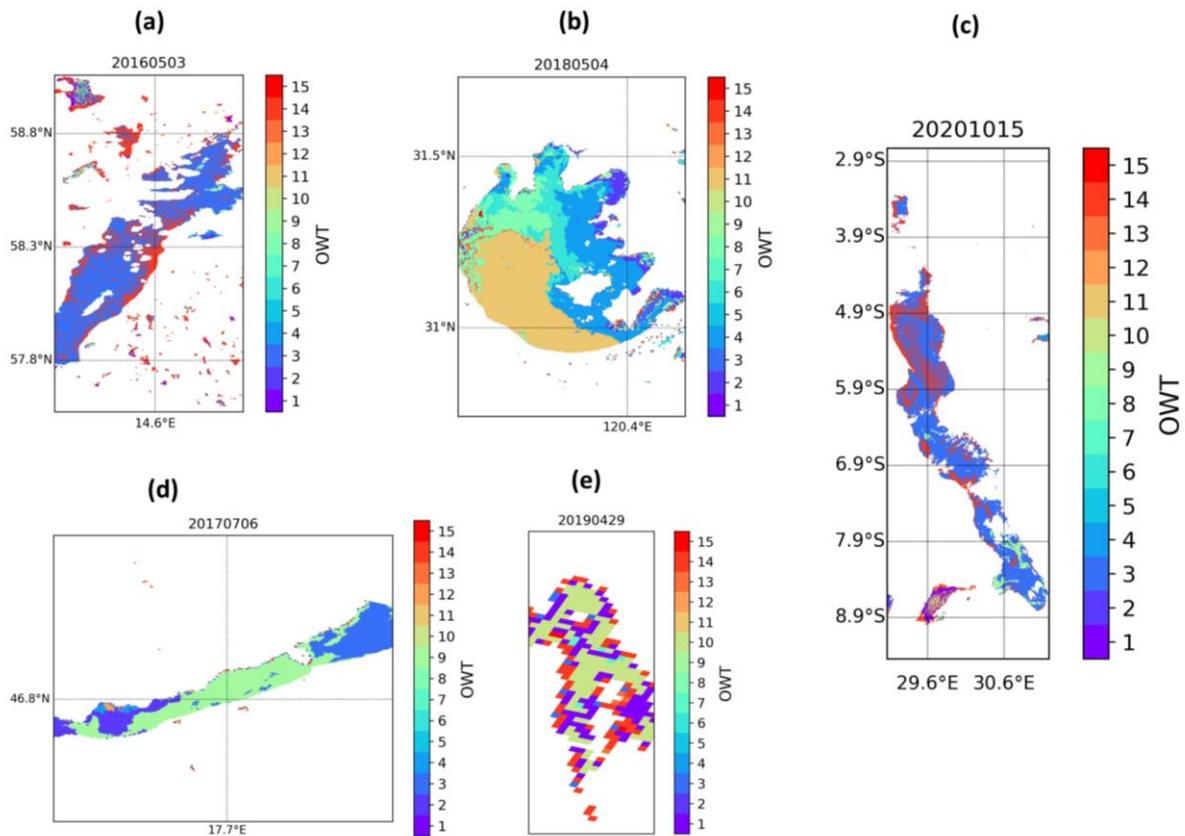
Figure 50 Same as Figure 49, but for OLCI L2 products

To further understand why many open water pixels in relatively clear lakes are classified as OWT 14, Figure 51 shows the spectra of the clear blue OWT 13 and the two adjacency OWTs (OWT 14 and 15). Despite the clear differences in the shape of these OWTs in the blue and NIR, confusion is likely to occur when the blue-green part of the spectrum has a relatively high amplitude (OWT13).
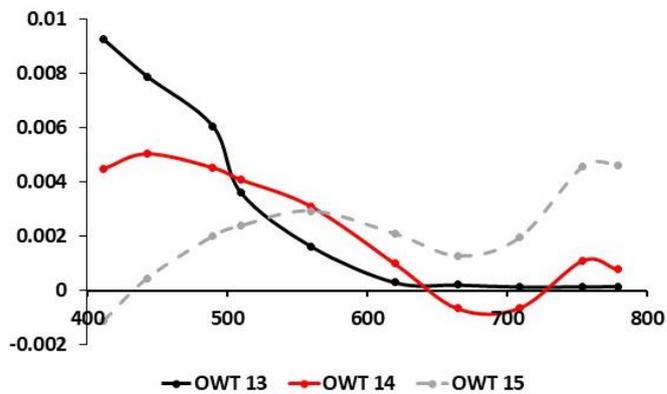
Figure 51 Spectra of OWT 13 (clear blue water), 14 and 15 (two new adjacency OWTs)

5.1.2 Enhanced adjacency effects identification using a threshold-based approach

Applying the criterion of a dominant OWTs 14 and 15 to identify adjacency affects was demonstrated in the previous section. Here, further refinements to this criterion are made to avoid the

misclassification in relatively clear lakes with a high blue LWLR. Rather than considering additional OWT additions, we approach the issue from a thresholding perspective. Figure 52 shows the frequency distribution of the sum of OWT-14 and 15 scores of all available pixels for MERIS and OLCI in a series of 'brown' lakes. In these lakes, OWT sum score for MERIS ranged from 1.4 to 1.65, while for OLCI the OWT sum score ranged from 1.3 to 1.65. Although OLCI shows a wider range in the OWT sum score compared to MERIS, the maximum values are similar between the two sensors in all lakes. In the clear lake Vättern the MERIS histogram shows a bimodal shape, with a value of 1.59 in the valley (Figure 52g).
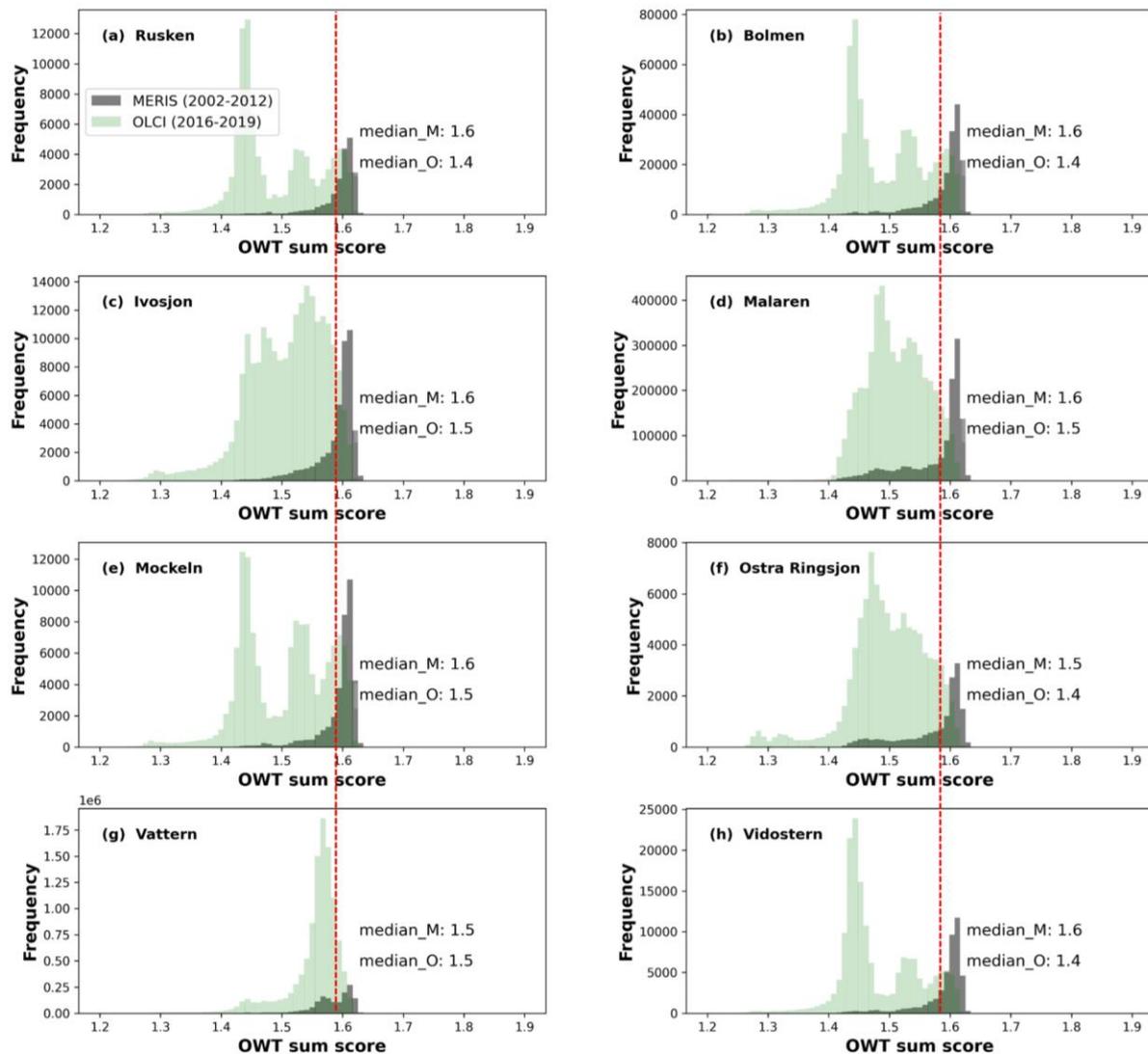
Figure 52 Frequency distribution of OWT sum score (for OWT-14 and 15) of all available pixels for MERIS and OLCI in Scandinavian lakes of (a) Rusken, (b) Bolmen, (c) Ivösjön, (d) Mälären, (e) Mockeln, (f) östra Ringsjön, (g) Vättern and (h) Vidöstern.

A threshold on the OWT sum score of 1.59 was determined to separate the pixels influenced by adjacency effects in the 'brown' lakes. Figure 53 shows the spatial distribution of OWT sum score (for OWT-14 and 15) in lakes Vattern, Taihu, Tanganyika, Balaton and Rusken. Note that MERIS scenes for each lake are the same as those in Figure 49. It is found that a threshold of 1.59 works adequately in all type of lakes, capturing all pixels potentially influenced by land adjacencies (Figure 53). Pixels at lake centres of Vättern and Tanganyika are no longer identified as influenced by adjacency effect (Figure 53 a and c). Similar results are shown for OLCI, with dramatically improved performance in clear lakes (comparing Figure 50 and Figure 54), suggesting that a threshold-based approach can be introduced to compensate the limitation of dominant-OWT approach in clear lakes.
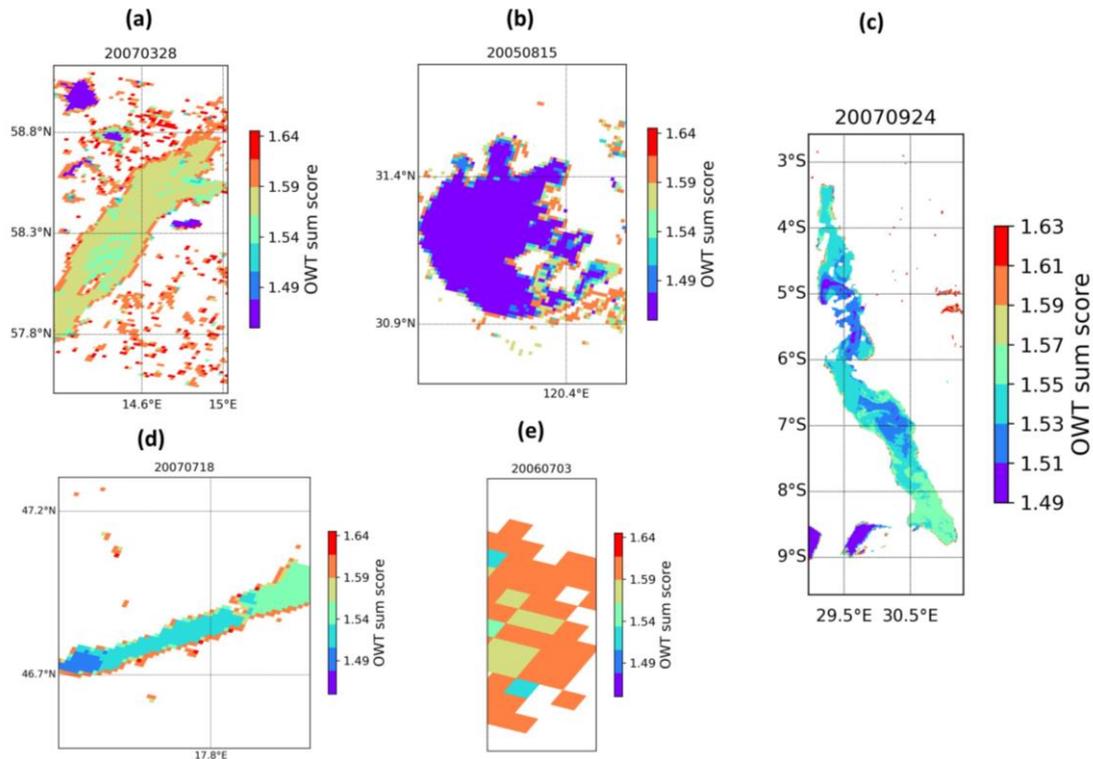
Figure 53 Spatial distribution of OWT sum score (for OWT-14 and 15) in lakes (a) Vättern, (b) Taihu, (c) Tanganyika, (d) Balaton and (e) Rusken from MERIS L2 products.
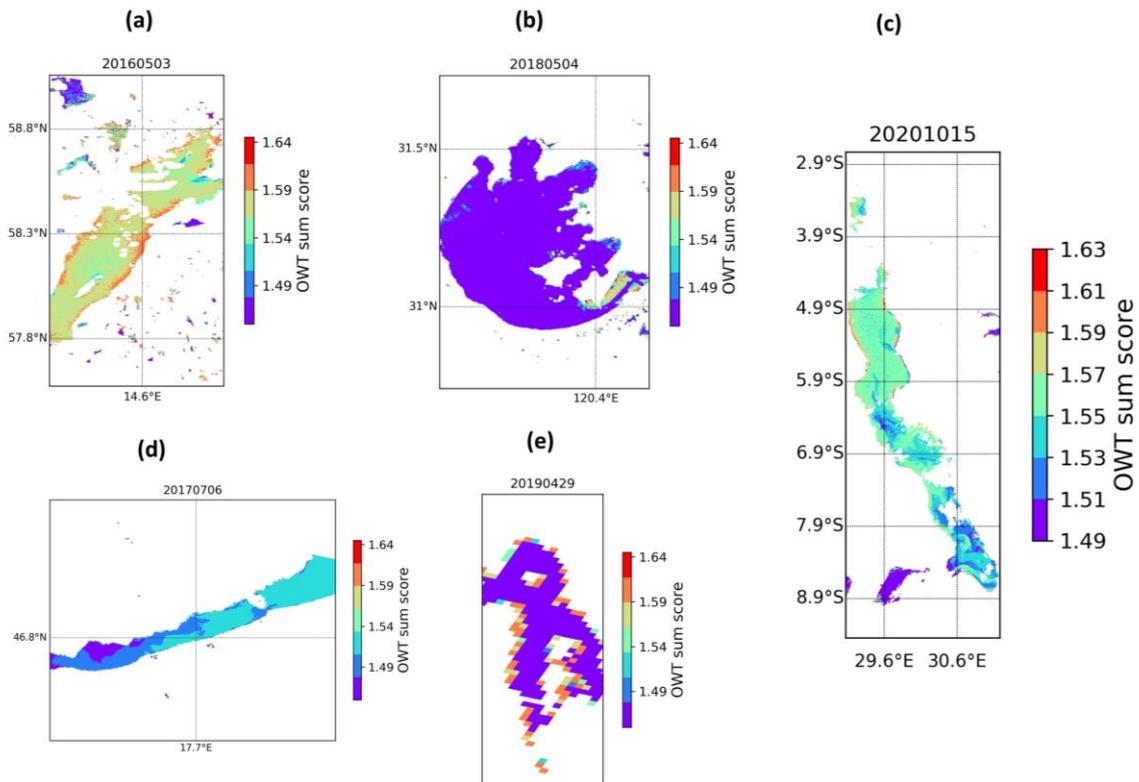

Figure 54 Same as Figure 24, but for OLCI L2 products

5.1.3 Conclusion: application of adjacency mask in Lakes_cci V2.0 processing

In the previous sections, two approaches (a dominant-OWT-based and a threshold-based approach) were evaluated in different lake types for MERIS and OLCI by adopting the two newly identified adjacency OWTs. It is suggested that a combination of the two approaches show adequate performance in all lakes tested. Specifically, one pixel will be identified as being influenced by adjacency effect if both of the following conditions are met:

- The dominant OWT is OWT 14 or 15
- The sum score of OWTs 14 and 15 is great than 1.59 (for MERIS and OLCI)

The proposed procedure is already applied in the Lakes_cci V2.0 LWLR processing chain to minimize the influence of land adjacency.

5.2 Application of climatology filtering on spatial data

5.2.1 Filtering of turbidity on spatial data of Lake Amadjuak (Lake ID 56)

The turbidity climatology based on lake median values for Lake Amadjuak shows that a very clear state of the water prevails. OLCI observations lead to slightly higher turbidity values than MERIS observations. If the weighted mean and standard deviation are used to define a daily acceptable upper limit of turbidity, the threshold values are quite similar (Figure 55). The following examples employ a threshold of mean + 3 × SD to the spatial data.

For day 250, the climatological threshold acts like an outlier filter. Only 27 out of 5691 turbidity data points are above the threshold (Figure 56).

On day 194, the threshold filtering can exclude the high turbidity data points, which arise from undetected ice cover (Figure 57). Low temperatures and no data points in LSWT point both towards a high probability of ice cover. 1525 of 1529 turbidity data points are successfully filtered out by the climatological threshold.
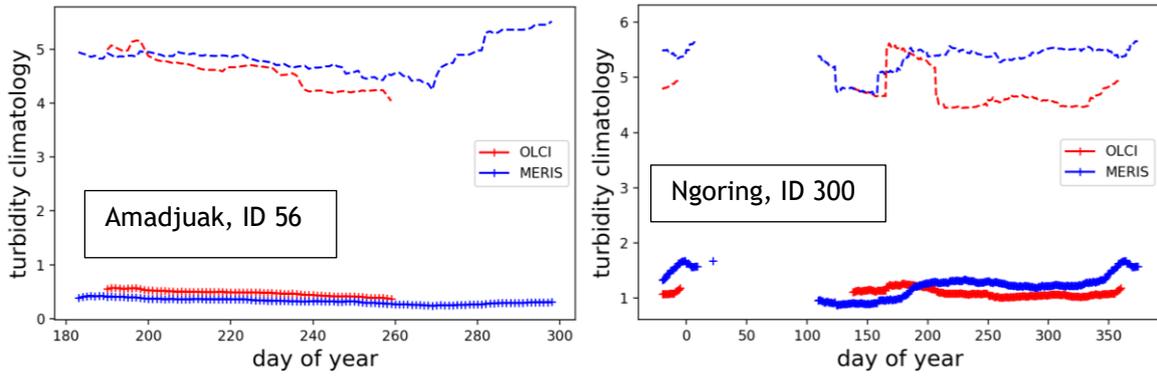
Figure 55 Turbidity climatology for Lake Amadjuak (LakeID 56), Canada, (left) and for Lake Ngoring, China (Lake ID 300, right) for OLCI and MERIS. The threshold in the filtering of images is defined as weighted mean (lines + crosses) plus three times the weighted standard deviation (thresholds shown as dashed lines).
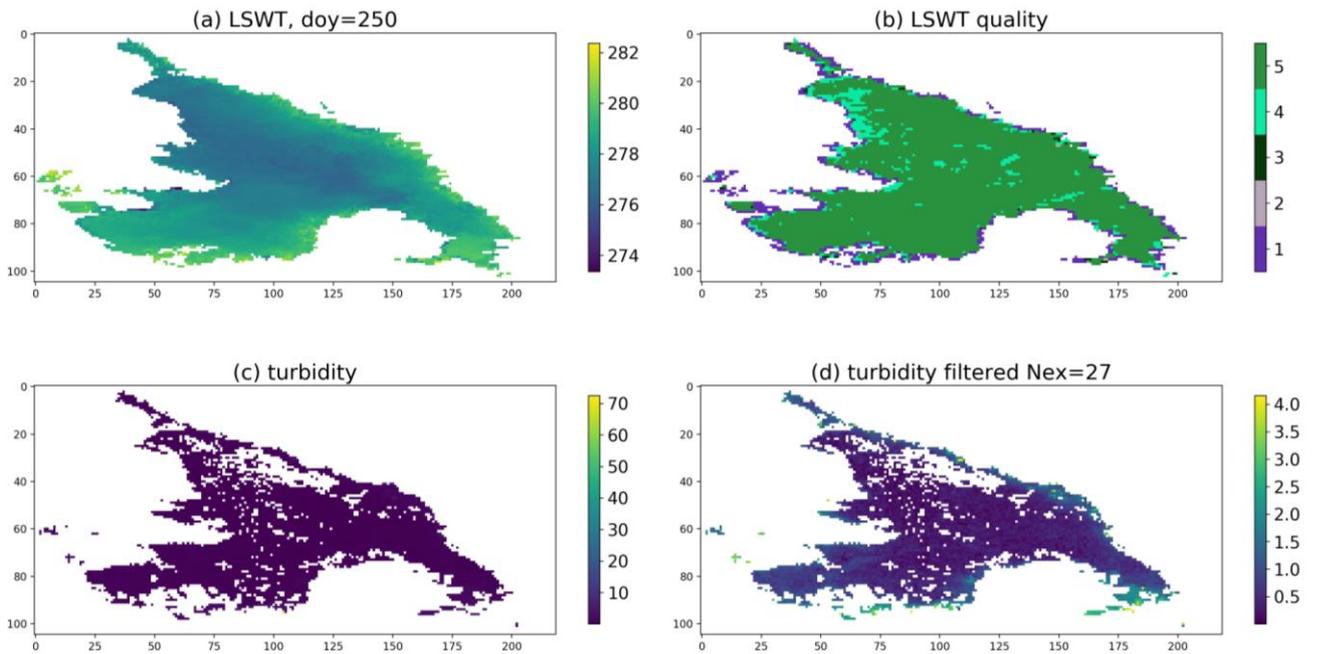
Figure 56 LSWT (upper panels: LSWT (a) and LSWT quality (b)) and turbidity product (c, d) of lake Amadjuak from 250th day of the year 2018 (OLCI). The turbidity threshold is set to 4.21 from the climatology and 27 pixels are filtered out (number of excluded pixels Nex=27).
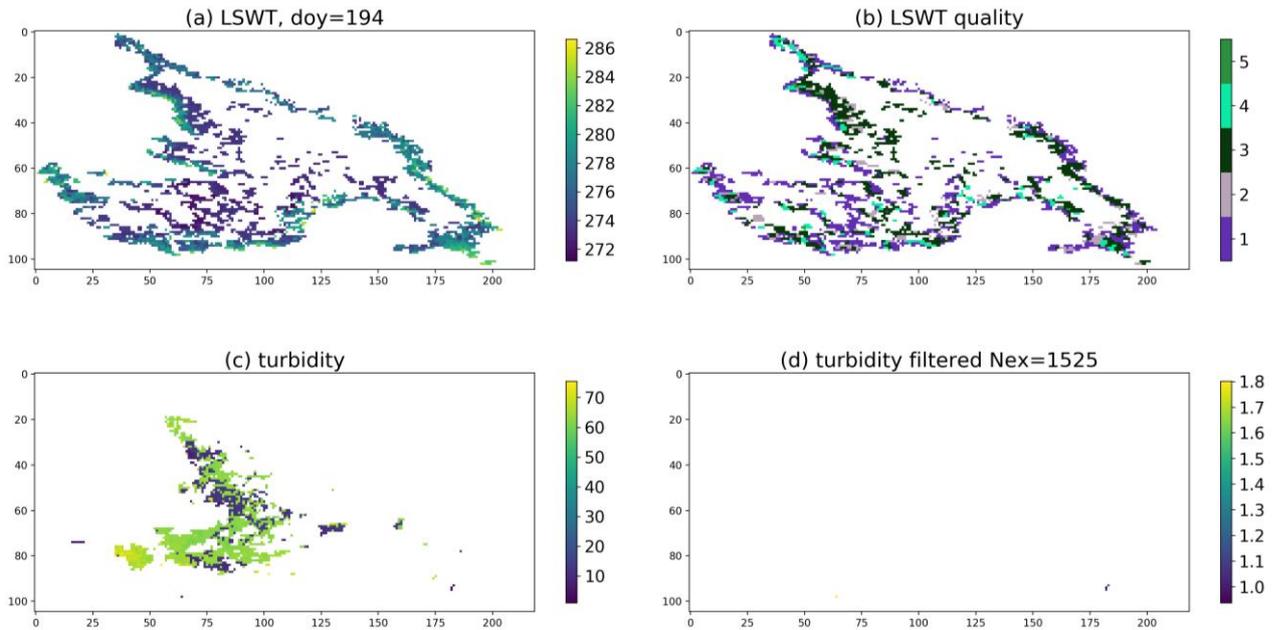
Figure 57 Filtering out ice influenced high turbidity values by climatological threshold on Lake Amadjuak (day 194, 2018, OLCI). LSWT (a, top left) LSWT quality (b, top right), unfiltered turbidity (c, bottom left), filtered turbidity (d, bottom right, number of excluded pixels Nex=1525). The pattern of LSWT measurements near the shore and sparsely scattered within the lake is common for winter conditions.

5.2.2 Filtering of spatial data on Lake Ngoring

The MERIS data appear more strongly affected by adjacency effects (see section 4.1 and 5.1) than the OLCI data, which has in part been attributed to the lower spatial resolution of MERIS RR imagery although other observation effects are not excluded. High turbidity values along the north-eastern shore on day 130 and along the north-western shore on day 205 are excluded by the climatology-based threshold filtering method (weighted climatological mean + 3×SD). The lake area increased from 578 km2 to 677 km2 during 2003 and 2010, which likely created shallow areas or flooded areas along the shore. Submerged vegetation or mixed pixels of land and water could explain the high values in those regions. Unfortunately, the climatology threshold method also cuts off an area of open water in the southwest on day 205. The spatial variability in this lake is likely too large for the simple threshold-based filtering approach to be fully successful, which is based on the daily median per lake. Although, we can assume different results of the median extraction, if the new OWT filter has been applied beforehand, the problem of this methodology would not be resolved. The variability of this lake's observations might decrease significantly, if these close-to-shore pixels are classified as the new classes 14 and 15 and therefore excluded from any water product evaluation. Median values (although less vulnerable to outliers) can be expected to become lower than currently deduced, so that filtering of strong natural spatial patterns can still take place.

The potential of the filtering approach of the climatological thresholds on spatial data can only be tested once the v.2 production has been realised. In there, both methodologies can be easily combined, as the new OWT classes are already applied and in place and new lake-median values excluding OWT 14 and 15 can be extracted.

A similar pattern of high values can also be found in the chl-a concentration product of the same days (Figure 59).
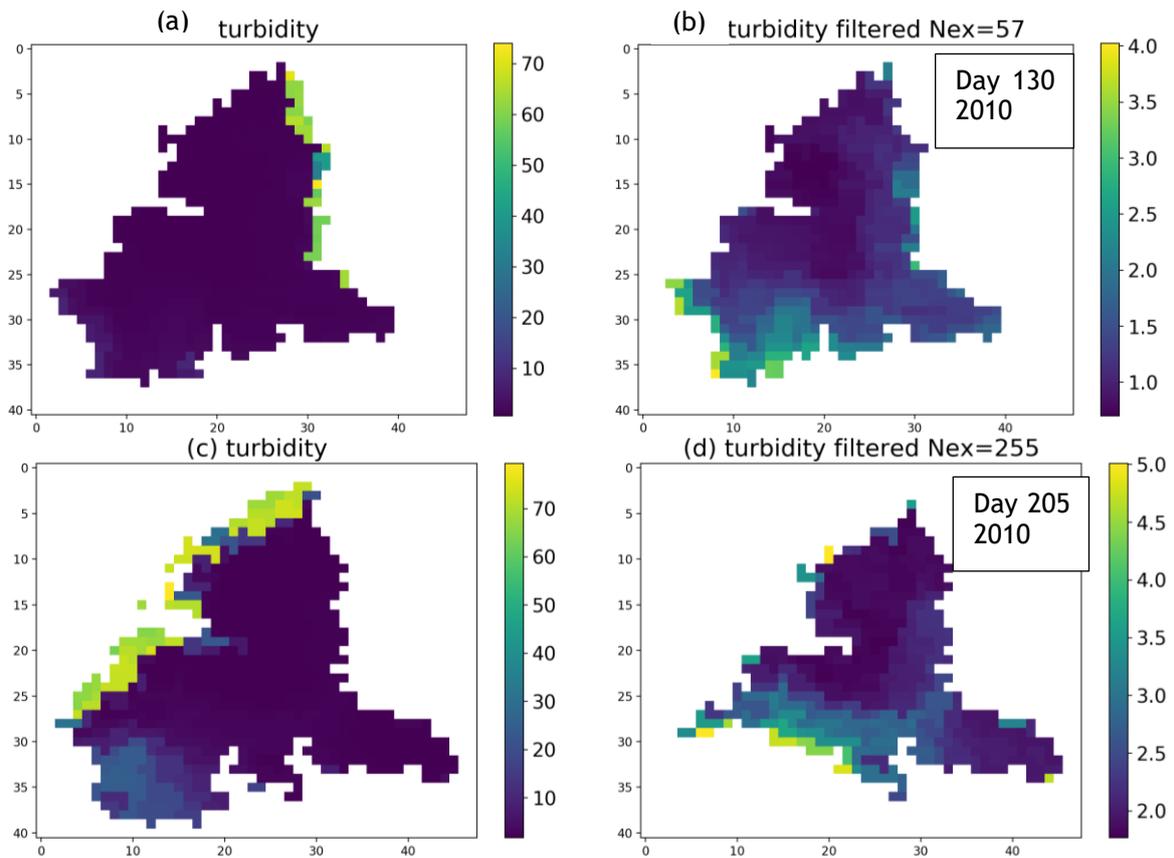
Figure 58 Effect of turbidity filtering with climatological threshold on Lake Ngoring, China. Day 130 (upper row, a + b) and 205 (bottom row, c + d) of year 2010, MERIS data. Unexpectedly high values are filtered out: excluded pixels Nex=57 along the eastern shore on day 130 (b) and Nex=255 along the western shore on day 205 (d). Additionally, the dynamic climatology-based threshold filtering also removed a section in the southwestern region on day 205, which had a naturally higher variability.
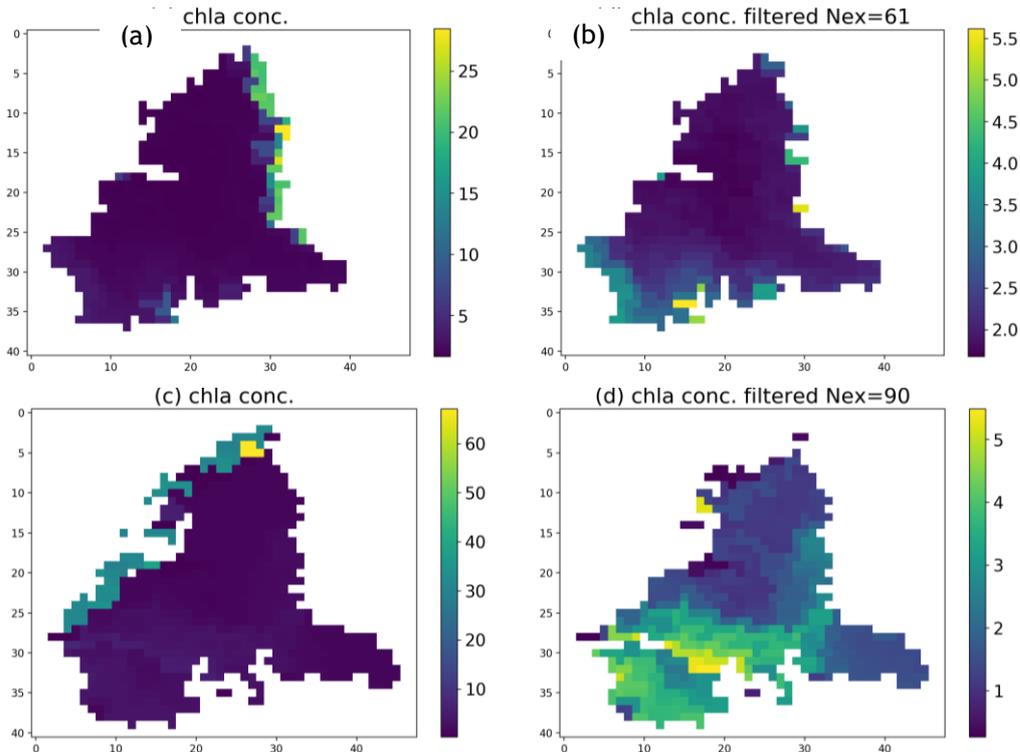
Figure 59 Effect of chla conc. filtering with climatological threshold on Lake Ngoring, China. Day 130 (upper row, a + b) and 205 (bottom row, c + d) of year 2010, MERIS data. Pixels with strong adjacency effect are filtered out (top row at the eastern shore, number of excluded pixels Nex=61 (b); bottom row at the western shore, number of excluded pixels Nex=90 (d); presumably adjacency affect).

5.3 Cross-correlation consistency analysis

5.3.1 LSWT consistency with reanalysis data

To analyse the consistency of water temperature products between different data resources, Climatologies of LSWT and lake mixed layer temperature (LMLT) were used in this analysis, where LSWT is the lake-median daily value from the v1.0 L3S products and LMLT was extracted from ERA 5 meteorological data (see section 2.2). Cross-correlation analysis was carried out between the climatology LSWT and LMLT to assess the consistency between these two products.

Consistency is expected between the observed skin temperature (LSWT) and the reanalysis temperature for the mixed water layer (LMLT). Figure 60 shows and example of the climatology data of LSWT and LMLT in Lake Huron and Lake Tana. These examples show high consistency between LSWT and LMLT, at least in terms of seasonality.
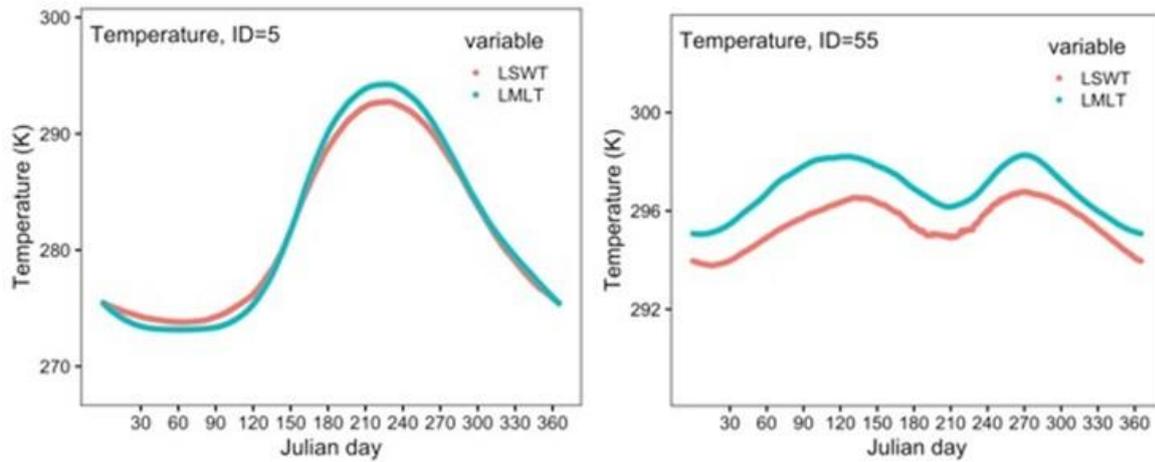
Figure 60: Example of the relationship between LSWT and LMLT. Left: Lake Huron. Right: Lake Tana in Ethiopia.

Most of the lakes (94.5%) included in CRDP v1.0 showed positive correlation between LSWT and LMLT with R > 0.8 (Figure 61), which indicate that there is a good consistency between LSWT product and LMLT product. Only Lake Tucurui in Brazil showed a negative relationship between climatology LSWT and LMLT (Figure 62 left), which may be caused by poor availability of LSWT data (Figure 62). In addition, a glacial lake in Greenland shows a positive relationship between climatology LSWT and LMLT, whereas the peaks of LSWT and LMLT are not synchronous (Figure 62 right).
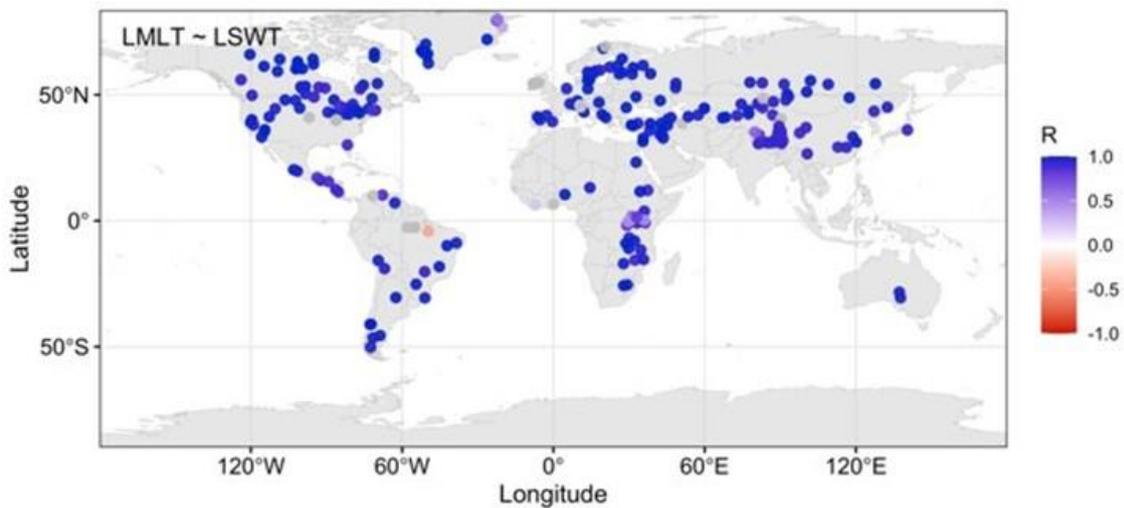
Figure 61: Correlation between climatology LSWT and LMLT for global lakes.
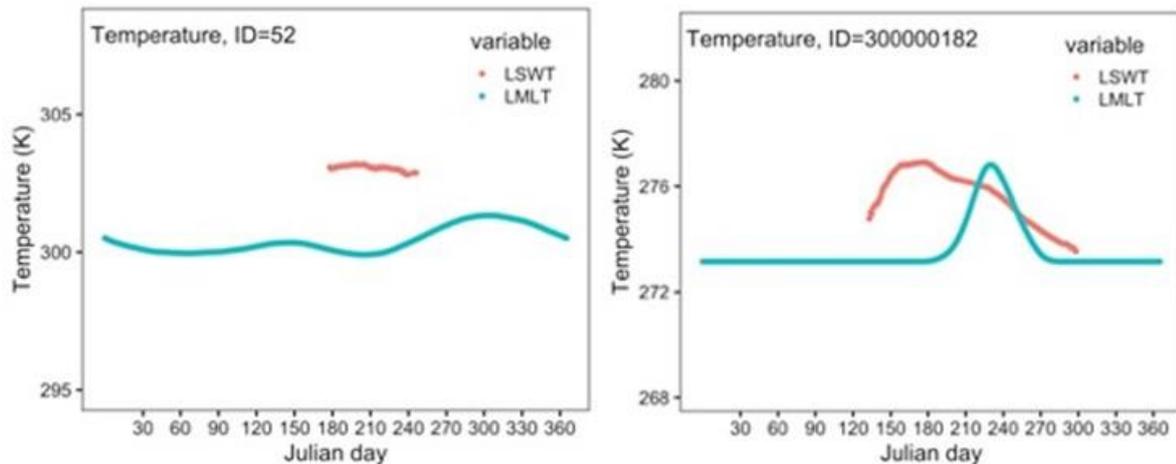
Figure 62: Left: Lake Tucurui in Brazil which showed a negative relationship between climatology LSWT and LMLT. Right: a glacier lake in Greenland, which showed apparently shifted peak between climatology LSWT and LMLT.

5.3.2 Analysis of Chl-a and turbidity climatologies between MERIS and OLCI

To check the consistency of climatologies derived from different sensors, cross-correlation analysis was carried out between Chl-a (turbidity) climatologies derived from MERIS and OLCI, where the climatologies were obtained from lake median Chl-a (turbidity) (section 2.2)

It is reasonable to assume that the seasonality detected from MERIS and OLCI products are consistent for the majority of observed lakes, because drastic ecosystem change is relatively rare and climate shifts are mostly expected to be gradual. For example, in Lake Titicaca (Figure 63), the peak Chl-a concentration is in June-July, the minimum Chl-a concentration is in December-January and this pattern is found in both the MERIS and OLCI time series. In Lake Issyk-Kul, Chl-a peak is in November and the Chl-a minimum is in April for both MERIS and OLCI time series.
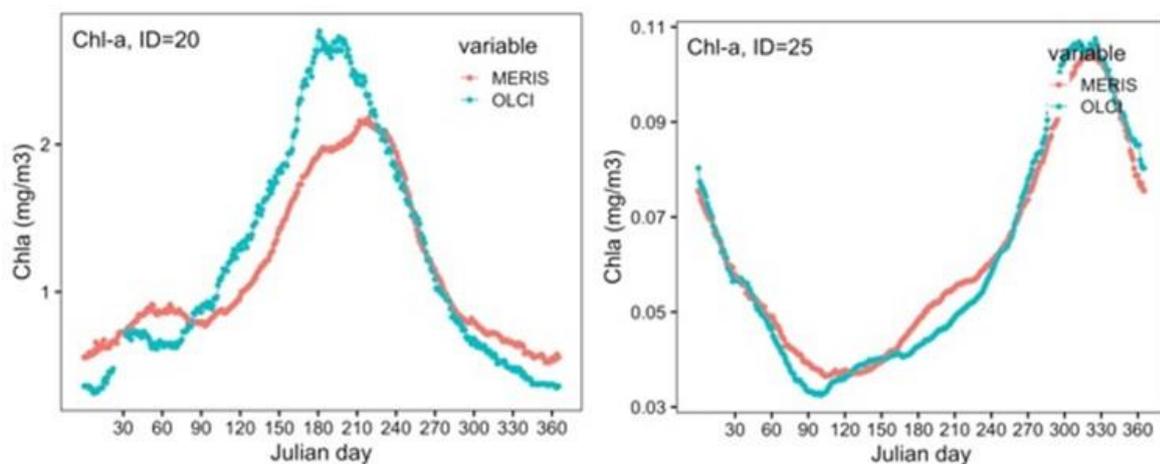
Figure 63: Example of consistent relationships of Chl-a climatologies extracted from MERIS and OLCI. Left: Lake Titicaca in south America. Right: Lake Issyk-Kul in Kirgizstan.

Correlations between Chl-a climatologies derived from MERIS and OLCI showed positive relationships in the majority of lakes (Figure 64), which indicates that seasonal patterns of Chl-a extracted from MERIS and OLCI are consistent. There are 22 lakes which showed R<0, which lakes are mainly located in high altitude areas (e.g., Tibetan plateau) and high latitude areas (e.g., northern Europe and North America). For example, Lake Ladoga in Russia (Figure 65 left), showed Chl-a peaks in August-

September during the MERIS observation period, has a Chl-a peak in April-May during OLCI observations. Lake Nettiling in Canada (Figure 65 right) showed opposite seasonal patterns between MERIS and OLCI. The potential reasons for those lakes which showed negative relationship between climatology data from MERIS and OLCI are: (1) the ecosystem status of the lake changed from 2002-2012 to 2016-2019, (2) the availability of data influenced the climatology, e.g. due to ice cover, or (3) lake size influenced the Chl-a retrieval, as 77% of the 22 lakes have a max-distance-to-land < 10 km. This would suggest the sensor data and/or processing have different sensitivities to adjacency effects, as we also observe in other analyses.
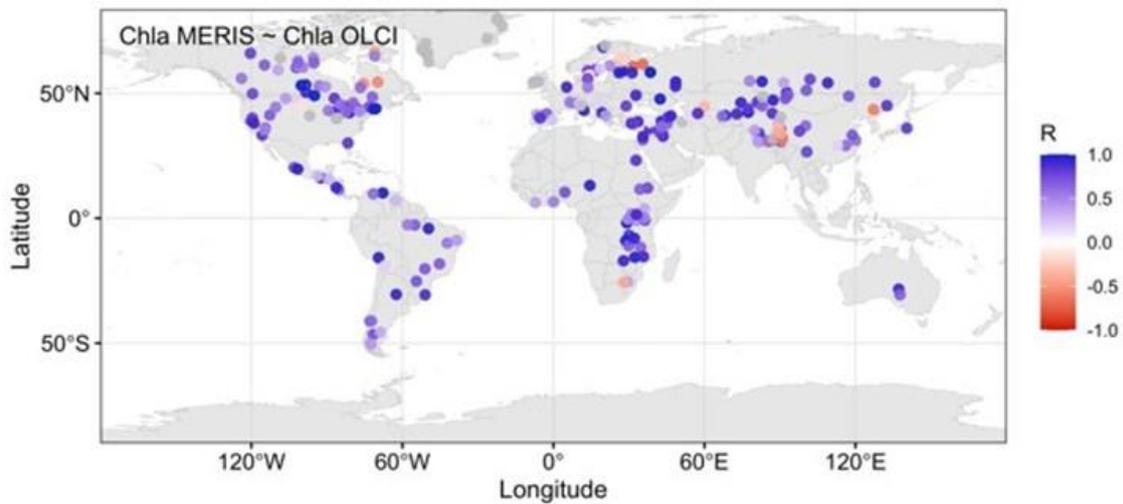
Figure 64: Correlation between Chl-a climatologies derived from MERIS and OLCI L3S products.
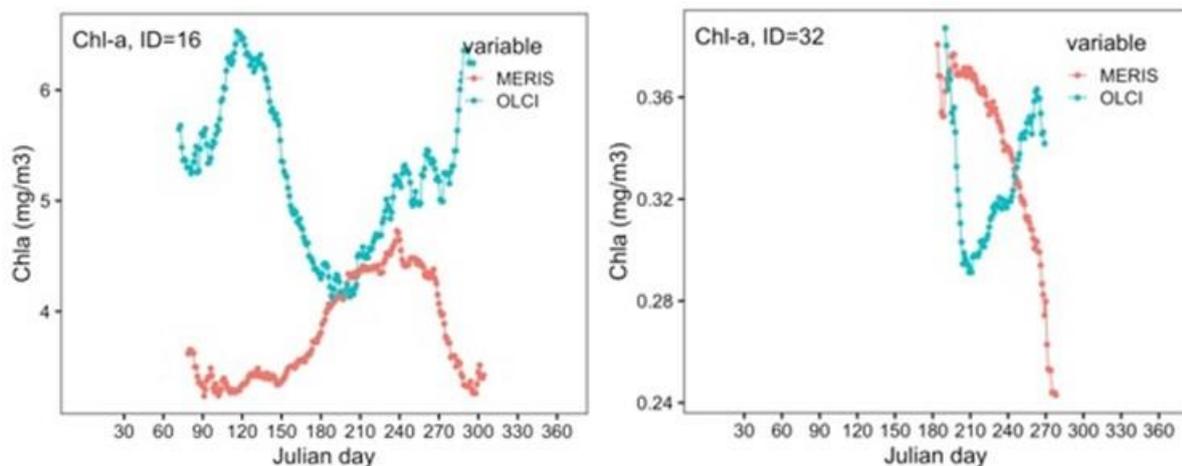
Figure 65: Examples of questionable relationships between of Chl-a climatologies derived from MERIS and OLCI L3S products. Left: Lake Ladoga in Russia. Right: Lake Nettiling in Canada.

For turbidity climatologies, most of the lakes showed positive relationships (74% of lakes R>0.5) between data derived from MERIS and OLCI (Figure 66), which indicates good consistency. There are 19 lakes with R<0 located in the Tibet area, west Asia, northern Europe, and North America. Potential reasons for those lakes are the same as those suggested for Chl-a retrieval. In this case, 74% of the 19 lakes affected had a maximum distance to land < 10 km.
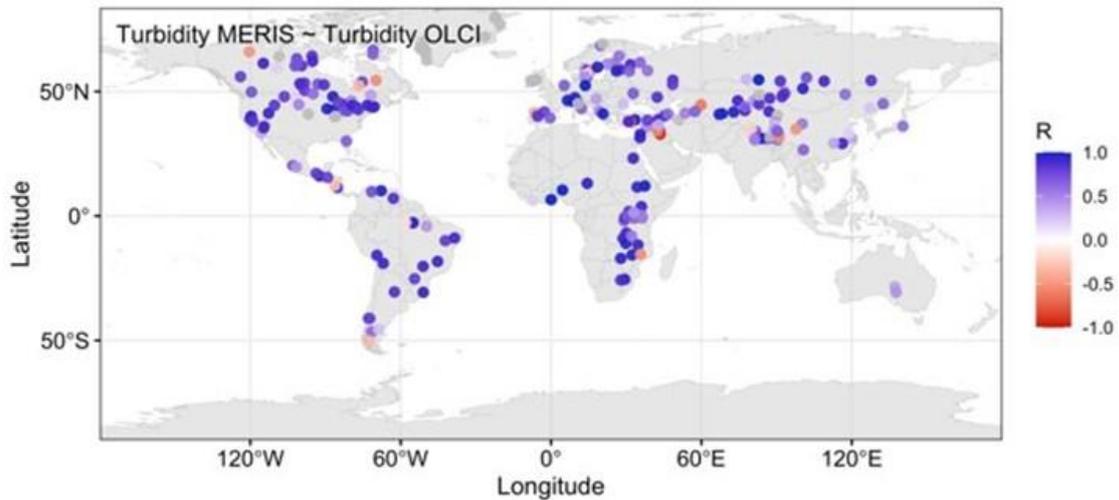
Figure 66: Correlation between climatology turbidity derived from MERIS and OLCI products for global lakes.

5.3.3 Relationship between turbidity and LWH

To explore if the turbidity of the lake generally follows the variation of lake water level, Lake median turbidity time series at the lake centre (maximum distance from land) were compared to lake water surface height (LWL) in each lake included in the CRDP v1.0 (section 2.1). The time series were first smoothed using LOESS to minimize the influence from outliers, and then cross correlation analysis were carried out between the smoothed timeseries turbidity and timeseries LWL for each lake to explore their potential relationships.

Figure 67 shows the relationship between turbidity and LWL for all included lakes. There are 152 lakes with valid results in this analysis because not all lakes have LWL data. Lakes for which timeseries could not be compared are shown in grey in Figure 67. For the lakes with valid turbidity and LWL timeseries, most (70%) show a negative relationship between turbidity and LWL. In these cases, high turbidity corresponds to low water level. 30% of lakes showed a positive relationship between turbidity and LWL, and these are mainly located in central Asia, north and south America.
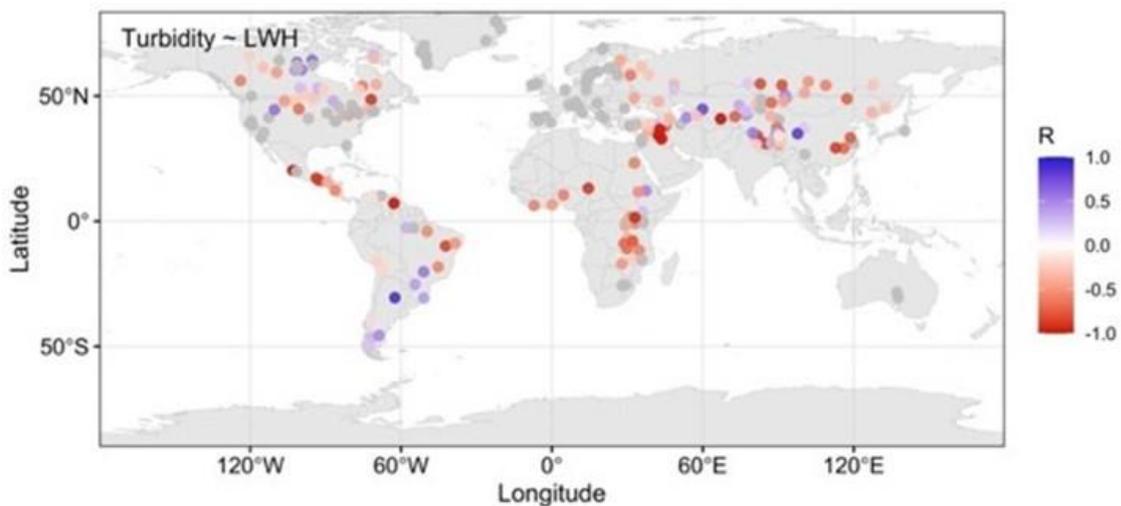
Figure 67: Relationship between turbidity and lake water height for global lakes, grey points are invalid results because of availability of timeseries data.

In terms of the positive relationship between turbidity and LWL, there are two cases: where turbidity and LWL showed positive relationships at the seasonal scale, for example in Lake Ilha Solteira in Brazil (Figure 68), high turbidity with high water surface height is observed during the first half of the year, and low turbidity with low water surface height in the second half of the year. The likely mechanism behind this behaviour is turbid water flowing into the lake in the rainy season, thus increasing both LWL and turbidity. Where turbidity and LWL show positive relationships at the annual scale, for example in Lake Mar Chiquita in Argentina (Figure 69), we see a decreasing trend of turbidity from 2004 to 2012, and the water surface height also showed a decrease trend in the same period. The mechanism behind this is less clear, but a dampening of flow patterns would likely result in lower transport of sediments into and within the lake.
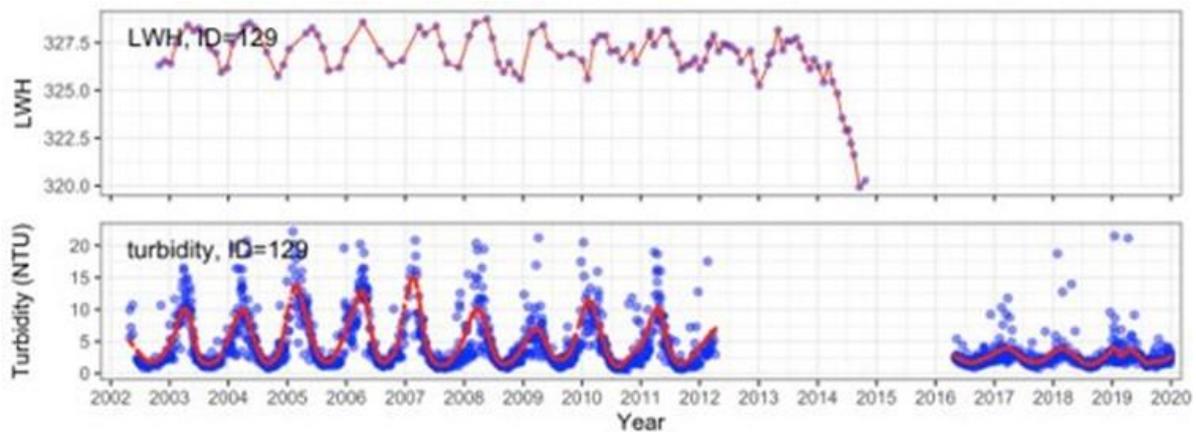
Figure 68: Example of the positive relationship between turbidity and LWL in Ilha Solteira Reservoir in Brazil.
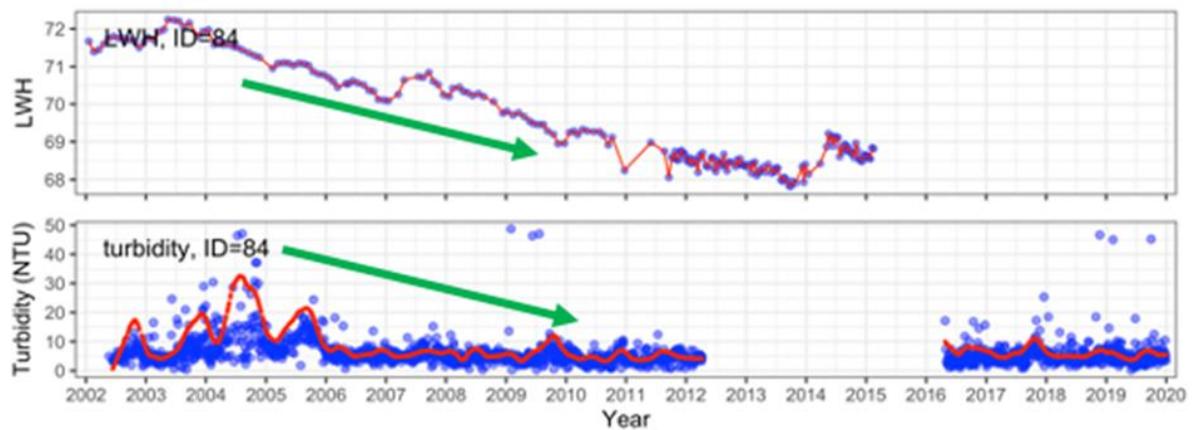
Figure 69: Example of the positive relationship between turbidity and LWL in Lake Mar Chiquita in Argentina.

Similarly, looking at negative relationships between turbidity and LWL, there are also two cases: where turbidity and LWL show negative relationships on the seasonal scale, for example in Lake Kainji in Nigeria (Figure 70), high turbidity but low water surface height is observed during September-October in each year. The potential mechanism behind this is clear water flowing into and diluting the lake or a heightened water table lessening resuspension events. Where turbidity and LWL showed negative relationships at the annual scale, for example in Qadisiyah reservoir in Iraq (Figure 71), we see a significant increase of turbidity in 2009, and then the turbidity decreased since 2010. Interestingly, the water surface height showed a significant decrease in 2009, and then increased since 2010. The extremely high turbidity event in 2009 is likely linked to the drop of water surface height (decrease of water area). Extremely elevated turbidity may be an observation artefact

associated with a low water table (bottom visibility) which ideally would be masked out in the L3S product.
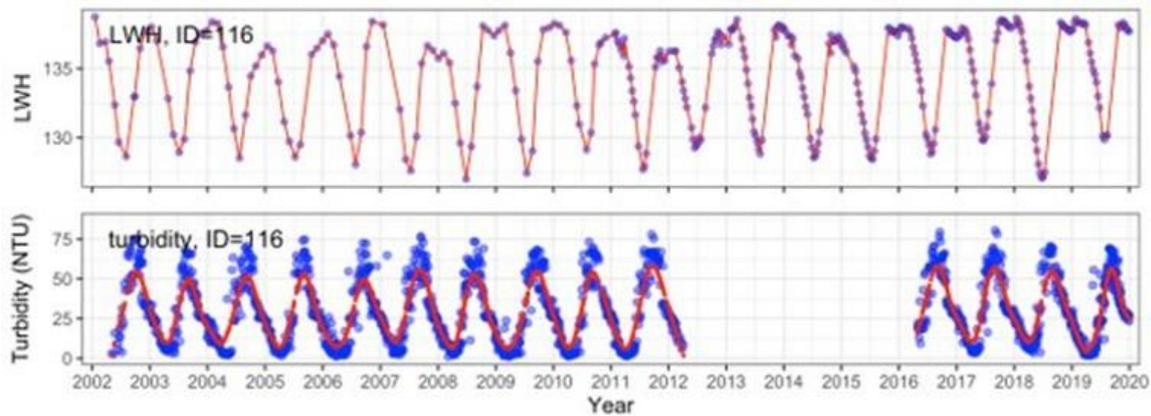
Figure 70: Example of negative relationship between turbidity and LWL in Lake Kainji in Nigeria.
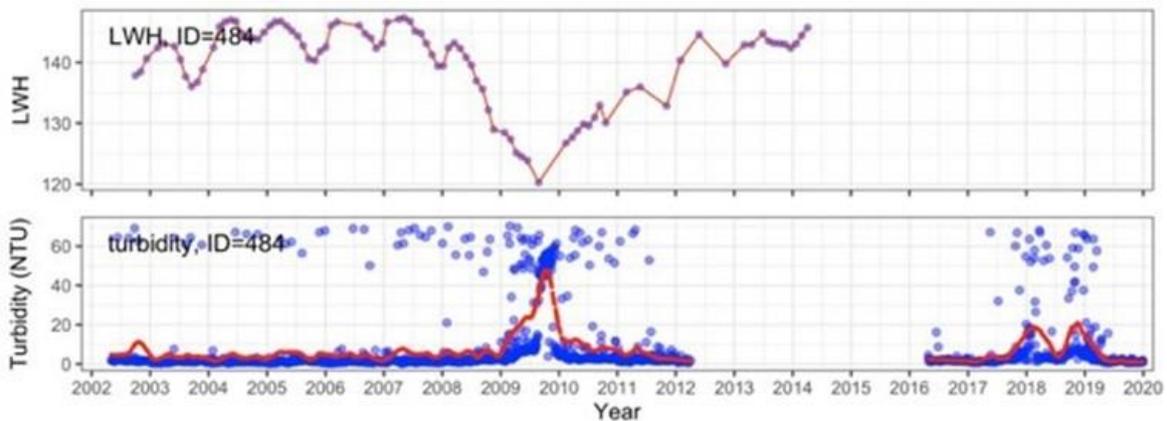
Figure 71: Example of negative relationship between turbidity and LWL in Qadisiyah Reservoir in Iraq.

5.3.4 Conclusions

At seasonal scales, consistency between LSWT and LMLT climatology is found for almost all the lakes, and the level of seasonal and annual consistency between Chl-a and turbidity climatologies derived from MERIS and OLCI was good for most of the lakes. Inconsistencies between MERIS and OLCI LWLR products may have systematic causes, be based in ecosystem shifts or infrequent pixel identification issues which influenced the climatologies.

6   Recommendations

The combination of LIC, LSWT and LWLR variables in a single L3S product creates new opportunities to evaluate shortcomings in individual pixel identification of these product branches, and to implement solutions either upstream (L2 processing) or downstream (L3S product flagging). Suspicious cases include ice observations at non-freezing temperatures in the LIC product, and high water leaving reflectance values of the LWLR product where an ice presence is apparent. In general, the latest thermal products (LSWT, LIC) show a higher degree of day-to-day stability, which can be exploited to resolve cases where the influence of observation artefacts is less easily distinguished from noise (e.g. LWLR).

Climatologies of all key variables are particularly useful to circumvent observation gaps and assess observed events in the context of the predictor variables. It is important to note that this would result in a product confidence flag (flagging a risk that data are not reliable) rather than directly invalidating observations.

Based on the analyses performed within this study, we have suggested some practical solutions and further recommendations for future investigations, which are summarized in the following sections.

6.1   Flagging of LWLR and derived products based on new OWTs

Two new OWTs (OWT-14 and OWT-15) were identified from MERIS and OLCI images, initially based on data from small, northern lakes and validated against a wider set of lake types. The analysis and results indicate that the new OWTs could be integrated in the data processing chain to identify pixels which are influenced by adjacency effects. It is not yet known how this will change the value distributions across all the considered lakes, as this requires a larger reprocessing effort, which is already ongoing towards CRDP v2.0. Once this work is completed, dynamic-threshold filtering can be revisited.

A combination of the two validated approaches shows adequate performance in all lakes tested. Specifically, an observation will be identified as being influenced by adjacency effect if both of the following conditions are met:

- The dominant OWT of the L2 Rw spectrum is OWT 14 or 15
- The sum of the OWT membership scores of OWTs 14 and 15 is greater than 1.59 (for MERIS and OLCI)

The proposed procedure is already incorporated in Lakes_cci CRDP V2.0 production and has also been extended to MODIS-Aqua.

6.2   Dynamic threshold filtering based on LSWT climatologies

The annual LSWT pattern is a clear indication of the probability of ice cover, including which occurs below the detection limit of LIC or LWLR pixel identification procedures. If the climatological temperature is well above freezing point, it is very likely that no ice can form and the LIC product should provide non-ice classifications.

Outlier values associated with low water temperatures can be confidently removed from the LWLR products. The turbidity product, because it is less affected by biological variability and highly sensitive to ice presence, may be used as a proxy to test for the ice risk. A procedure has been proposed in the form of a decision tree, which sets lake-specific turbidity thresholds for each day of the year, using any available LSWT climatology data and lowering the realistic bounds for turbidity where the LSWT climatology is not informative.

Once LSWT climatologies are available for all lakes, the procedure can be implemented directly after producing daily L3 LWLR products and before generating the L3S product.

Turbidity and Chl-a climatologies may also be directly used to flag suspect observations, but such procedures should be treated with caution to prevent masking out extreme events.

All climatologies are currently based on daily lake median values to reduce the spatial dimensionality of the dataset. The number of observations available on a given day can be low due to cloud or ice cover or the extent of the sensor swath, which needs to be taken into consideration. For LSWT, lake medians were calculated for the quality classes, which may have a spatial bias.

6.3   Consider spatial heterogeneity in extracted data sets

Spatial heterogeneity has not been taken into account in any of the climatologies or per-OWT percentiles we considered. But spatial patterns can be strong and are thus not well represented by a single average value of the lake. For example, if the observations (valid pixels) cover only parts of the lake, most likely the average is not representative. Ideally, for each day the lake has been observed to its full extent, which is rarely the case. In addition to restrictions in orbit repetitions, there is also cloud and ice cover hindering a full coverage. Already in ideal conditions the presence of pronounced spatial pattern like strong gradients in turbidity or chl-a concentration cannot be covered by a single daily aggregated value, and a filtering based on this kind of climatology will exclude valid pixels inevitably. Cloud cover prevents observations more randomly than ice coverage, so that representativeness becomes systematically lower during times of ice cover. Of course, if the patterns of spatial coverage follow a stable annual cycle, the derived climatologies reclaim their descriptiveness of the observed data and can be applied as simple threshold tests. Nevertheless, climatologies based on daily averages have to be interpreted as depending on spatial distribution of data.

Therefore, we recommend including either a classification by bathymetry and/or distance from shore and calculate average values inside these classes. Or, for larger lakes, subdivisions could be introduced which reflect prevailing patterns of dominant OWTs, if they are not strongly correlated with the distance to shore. Lake basins of different depths or bathymetry in general, and artificial dams can be reasons for optically observed spatial patterns.

But dividing the lake data, effects close to the shorelines which might be caused by adjacency effects would have to be filtered out before such a distance to shore based climatology (as done for version CRDP v2.0). Otherwise, the climatologies based on observations close to shore will be strongly affected by processing artefacts, which are not an issue if the daily median value of the entire lake is the basis of further analysis.

Annex A. Project Acronyms

This is a generic list containing all the acronyms used in the project.

AATSR	Advanced Along Track Scanning Radiometer
AATSR	Advanced Along Track Scanning Radiometer
AERONET-OC	AErosol RObotic NETwork - Ocean Colour
AMI	Active Microwave Instrument
AMSR-E	Advanced Microwave Scanning Radiometer for EOS
APP	Alternating Polarization mode Precision
ASAR	Advanced Synthetic Aperture Radar
ASLO	Association for the Sciences of Limnology and Oceanography
ATBD	Algorithm Theoretical Basis Document
ATSR	Along Track Scanning Radiometer
AVHRR	Advanced very-high-resolution radiometer
BAMS	Bulletin of the American Meteorological Society
BC	Brockman Consult
C3S	Copernicus Climate Change Service
CCI	Climate Change Initiative
CDR	Climate Data Record
CEDA	Centre for Environmental Data Archival
CEMS	Centre for Environmental Monitoring from Space
CEOS	Commitee on Earth Observation Satellites
CGLOPS	Copernicus Global Land Operation Service
CIS	Canadian Ice Service
CLS	Collecte Localisation Satellite
CMEMS	Copernicus Marine Environment Monitoring Service
CMUG	Climate Modelling User Group
CNES	Centre national d'études spatiales
CNR	Compagnie Nationale du Rhône
CORALS	Climate Oriented Record of Altimetry and Sea-Level
CPD	Communiation Plan Document
CR	Cardinal Requirement
CRG	Climate Research Group
CSWG	Climate Science Working Group
CTOH	Center for Topographic studies of the Ocean and Hydrosphere
DUE	Data User Element
ECMWF	European Centre for Medium-Range Weather Forecasts
ECV	Essential Climate Variable

ELLS-IAGRL	European Large Lakes Symposium-International Association for Great Lakes Research
ENVISAT	Environmental Satellite
EO	Earth Observation
EOMORES	Earth Observation-based Services for Monitoring and Reporting of Ecological Status
ERS	European Remote-Sensing Satellite
ESA	European Space Agency
ESRIN	European Space Research Institute
ETM+	Enhanced Thematic Mapper Plus
EU	European Union
EUMETSAT	European Organisation for the Exploitation of Meteorological Satellites
FAQ	Frequently Asqued Questions
FCDR	Fundamental Climate Data Record
FIDUCEO	Fidelity and Uncertainty in Climate data records from Earth Observations
FP7	Seventh Framework Programme
GAC	Global Area Coverage
GCOS	Global Climate Observing System
GEMS/Water	Global Enfonment Monitoring System for freshwater
GEO	Group on Earth Observations
GEWEX	Global Energy and Water Exchanges
GloboLakes	Global Observatory of Lake Responses to Environmental Change
GLOPS	Copernicus Global Land Service
GTN-H	Global Terrestrial Network – Hydrology
GTN-L	Global Terrestrial Network – Lakes
H2020	Horizon 2020
HYDROLARE	International Data Centre on Hydrology of Lakes and Reservoirs
ILEC	International Lake Environment Commettee
INFORM	Index for Risk Management
IPCC	Intergovernmental Panel on Climate Change
ISC	International Science Council
ISO	International Organization for Standardization
ISRO	Indian Space Research Organisation
JRC	Joint Research Centre
KPI	Key Performance Indicateurs
LEGOS	Laboratoire d'Etudes en Géophysique et Océanographie Spatiales
LIC	Lake Ice Cover
LSWT	Lake Surface Water Temperature
LWE	Lake Water Extent
LWL	Lake Water Level
LWLR	Lake Water Leaving Reflectance

MERIS	MEdium Resolution Imaging Spectrometer
MGDR	Merged Geophysical Data Record
MODIS	Moderate Resolution Imaging Spectroradiometer
MSI	MultiSpectral Instrument
MSS	MultiSpectral Scanner
NASA	National Aeronautics and Space Administration
NERC	Natural Environment Research Council
NetCDF	Network Common Data Form
NOAA	National Oceanic and Atmospheric Administration
NSERC	Natural Sciences and Engineering Research Council
NSIDC	National Snow & Ice Data Center
NTU	Nephelometric Turbidity Unit
NWP	Numerical Weather Prediction
OLCI	Ocean and Land Colour Instrument
OLI	Operational Land Imager
OSTST	Ocean Surface Topography Science Team
PML	Plymouth Marine Laboratory
PRISMA	PRecursore IperSpettrale della Missione Applicativa
Proba	Project for On-Board Autonomy
R	Linear Correlation Coefficient
RA	Radar Altimeter
RMSE	Root Mean Square Error
SAF	Satellite Application Facility
SAR	Synthetic Aperture Radar
SeaWIFS	Sea-viewing Wide Field-of-view Sensor
SIL	International Society of Limnology
SLSTR	Sea and Land Surface Temperature Radiometer
SoW	Statement of Work
SPONGE	SPaceborne Observations to Nourish the GEMS
SRD	System Requirements Document
SSD	System Specification Document
SST	Sea Surface Temperature
STSE	Support To Science Element
SWOT	Surface Water and Ocean Topography
TAPAS	Tools for Assessment and Planning of Aquaculture Sustainability
TB	Brightness Temperature
TM	Thematic Mapper
TOA	Top Of Atmosphere
TR	Technical Requirement
UNEP	United Nations Environment Programme
UoR	University of Reading

US	United States
VIIRS	Visible Infrared Imaging Radiometer Suite
WCRP	World Climate Research Program
WHYCOS	World Hydrological Cycle Observing Systems
WMO	World Meteorological Organization
WP	Work Package

References

Spyrakos, E., O'Donnell, R., Hunter, P.D., Miller, C., Scott, M., Simis, S.G., Neil, C., Barbosa, C.C., Binding, C.E., & Bradt, S., 2018. Optical types of inland and coastal waters. Limnol. Oceanogr. 63, 846-870.